Analysis of Plasmons Sustained on the Surface of Graphene

by

Keenan Lyon

A thesis
presented to the University of Waterloo
in fulfillment of the
thesis requirement for the degree of
Master of Mathematics
in
Applied Mathematics

Waterloo, Ontario, Canada, 2014

I hereby declare that I am the sole author of this thesis. This is a true copy of the thesis, including any required final revisions, as accepted by my examiners.

I understand that my thesis may be made electronically available to the public.

Abstract

This thesis is broken into two parts, both dealing with the role of two-dimensional graphene in electronic and optical applications. The first section develops a phenomenological relationship for the polarizability of the graphene sheet using a hybrid semi-classical and QFT-derived (Quantum Field Theory) model for different energy regimes. Fits are made and our results are compared to data from two distinct experimental setups. The effects of contamination and rippling of the sheet are considered. The second section shows a phenomenological model for the rough surfaces of graphene and its underlying substrate for a sheet grown on a conducting material. Three different perturbative mathematical models are then explored to justify the shift in the plasmon frequency and the energy loss dispersion due to roughness, using input from experimental roughness data. The models are compared and corrected to include physical effects like crumpling.

Acknowledgements

I am thankful for the friends and family that have made these two years merry and cheerful, in and out of the office.

A special shout out to A. Tavakoli, MMath, for never accepting my answer for what a 'plasmon' is, to R. Peierls for guiding me into PhD studies in physics, and to Wikipedia, who has helped me more than I can give her credit for.

Last but not least, I am grateful towards Prof. Mišković for helping me on my journey as a researcher, for being a great mentor, and for indulging a young scientist with carefree, tender, and airy poetry.

Table of Contents

List of Figures

Chapter 1

Introduction

1.1 Graphene: Physics in Flatland

Graphene has many peculiar features, the most noteworthy being its two-dimensionality. Two-dimensional materials for decades were predicted to be experimentally unviable; this is due to the Mermin-Wagner theorem, which states that the long-wavelength thermal and quantum fluctuations would make the material ripple and curve, meaning a flat structure is an unstable energy state for the system [27]. However, its discovery in 2004 by Geim and Novosolev using scotch tape on graphite, which is composed of many layers of spaced graphene, showed that a stable configuration is possible. Graphene is the most recent in a succession of discoveries regarding the assembly of carbon atoms into different configurations, with fullerene, or buckyballs, coming in 1985 [32]; these are stable molecules of 60 carbon atoms arranged in a geodesic structure. Carbon nanotubes, with a disputed discovery date between 1952 and 1991, are cylindrical lattices with small radii and enormous tensile strength, and can be considered as 'rolled up' graphene in terms of the bonding and hexagonal lattice structure. The overarching theme of all these carbon nano-structures is the sp^2 orbital bonding that gives these carbon allotropes their unusual properties, including their feature of having unbonded π orbitals which yield many of the electronic properties. Throughout our thesis we address this two-dimensional feature of our graphene, a theme that affects the movement of electrons in the sheet, the roughness of the graphene membrane, and the mathematical description of it within our electromagnetic boundary conditions.

The topic of two-dimensionality does not stop at the lattice structure. The influence of the unbonded sp^2 orbitals above and below each carbon atom, along with the hexagonal lattice that threads our carbon atoms, yields a linear dispersion relation for frequencies between the visible and THz range, depending on the Fermi energy of the graphene. The photon-like nature of fermionic quasi-particles (meaning electrons and holes with zero effective mass) for these energies and the ability to experimentally investigate them makes graphene a tool for research into fundamental physics concepts like Pauli blocking, Klein tunneling [55], Landau quantization of the fermionic quasi-particles [26], and the quantum Hall effect.

On the more applied side of things, the electrical conductivity of graphene, even at room temperature, is stronger than any known material, hence graphene's being heralded as the new innovation to upgrade transistors, electrical circuits and semiconductors into faster and smaller variations [53]. Plasmons with tunable resonance frequency on the graphene surface is a trending topic in current research, and we describe them next.

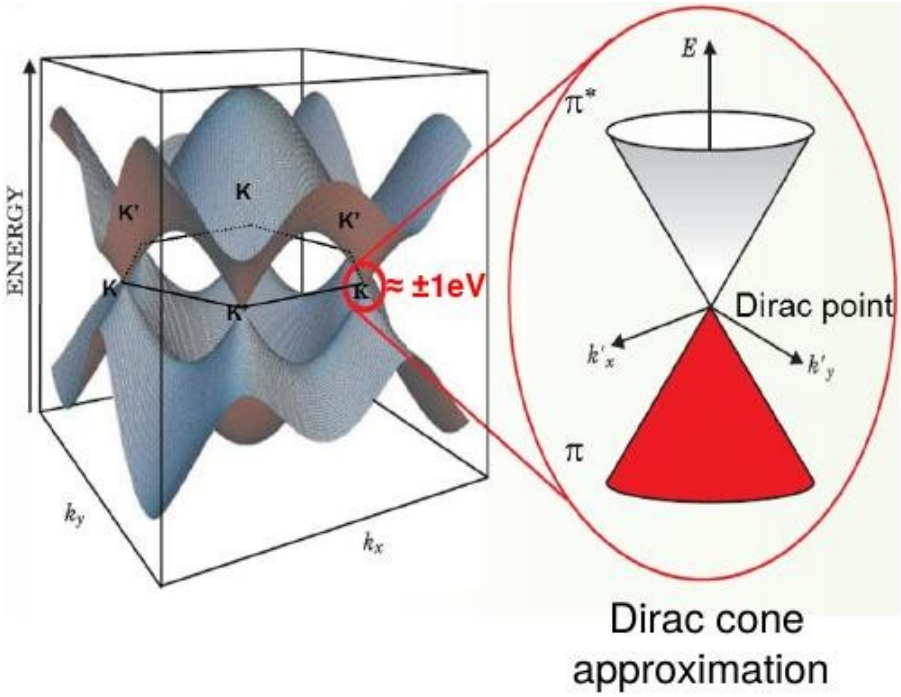

Figure 1.1: Model of the energy dispersion of graphene within the tight-binding approximation. The 6 symmetric self-crossings in the band energy structure are where the dispersion relation relating energy to the crystal momentum in the graphene lattice are effectively linear, known as the Dirac cone regime. Other symmetry points (see Fig. 3.1) are associated with different regimes that exhibit special properties. Adapted from [42]

1.2 Graphene: A Host for Tunable Plasmons

The many optical and electrical properties of graphene make it an attractive option for the development of new opto-electronic devices and in the enhancement of current technologies. Its small size allows its incorporation into semiconductors, conductors, dielectrics, metals and other nano-structures. Aside from its size, an advantage of graphene is the effect that doping and gating have on the resonance of electron oscillations confined to the surface of the sheet, known as plasmons [21]. Graphene in the low energy regime has a band structure effectively described via a quasi-particle picture with photon-like particles occupying eigenstates of the Hamiltonian, computed within a tight-binding approximation. Tunability of the plasmon works because of the strong electron-electron interactions within the graphene sheet [15], causing the effective mass of these quasi-particles in graphene to modulate with the Fermi energy, and hence shift the resonant frequency. The ability to tune these plasmons gives graphene a character unseen in traditional optical devices which have fixed resonance frequencies. The success of graphene in this respect has spurred the investigation of the tunability of similar 2D crystals to discover their applications in opto-electronics.

Current applications for graphene plasmons include efficient photocells, frequency modulators, displays, and sensors, and is seen as a probable successor to liquid crystals due to the speed of graphene's response [3]. The biological and chemical sensing technique of surface plasmon resonance has been shown to increase its sensitivity to detected particles when the system is coupled to a graphene sheet, along with the fact that the carbon structure of graphene makes it an effective tool for chemical bonding. The extremely-high localiza-

tion and confinement of the plasmons in graphene, along with its long lifetime and efficient light-matter interactions also make it the subject of heavy research for opto-electronic uses [21].

The main issues with using plasmons in graphene for applications center around the low optical absorption of the single layer of carbon atoms, the challenge of coupling to certain systems due to the strong bonding capabilities of graphene, and the issues of disorder, randomness, contamination and finite temperature in the structure, which tend to ripple and shift the spectrum of graphene plasmons and reduce their lifetime [6]. We therefore have the high sensitivity of graphene being both a celebrated element of its two-dimensional structure and as the part of its nature that is hardest to control. In this thesis, we attempt to uncover some of the effects of random height fluctuations in the structure of the graphene sheet and the underlying substrate that the carbon nano-structure is frequently grown on.

1.3 Outline of Thesis

The purpose of this thesis is to investigate the behaviour of graphene plasmons in two different contexts: one context uses them as a method of energy absorption that can be detected via spectroscopic analysis, and the other context considers graphene plasmons as self-excited modes on the surface that are solutions to electromagnetic boundary conditions. The objective of our first investigation is to determine a semi-classical equation for the optical conductivity of graphene in an energy region that covers two separate regimes of spectroscopic experiments, and to test our theory by comparing it to experimental results. Our second objective is to arrive at a reasonable description of the effect that rough surfaces have on the plasmonic and structural nature of graphene.

Chapter 2 begins this thesis with an explanation of the electromagnetic background necessary to describe plasmons in later chapters, including Maxwell's equations, boundary conditions, the quasi-static approximation, the equations for s- and p- polarized light reflecting from an interface, and the dispersion equation for graphene plasmons on an interface. Results from this chapter are used later to experimentally verify our model for graphene conductivity by comparing it with ellipsometry, which measures changes in light polarization to extract information about a material. We also use this chapter to understand the bound, oscillatory nature of plasmons on an interface which dominates the theory behind Chapter 5.

Chapter 3 is an introduction into the electronic properties of graphene we will be using throughout the thesis. This chapter highlights the relevance of graphene's two-dimensional nature, the linear energy dispersion relation for low frequencies in graphene, the universal absorbance of light in this low energy regime due to the photon-like nature of graphene quasi-particles, the Random Phase Approximation (RPA), Fermi Liquid theory, the phase space of excitations, the resonant frequencies in graphene at different energies and the applicability of a two-fluid two-dimensional hydrodynamic model to describing graphene at higher energies. Results from this chapter have their application throughout the thesis, with the hydrodynamic model combined with the universal absorbance of light composing the two-dimensional conductivity we compare to our experimental spectroscopic results, and the RPA approximation yielding equations for the conductivity we use for low energies to analyze the effective dispersion relation for a rough surface.

Chapter 4 delves into one of our two objectives; it contains the necessary equations relating the functions describing graphene's polarizability to parameters that can be exper-

imentally measured. This includes a derivation of the energy loss of inelastically scattered electrons, and a phenomenological fit to the energy loss data. We then use our fitting parameters, now inserted into the conductivity of the graphene, to check the region of low energy probed by ellipsometry. We test ideas like contamination and rippling of the graphene to help explain our results, then use the f-sum rule to justify some of our findings.

Chapter 5 is broken in two parts. The first deals with the mathematical and physical underpinnings of stochastic methods and rough surfaces. We look at ways to describe roughness, and test out both theoretical and experimental results that justify our treatment of graphene as a stochastically rippled surface. The second part of the chapter inputs these results into three different methods for determining the effect of roughness on the plasmon dispersion relation, which relates the wavenumber to the frequency of a plasmon constrained to the surface. These methods use a combination of Green's functions, potentials as solutions to Laplace's and Poisson's equations, and a smoothing method that allows us to deal analytically with the stochastic variables. Some numerical results are shown to present predictions that the methods make.

Chapter 6 closes out the thesis with a brief summary of the work performed within the thesis and future work that can be undertaken in this burgeoning field.

Chapter 2

Electromagnetic Theory and Plasmons

2.1 Maxwell's Equations

A proper understanding of the nature of plasmons, and how they exhibit themselves on a graphene sheet, necessitates a thorough understanding of electromagnetic (EM) theory. Analysis of graphene's opto-electronic properties requires a theory that describes both the physical matter of the material and the fields that fluctuate near it. We begin with Maxwell's equations, which describe macroscopically the electromagnetic effect of several charges and fields. Although we are dealing with nano-structures throughout the paper, we are justified in using the classical framework as the materials we investigate have a high density of free charge carriers, yielding an almost continuous spectrum of electron energy levels [25]. The equations are below, with boldface representing vector quantities in 3D space.

$$\nabla \cdot \mathbf{D} = \rho_{ext} \tag{2.1}$$

$$\nabla \times \mathbf{E} = -\frac{\partial \mathbf{B}}{\partial t} \tag{2.2}$$

$$\nabla \cdot \mathbf{B} = 0 \tag{2.3}$$

$$\nabla \times \mathbf{H} = \mathbf{J}_{ext} + \frac{\partial \mathbf{D}}{\partial t} \tag{2.4}$$

where, under the assumptions of linear, isotropic and non-magnetic materials, $\mathbf{D} = \epsilon\epsilon_0\mathbf{E}$ and $\mathbf{B} = \mu\mu_0\mathbf{H}$, ϵ and μ are the relative permittivities that characterize the response of a given material to electric and magnetic fields respectively, ϵ_0 and μ_0 are the vacuum dielectric and magnetic permittivities, ρ_{ext} is the external charge density, $\mathbf{J}_{ext}$ is the external current density, $\mathbf{D}$ is the electric displacement vector, $\mathbf{H}$ is the magnetizing field, $\mathbf{B}$ is the magnetic field and $\mathbf{E}$ is the electric field. Throughout the text we assume $\mu = 1$, meaning our materials are not magnetizable. These equations in general are both spatially and time dependent. The relationship between what we label 'external' and 'internal' variables has a clear physical distinction: external contributions (e.g. from incident light) drive a system, and anything labeled as internal (e.g. charge density of electrons bound to ions in a dielectric) respond to these stimuli.

Equation 2.1 is of special note in the discussion of plasmonic effects: $\mathbf{D}(\mathbf{r}, t)$ is known as the electric displacement, the electric field induced by free charges i.e. ones not bound to any material. Contributions to this vector quantity only include external stimuli and not

the internal charge density (see the first Maxwell's equation Eq. 2.1). Given that plasmons are collective modes, or oscillations, of free particles inside or on the surface of a material, this quantity $\mathbf{D}(\mathbf{r},t)$, and more specifically the constitutive dielectric function $\epsilon(\mathbf{r},t)$ that relates it to the electric field $\mathbf{E}(\mathbf{r},t)$, are the main scope of our forays into electromagnetic theory.

The other constitutive relation that will receive much attention in the coming chapters is the relation between internal current density and the electric field. The two equations we will focus on are therefore:

$$\mathbf{J}_{int}(\mathbf{r},t) = \int d\mathbf{r}'dt'\sigma(\mathbf{r}-\mathbf{r}',t-t')\mathbf{E}(\mathbf{r}',t') \tag{2.5}$$

$$\mathbf{D}(\mathbf{r},t) = \epsilon_0 \int d\mathbf{r}'dt'\epsilon(\mathbf{r}-\mathbf{r}',t-t')\mathbf{E}(\mathbf{r}',t') \tag{2.6}$$

where the response function $\sigma(\mathbf{r},t)$ is called the electrical conductivity of the material. Since the materials we are investigating (e.g. graphene, glass and dielectrics) are media with very little temporal or spatial dispersion, and are linear media (the photons are not absorbed in harmonic generation processes), we are justified in assuming response functions constitute these relations. Transforming the relations via Fourier transforms $\int dtd\mathbf{r}e^{-i(\mathbf{k}\cdot\mathbf{r}-\omega t)}(\cdots)$ breaks our EM fields into plane wave components

$$\mathbf{J}_{int}(\mathbf{k},\omega) = \sigma(\mathbf{k},\omega)\mathbf{E}(\mathbf{k},\omega) \tag{2.7}$$

$$\mathbf{D}(\mathbf{k},\omega) = \epsilon_0\epsilon(\mathbf{k},\omega)\mathbf{E}(\mathbf{k},\omega) = \epsilon_0\mathbf{E}(\mathbf{k},\omega) + \mathbf{P}(\mathbf{k},\omega) \tag{2.8}$$

where $\mathbf{P}(\mathbf{k},\omega)$ is defined as the polarization field in the macroscopic Maxwell's equations. The link between the dielectric function and the conductivity is given by $\mathbf{J}_{int} = \frac{\partial}{\partial t}\mathbf{P}$, the definition of the internal current density. In frequency space, this yields the so-called dielectric response function

$$\epsilon(\mathbf{k},\omega) = 1 + \frac{i\sigma(\mathbf{k},\omega)}{\epsilon_0\omega} \tag{2.9}$$

This relation is only valid in three dimensions when $\mathbf{J}$ represents the current density. We will see how this relation changes in two dimensions (see Appendix 2).

The inclusion of the wavenumber $\mathbf{k}$ in these equations implies a spatially non-local response. However, by the same line of reasoning as that we used to justify Maxwell's equations, we may say that the wavelengths of the light waves and plasmon waves we investigate are much longer than the size of graphene's Brillouin zone or the mean free path of electrons in a metal, for example. Therefore, many of our derivations will include only a frequency ω response by considering the so-called optical limit of $\mathbf{k} \to 0$ (see Eq. 3.22). More advanced models for the polarization of materials (related again to the conductivity and the dielectric function), like the Random Phase Approximation (RPA), and the consideration of plasmons in waveguides [17] keep this non-locality. We will be using these relations often in the rest of the text.

2.1.1 Wave Equation and Boundary Conditions

Any system of PDEs, including Maxwell's equations above, must be implemented physically with the use of boundary conditions. It is well known that free space EM waves exhibit transverse behaviour, with oscillating electric and magnetic fields oriented perpendicular to the direction of motion of the light wave. Changing the medium to a dielectric affords

the possibility of longitudinal waves, also known as 'volume plasmons', where the EM fields oscillate parallel to the wave propagation direction. Labeling plasmons and collective oscillations as 'waves' is no accident. Combining Eqs. 2.2 and 2.4 with $\mathbf{J}_{ext} = 0$ yields

$$\nabla \times \nabla \times \mathbf{E} = -\mu_0 \frac{\partial^2 \mathbf{D}}{\partial t^2} \tag{2.10}$$

This equation can be simplified using the identities $\nabla \times \nabla \times \mathbf{E} = \nabla(\nabla \cdot \mathbf{E}) - \nabla^2 \mathbf{E}$, $\epsilon \nabla \cdot \mathbf{E} = \nabla \cdot (\epsilon \mathbf{E}) - \mathbf{E} \cdot \nabla \epsilon$, the Maxwell's equation $\nabla \cdot \mathbf{D} = 0$ if there is no external stimulation, and $\nabla \epsilon \approx 0$ for local dielectric profiles, yielding

$$\nabla^2 \mathbf{E}(\mathbf{r}, t) - \frac{\epsilon}{c^2} \frac{\partial^2 \mathbf{E}(\mathbf{r}, t)}{\partial t^2} = 0 \text{ or } \nabla^2 \mathbf{E}(\mathbf{k}, \omega) + k_0^2 \epsilon \mathbf{E}(\mathbf{k}, \omega) = 0 \tag{2.11}$$

as the speed of light $c = 1/\sqrt{\epsilon_0 \mu_0}$ and $k_0 = \omega/c$. This is exactly the wave equation, and it provides us some insight into the behaviour of these plasmons. The same equation holds for the magnetic field $\mathbf{H}$ under the same assumptions with $\mu = 1$ [37], giving

$$\nabla^2 \mathbf{H}(\mathbf{k}, \omega) + k_0^2 \mathbf{H}(\mathbf{k}, \omega) = 0. \tag{2.12}$$

The special behaviour occurs at the interfaces. Collective oscillations constrained to the edge of the material result because of the change of medium, and they are known as 'surface plasmons'. These exist as eigenmodes of the wave equation with the boundary conditions of the system, and can also be maintained without external excitation.

The boundary conditions at a flat planar interface [56] involve the continuity of the fields found in Maxwell's equations, with either transverse or normal components being continuous depending on whether the relation is the curl or the divergence of the field.

$$\mathbf{E}_{2t} = \mathbf{E}_{1t} \tag{2.13}$$
$$\mathbf{H}_{2t} - \mathbf{H}_{1t} = \mathbf{J}_s \times \hat{\mathbf{n}} \tag{2.14}$$
$$D_{2n} - D_{1n} = \rho_s \tag{2.15}$$
$$B_{2n} = B_{1n} \tag{2.16}$$

with normal, tangential (in-plane) and surface indices shown. $\mathbf{J}_s$ is the surface current density, ρ_s is the surface charge density, and the vector $\hat{\mathbf{n}}$ points in the $\hat{z}$ direction, perpendicular to the surface. For graphene, our charge carriers are electrons and holes, oscillating in response to these fields.

Mathematically, graphene will be treated as a two-dimensional material, and therefore will only ever appear in the boundary conditions of our problem. For a system where no other charges are present, $\rho_{ext} = \rho_s \delta(z)$ for a graphene sheet in the xy-plane. We will see later on that the definitions of normal or transverse components become skewed when working on rough (i.e. not flat) surfaces, and therefore require adapted boundary conditions.

2.1.2 Electrostatic and Quasi-static Approximations

Although the full Maxwell's equations describe the entirety of classical electrodynamics on the macroscopic scale, they can be hard to work with and solve, especially with the implementation of boundary conditions. We must frequently then make approximations suitable to the system in question. We briefly consider two of these.

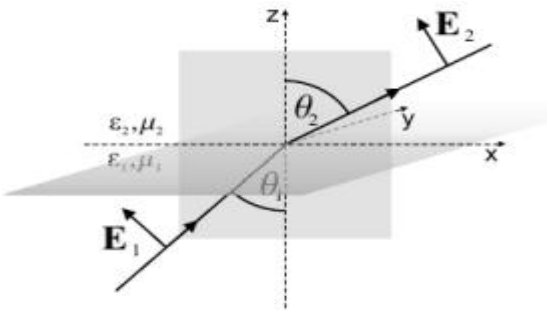

Figure 2.1: Interface between two dielectric media ϵ_1, ϵ_2. The electric field shown here is along the plane of incidence, and is known as either p-polarized or transverse magnetic (TM). If the magnetic field is along the plane of incidence, the wave is called s-polarized or transverse electric (TE). Along with the transmitted wave is a reflected wave with the same angle θ_1 in medium 1. Adapted from [47]

The electrostatic approximation makes an assumption that the magnetic field (and hence any electric currents, via Eq. 2.2) must not vary in time quickly. In equation form,

$$\vec{\nabla} \times \mathbf{E} = \frac{\partial \mathbf{B}}{\partial t} = 0 \tag{2.17}$$

Since the electric field is now irrotational, we may derive Poisson's equation for the electrostatic potential ϕ in this limit, while using Eq. 2.1 and the assumption of a homogenous medium with constant ϵ:

$$\mathbf{E} = -\vec{\nabla}\phi \tag{2.18}$$

$$\nabla \cdot (\epsilon \mathbf{E}) = \frac{\rho_{ext}}{\epsilon_0} \tag{2.19}$$

$$\epsilon \nabla^2 \phi = -\frac{\rho_{ext}}{\epsilon_0}. \tag{2.20}$$

This statement derives from the previous two. We arrive at a homogenous equation by setting $\rho_{ext} = 0$, so that Eq. 2.20 becomes

$$\nabla^2 \phi = 0, \tag{2.21}$$

giving us Laplace's equation. The boundary conditions at an interface can also be expressed in terms of the potential ϕ. Assuming media with dielectric constants ϵ_1, ϵ_2,

$$\phi_1|_{z=0} = \phi_2|_{z=0} \tag{2.22}$$

$$\epsilon_1 \frac{\partial}{\partial z}\phi_1|_{z=0} - \epsilon_2 \frac{\partial}{\partial z}\phi_2|_{z=0} = \frac{\rho_s}{\epsilon_0} \tag{2.23}$$

where ρ_s is non-zero if there is a charge density lying on the surface. This is a curious situation where we are able to assume zero charge density anywhere and can therefore use Laplace's equation, and yet in the boundary condition we will be able to put a graphene sheet that has many charge carriers. Such idealized situations occur frequently in theoretical treatments of physical problems.

We make note that, due to Maxwell's third equation Eq. 2.3, the $\mathbf{B}$ field is *only* rotational, and can therefore be expressed as a curl of a vector potential $\mathbf{B} = \nabla \times \mathbf{A}$, regardless of any approximation.

The second approximation, known as the quasi-static regime, is similar in scope to the electrostatic case. If we are working with charged particles (e.g. electrons) moving near the speed of light in our materials, and we have time-varying fields, there is a delayed response, and the field experienced by an observer at a point will be at a retarded time. As this time changes depending on the location of the charged objects causing the time-varying field, this results in a very complex equation. The problem can be reformulated in terms of a retarded potential

$$\phi(\vec{r}, t) = \frac{1}{\epsilon_0} \int \frac{\rho_{ext}(\vec{r}', t_r)}{|\vec{r} - \vec{r}'|} d^3\vec{r}' \text{ for } t_r = t - \frac{|\vec{r} - \vec{r}'|}{c} \tag{2.24}$$

but within the quasi-static regime can be formulated as

$$\phi_{quasi}(\vec{r}, t) = \frac{1}{\epsilon_0} \int \frac{\rho_{ext}(\vec{r}', t)}{|\vec{r} - \vec{r}'|} d^3\vec{r}'. \tag{2.25}$$

The difference from the electrostatic regime is that now the equation for the electric field will be allowed to depend on the time-varying magnetic field (i.e. the time varying vector potential). This therefore yields

$$\mathbf{E} = -\vec{\nabla}\phi - \frac{\partial \mathbf{A}}{\partial t}, \qquad \mathbf{B} = \nabla \times \mathbf{A} \tag{2.26}$$

for vector potential

$$\mathbf{A}_{quasi}(\vec{r}, t) = \mu_0 \int \frac{\mathbf{J}_{ext}(\vec{r}', t)}{|\vec{r} - \vec{r}'|} d^3\vec{r}', \tag{2.27}$$

derivable by the same method as that for the scalar potential ϕ.

Both of these approximations rely on a system staying close enough to equilibrium that the charge movement is either negligible (electrostatic) or non-retarded (quasi-static). As long as the velocities considered are much slower than light speed, these approximations should be valid.

2.1.3 Reflection Coefficients with a Graphene Sheet

One useful tool we will need in our future calculations is the modified version of Fresnel's equations, which describe the amount of reflected and transmitted light that an incident wave separates into at a planar interface. Given that two of Maxwell's equations and two boundary conditions deal with fields perpendicular to the interface, it is always possible to determine the reflectance and transmission given information about the angle of incidence (to determine the relative size of the x- and z- components) and the dielectric functions of the two media.

Consider first the case of p-polarization, where the magnetic field lies in the y-direction. Using the wave equation we derived in Eq. 2.12, we can write our fields in media $1, 2$ (see Figure 2.1) as

$$H_{1y} = (a_1 e^{i\kappa_{1z} z} + b_1 e^{-i\kappa_{1z} z}) e^{ik_{1x} x} \tag{2.28}$$

$$H_{2y} = (a_2 e^{i\kappa_{2z} z} + b_2 e^{-i\kappa_{2z} z}) e^{ik_{2x} x} \tag{2.29}$$

for $\kappa_{iz} = (\sqrt{\epsilon_i}\omega/c)\cos(\theta_i)$ and $k_{ix} = (\sqrt{\epsilon_i}\omega/c)\sin(\theta_i)$. These waves follow the assumption that there is no spatial propagation in the y-direction, which can be made so given a judicious choice of coordinates and the dispersion-less media. We consider Eqs. 2.13 and 2.14 from above, which read as

$$\hat{n} \times (\mathbf{E}_2 - \mathbf{E}_1)|_{z=0} = 0, \qquad \hat{n} \times (\mathbf{H}_2 - \mathbf{H}_1)|_{z=0} = \mathbf{J}_s. \tag{2.30}$$

The equation for the $\mathbf{E}$ field can be extracted via Eq. 2.4:

$$\frac{\partial}{\partial t}(\epsilon_0 \epsilon_i \mathbf{E}_i) = \nabla \times \mathbf{H}_i \longrightarrow \mathbf{E}_i = \frac{1}{i\omega\epsilon_0\epsilon_i}\nabla \times \mathbf{H}_i, \tag{2.31}$$

recalling that the current density $\mathbf{J}_s$ is restricted to the graphene sheet in the xy-plane, and therefore only appears in the boundary conditions. The equation for the current density $\mathbf{J}_s$ can be found using the constitutive relation $J_x = \sigma E_x|_{z=0}$ at the point $z = 0$, where the x-component of the electric field is

$$E_x|_{z=0} = \frac{\kappa_{2z}(a_2 - b_2)}{\epsilon_0\epsilon_2\omega} e^{ik_{1x}x} \tag{2.32}$$

by combining Eqs. 2.29 and 2.31. Noting that $k_{1x} = k_{2x}$ based on wavenumber conservation at the interface, the boundary conditions become:

$$\frac{\kappa_{1z}}{\epsilon_1}(a_1 - b_1) - \frac{\kappa_{2z}}{\epsilon_2}(a_2 - b_2) = 0 \tag{2.33}$$

$$(a_1 + b_1) - (a_2 + b_2) = J_x = \frac{\sigma\kappa_{2z}}{\epsilon_0\epsilon_2\omega}(a_2 - b_2), \tag{2.34}$$

or, in matrix form:

$$\begin{bmatrix} a_1 \\ b_1 \end{bmatrix} = \frac{1}{2}\begin{bmatrix} 1 + \frac{\epsilon_1\kappa_{2z}}{\epsilon_2\kappa_{1z}} + \frac{\sigma\kappa_{2z}}{\epsilon_0\epsilon_2\omega} & 1 - \frac{\epsilon_1\kappa_{2z}}{\epsilon_2\kappa_{1z}} - \frac{\sigma\kappa_{2z}}{\epsilon_0\epsilon_2\omega} \\ 1 - \frac{\epsilon_1\kappa_{2z}}{\epsilon_2\kappa_{1z}} + \frac{\sigma\kappa_{2z}}{\epsilon_0\epsilon_2\omega} & 1 + \frac{\epsilon_1\kappa_{2z}}{\epsilon_2\kappa_{1z}} - \frac{\sigma\kappa_{2z}}{\epsilon_0\epsilon_2\omega} \end{bmatrix}\begin{bmatrix} a_2 \\ b_2 \end{bmatrix} = M^{(p)}\begin{bmatrix} a_2 \\ b_2 \end{bmatrix}. \tag{2.35}$$

This is known as the transfer matrix of the problem [60], and can be compounded to yield the reflection and transmission emanating from many layers (see Eq. 4.24). For our purposes, $b_2 = 0$, so the reflectance coefficient for p-polarized light, defined as the ratio of the reflected light coefficient to the incident, is $r_p = M_{21}^{(p)}/M_{11}^{(p)} = b_1/a_1$, given that a_1 is the coefficient of the wave in medium 1 traveling in the $+z$ direction, and b_1 corresponds to $-z$ movement. The transmission coefficient, defined as the ratio between a_2 and a_1, is $t_p = 1/M_{11}^{(p)}$, and defines the 'amount' of light that passes through the material.

The case of s-polarization is similar, with electric fields now oscillating parallel to the y-axis. We choose E_{1y} and E_{2y} to have the same expression as H_{1y} and H_{2y} from Eqs. 2.28 and 2.29, as the two satisfy a similar wave equation (Eq. 2.11). Now to obtain our form for $\mathbf{H}$, we use Eq. 2.2:

$$-\frac{\partial}{\partial t}(\mu_0 \mathbf{H}_i) = \nabla \times \mathbf{E}_i. \tag{2.36}$$

Meanwhile, we have the current $\mathbf{J}_s = J_y\hat{y} = (a_2 + b_2)\sigma e^{ik_{2x}x}\hat{y}$, as it must always parallel to the electric field. This gives boundary conditions for s-polarization of

$$(a_1 + b_1) - (a_2 + b_2) = 0 \qquad \frac{\kappa_{1z}}{\mu_0\omega}(a_1 - b_1) - \frac{\kappa_{2z}}{\mu_0\omega}(a_2 - b_2) = \sigma(a_2 + b_2) \tag{2.37}$$

and an s-polarization transfer matrix of

$$M^{(s)} = \frac{1}{2}\begin{bmatrix} 1+\frac{\kappa_{2z}}{\kappa_{1z}}+\frac{\sigma\mu_0\omega}{\kappa_{1z}} & 1-\frac{\kappa_{2z}}{\kappa_{1z}}+\frac{\sigma\mu_0\omega}{\kappa_{1z}} \\ 1-\frac{\kappa_{2z}}{\kappa_{1z}}-\frac{\sigma\mu_0\omega}{\kappa_{1z}} & 1+\frac{\kappa_{2z}}{\kappa_{1z}}-\frac{\sigma\mu_0\omega}{\kappa_{1z}} \end{bmatrix}. \tag{2.38}$$

Once again, the reflectance for this polarization is $r_s = M_{21}^{(s)}/M_{11}^{(s)}$, and the transmission is $t_s = 1/M_{11}^{(s)}$. We have observed in this derivation the use of many of the assumptions we had earlier mentioned; the macroscopic view of both Maxwell's equations, giving us the wave equation, and the locality assumptions that give us local dielectric functions ϵ_1, ϵ_2.

In the special case of $\epsilon_1 = \epsilon_2 = 1$ (suspended graphene) and $\theta_1 = \theta_2 = 0$, our expression for the transmission $t = t_p = t_s$ becomes

$$t = \frac{1}{\frac{1}{2}(1+(1)+\frac{\sigma k_z}{\epsilon_0\omega})} \approx 1 - \frac{1}{4\pi\epsilon_0}\left(\frac{2\pi\sigma k}{\omega}\right) = 1 - \frac{1}{4\pi\epsilon_0}\left(\frac{2\pi\sigma}{c}\right) \tag{2.39}$$

as $k_z = k = \omega/c$. The actual transmittance of light is given by $T = |t|^2$ for the zero incidence angle in a free medium, and gives the fraction of the power that passes into the medium. To first order in σ, we obtain [12]

$$T = |t|^2 = 1 - 2\frac{1}{4\pi\epsilon_0}\frac{2\pi}{c}\Re\sigma(\omega) \text{ and therefore } 1 - T = A = \frac{1}{4\pi\epsilon_0}\frac{4\pi}{c}\Re\sigma(\omega) \tag{2.40}$$

where we have listed the absorbance A and its proportionality to the conductivity of graphene, which we have chosen in the optical limit to reflect our other assumptions about locality.

Analyzing the reflectance of light and radiation off of various materials is the basis of ellipsometry, an experimental technique that will allow us to probe graphene at a low frequency level with high precision. Since graphene is a two-dimensional material, we do not expect energy losses to come from penetration inside it (unlike a metal, which exhibits near perfect reflection). We will see the largest effect of the graphene when the conductivity σ is the largest e.g. when the electrons are moving collectively. This happens closest to the plasmon resonance, a topic we will now investigate.

2.2 Plasmons

We have mentioned before about plasmons being charge oscillations: when charges are moving to try and screen an electric field, they tend to overshoot and are hence pulled back by the charge disturbance, which causes an oscillation [21]. What makes surface plasmons so fascinating is their constraint to the interface between two media, and the experimental ability to manipulate them to induce resonance for sensors or cause extreme charge accumulations. However, we must first find out under what conditions these plasmons exist, be it for graphene on the surface of our interface or not.

2.2.1 EM Equations for Plasmons at an Interface

It has been stated that for a planar interface, we can consider no spatial propagation in the y-direction, leaving us with two possibilities: the s- and p- polarized modes. To find the relationship between the frequency and wavenumber of our plasmon, we need to consider solutions to the wave equation that both satisfy the boundary condition and decay away

from the surface for fields perpendicular to the planar interface. p-polarization means that only the E_x, E_z and H_y will be non-zero in media $m = 1, 2$. Motivated by the wave equation in Eq. 2.12 and following the same logic as in Eqs. 2.28 and 2.29 for p-polarized waves, we write our vectors in the form [4]

$$\mathbf{E}_m = (E_{m,x}, 0, E_{m,z})e^{ik_x x}e^{-\kappa_{mz}|z|} \tag{2.41}$$

$$\mathbf{H}_m = (0, H_{m,y}, 0)e^{ik_x x}e^{-\kappa_{mz}|z|} \tag{2.42}$$

noting that $k_x = k_{1x} = k_{2x}$ due to conservation of the wavenumber over the interface, and that $z = 0$ is the boundary between the two media in the xy-plane. We also note that, in order to have a surface plasmon, the wavenumbers κ_{1z}, κ_{2z}, the components of the wavevector perpendicular to the interface, must have positive real parts so that the waves decay away from the surface. This feature of the localization of plasmons to the surface is especially useful in applications, as it not only shows the high efficiency of energy transfer within the medium but it also meets the demand of modern electronics to have small, non-interacting components with fast response times and strong fields. Research into waveguides for opto-electronic applications is an area of development where these local plasmons find their groove [59].

The coefficients $E_{m,x}, E_{m,z}$ and $H_{m,y}$, along with the frequency dispersion relation, can now be determined via Maxwell's equations and the boundary conditions at the interface. Using Eqs. 2.2 and 2.4, using the fact that $\mathbf{J}_{ext} = 0$ for our system, gives

$$(-1)^m \kappa_{mz} E_{m,x} - ik_x E_{m,z} = i\omega\mu_0 H_{m,y} \tag{2.43}$$

$$(-1)^{m+1} \kappa_{mz} H_{m,y} = -i\omega\epsilon_0\epsilon_m E_{m,x} \tag{2.44}$$

$$ik_x H_{m,y} = -i\omega\epsilon_0\epsilon_m E_{m,z} \tag{2.45}$$

using the appropriate Fourier transforms. Solving this system of three equations gives

$$E_{m,x} = i\frac{\kappa_{mz}}{\omega\epsilon_0\epsilon_m} H_{m,y}(-1)^{m+1} \tag{2.46}$$

$$E_{m,z} = -\frac{k_x}{\omega\epsilon_0\epsilon_m} H_{m,y} \tag{2.47}$$

$$\kappa_{mz}^2 = k_x^2 - \epsilon_m \frac{\omega^2}{c^2}. \tag{2.48}$$

If we wish to consider the effect that graphene has on the plasmons at the interface, we use the boundary conditions just as in Section 2.1.3, so that Eqs. 2.13 and 2.14 give, respectively,

$$H_{1,y} = -\frac{\kappa_{2z}\epsilon_1}{\kappa_{1z}\epsilon_2} H_{2,y} \tag{2.49}$$

$$H_{2,y} - H_{1,y} = \sigma E_{1,x}, \tag{2.50}$$

where σ is defined via a constitutive relation as in Eq. 2.34. Combining the above two equations, along with Eq. 2.46, yields

$$\frac{\epsilon_1}{\kappa_{1z}} + \frac{\epsilon_2}{\kappa_{2z}} + \frac{i\sigma}{\epsilon_0\omega} = 0, \tag{2.51}$$

which is the dispersion relation for plasmons on a graphene sheet between two media with dielectric functions $\epsilon_{1,2}$ when used in tandem with Eq. 2.48. We now consider two limiting

cases of this equation, the first being the case of no graphene. Our dispersion relation is then

$$\frac{\kappa_{2z}}{\kappa_{1z}} = -\frac{\epsilon_2}{\epsilon_1}. \tag{2.52}$$

This expression reveals one very unique property of surface plasmons at the interface without graphene - they will only exist between two materials with dielectric functions with oppositely signed real parts. Materials with dielectric functions with positive real part include materials with not too many free electrons (e.g. air, glass), so that an applied electric field moves charges along with it. The opposite is the case for metals and conductors, whose free electrons oscillate oppositely out of phase with the driving electric field, causing high reflectivity. The oscillation of these plasmons is therefore usually exhibited at air/metal or glass/metal planar setups.

Combining Eq. 2.52 with Eq. 2.48 gives a plasmon dispersion for p-polarization modes for this limiting case as

$$k_x = k_0 \sqrt{\frac{\epsilon_1 \epsilon_2}{\epsilon_1 + \epsilon_2}}, \tag{2.53}$$

which relates the frequency (through $k_0 = \omega/c$) to the wavenumber of the collective oscillation (the plasmon).

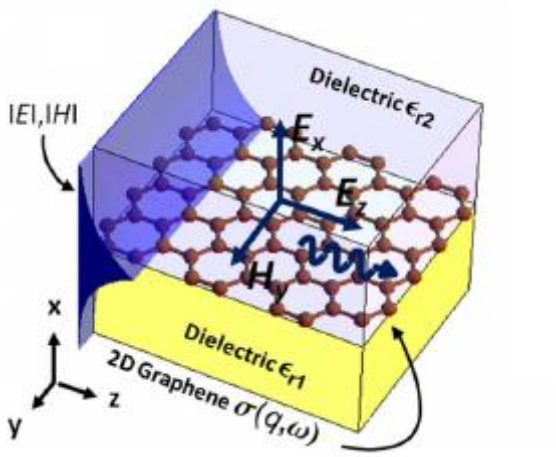

Figure 2.2: Propagation of plasmon on a two-dimensional graphene lattice. The coupled EM wave is *p*-polarized in this diagram and the decay of the electric field perpendicular to the interface shows that the plasmon is a localized mode. Adapted from [24]

It is of note that although we are dealing with electron oscillations, we have been working in the framework of electromagnetism, and our solution for this 'plasmon' is exactly a photon wave. The reason for this is the strong coupling between the electron modes and the photon that follows them. The collective quasi-particle is known as a surface plasmon polariton. The behaviour of the plasmon polariton varies greatly with wavenumber, with high wavelengths yielding light-like oscillations, while low ones become almost electrostatic in their scope. We will see later on that we can treat the plasmon's electronic fluctuations via a different model than the electrodynamic one, namely a hydrodynamic model, treating the moving particles in the graphene as a fluid flow.

Our interest in later chapters will focus on the surface plasmon, the limiting case of a surface plasmon polariton where k_x, our wavenumber, is far below the light-line $\omega = ck_x$,

giving it an electrostatic character, the opposite of the light-like behaviour one would see for photon-coupled propagation. To see deeper why this is the case, a plasmon that is fully constrained to the surface yields a system that satisfies Laplace's equation, due to the lack of outward damping giving potentials outside the surface. Wave solutions for the plasmon that satisfy Laplace's equation, just as in Eqs. 2.41 and 2.42, will have the form

$$\begin{aligned} \phi(z) &= A_2 e^{ik_x x} e^{-\kappa_{2z} z} & z < 0 \quad (2.54) \\ \phi(z) &= A_1 e^{ik_x x} e^{\kappa_{1z} z} & z > 0, \quad (2.55) \end{aligned}$$

where we have mentioned that $k_x = k_{1x} = k_{2x}$ to satisfy Laplace's equation properly. Due to continuity of ϕ at $z = 0$ and continuity of $\epsilon \partial\phi/\partial z$ at $z = 0$, we have $A_1 = A_2$ as well as

$$\epsilon_1 + \epsilon_2 = 0. \quad (2.56)$$

Plugging this into Eq. 2.53 shows that $k_x \to \infty$ for these surface plasmons that behave electrostatically.

Our second limiting case will be that where graphene is between two media with dielectric function $\epsilon = \epsilon_m$, so the plasmon dispersion in Eq. 2.51 becomes

$$1 + i\frac{\sigma}{2\omega\epsilon\epsilon_0}\sqrt{k_x^2 - \epsilon\frac{\omega^2}{c^2}} = 0. \quad (2.57)$$

We are interested in the equivalent limit in the case of no graphene, $k_x \to \infty$, for surface plasmons on graphene. This will be the case of $k_x^2 \gg \epsilon\omega^2/c^2$, where the plasmon behaves less like a photon of the form $\omega \sim k_x$ and instead takes on a quasi-static character. For this dispersion relation to be valid, the imaginary component of the conductivity must be positive, which in graphene occurs, as we will see later, for the intraband component of the conductivity σ_D from Eq. 3.28. Eq. 2.51 now becomes, in this limit,

$$1 + i\frac{ie^2 E_F}{\pi\hbar^2\omega}\frac{1}{2\omega\epsilon\epsilon_0}k_x = 0 \longrightarrow \omega^2 = \frac{e^2 E_F}{\pi\hbar^2 2\epsilon\epsilon_0}k_x \quad (2.58)$$

Putting this equation for ω^2 into the limit $k_x^2 \gg \epsilon\omega^2/c^2$ required for quasi-static surface plasmon behaviour gives

$$\frac{k_x}{k_F} \gg \frac{2v_F}{c^2}\frac{e^2}{4\pi\hbar\epsilon_0} = \frac{2v_B v_F}{c^2} \quad (2.59)$$

where v_B is known as the Bohr velocity, and v_F and k_F are the Fermi velocity and Fermi wavenumber defined in Eq. 3.1 and 3.13. The importance of this equation is that it justifies our use of both the quasi-static approximation in graphene and what we later call the optical limit in Eq. 3.22, as our restriction of $k_x \to \infty$ is lifted in favour of Eq. 2.59.

Our focus has been on *p*-polarized modes and not *s*-polarized modes for two reasons. The first is that it can be shown [37] that for the interface without graphene, plasmons do not exist for this polarization. The presence of the graphene changes this, but the strength of such plasmons is limited by the region where the graphene conductivity is negative, which only occurs in special circumstances in a limited region [4].

One thing we will observe is that the resonance frequencies that cause collective oscillations in graphene are much lower than those for most dielectric substrates that graphene rests near. Therefore, concerns about interference or combinations of plasmon modes are unwarranted, and approximating our dielectric functions as being purely real is justified at low enough frequencies [24].

A final note about plasmons and the equations above goes as follows: generally in problems involving waves, imaginary parts correspond to oscillations and real parts to damping. The dispersion equation in Eq. 2.53 for p-polarized waves implies, if ϵ_1, ϵ_2 are entirely real, a plasmon without damping that is forever constrained to the surface. In reality, however, these dielectric functions have delayed reactions to incident fields, represented by them having an imaginary part. The imaginary part will therefore also appear in the wavenumbers, causing the z-components of the electromagnetic waves to oscillate into space and lose energy. Much of the future of applications of plasmonics, including those portending to graphene, relies on the maintenance of strong excitations over long distances for extended time periods, a goal made difficult by the lack of coherency in the dielectric response. Graphene as a tool magnifies plasmons to a great degree, hence its interest for plasmonics and our research in this thesis.

Chapter 3

Electronic Properties of Graphene

This chapter encapsulates the very broad category of electron interactions, which covers all interactions of electrons (and holes) with light and matter. For low energies, where interaction with light is strong, graphene's optical properties become of interest. Graphene plasmonics, a main branch of this research, seeks to explore the theory and applications of localized collective oscillations for a graphene sheet. The main reasons why graphene plasmonics is a blossoming field are due to the material's strongly responsive electrons, its linear band-structure, and its strong electronic tunability due to doping and gating. At higher-energies, optical exploration of graphene's structure is no longer viable, but fast-incident electrons still couple with other electrons in graphene and probe the modes at these energies, which is the basis of the experimental technique of Electron Energy Loss Spectroscopy. This chapter seeks to briefly explore how these properties come about and why they can be used in our research for plasmon and electron interactions. For the remainder of the chapter, we switch to Gaussian electrostatic units, where $4\pi\epsilon_0 = 1$.

3.1 Atomic and Band Structure

Graphene is a honeycomb lattice made up of sp^2-hybridized carbon atoms arranged in a 2-dimensional structure. Three evenly spaced σ-bonds are in-plane, while a delocalized π bond, the main contributor to the conductivity of the graphene lattice, lies perpendicular to the sheet. Both the unit cell and the reciprocal cell are rhombuses, the direct lattice being composed of two overlapping triangular lattices (labeled by A,B). The spacing between the carbon atoms is approximately 0.142 nm, and with the high electron density of these atoms, classical electromagnetic theory will work well here.

Labeled in the reciprocal lattice in Figure 3.1 are four key 'symmetry' points, that either represent saddle points in the energy dispersion or self-crossings. The point M will be important later, as transitions in the UV region of the EM spectrum occur between π and π^* energy bands that occur at this point. The point Γ has an even larger difference in its states, and transitions at this point will occur for very high energies reachable by Electron Energy Loss Spectroscopy (EELS), an experimental method we will investigate in later chapters. Fig. 3.2 shows the band structure and the relevant Fermi surface for graphene.

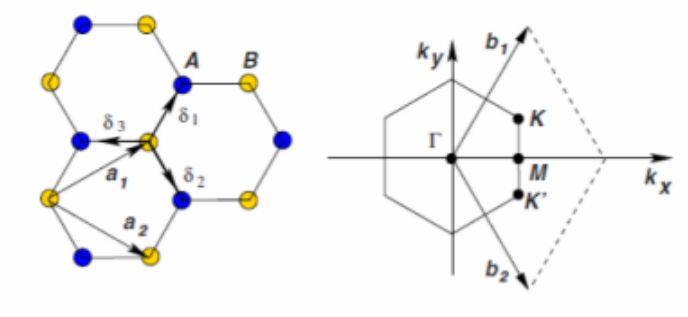

Figure 3.1: (a) Graphene exhibits a honeycomb lattice structure, and the different valleys A and B make up one elementary cell of two electrons. The lattice vectors $\vec{a}_1$ and $\vec{a}_2$ show the directions that elementary cells can be repeated in to form an entire lattice. (b) The 1st Brillouin zone is the momentum space dual to the elementary cell. For example, a function of the wavenumber at point $\mathbf{b}_1$ has the same properties as a function with wavenumber $k = 0$. Adapted from [7]

Low-Energy Physics

As shown in Fig. 1.1, different circled regions, representing gaps between the conduction and valence bands, can be modeled within different approximations. Of particular interest in graphene, as mentioned in the introduction, is called the *low-energy* spectrum, circled in red in Fig. 1.1. Electronic interactions in this region are dominated by the unusual energy dispersion near the Dirac point, as we investigate below.

The points K, K' are locations that, within the tight-binding model for nearest-neighbour interactions, give a zero Hamiltonian, corresponding to self-crossing. In other words, there is a meeting point between the valence and conduction bands (under ideal conditions, like zero temperature). What is unique to graphene, and of great interest for plasmonic applications, is the linear band dispersion near these points:

$$\varepsilon_{K,K'}(\vec{k}) = \hbar k v_F \tag{3.1}$$

where ε is the energy derived from the tight-binding Hamiltonian, and $v_F \approx 10^6 m/s$ is the Fermi velocity. Because this dispersion is linear, it is similar to the photonic dispersion relationship. This implies that the electrons near these conical energy dispersions behave like massless particles, and follow the 2D Dirac equation [26]

$$-iv_F\vec{\sigma}\cdot\nabla\psi(r) = E\psi(r) \tag{3.2}$$

with two-component spinor eigenfunctions

$$\psi_\pm = \frac{1}{\sqrt{2}}\begin{bmatrix} 1 \\ \pm e^{i\theta_{\vec{k}}} \end{bmatrix} e^{i\vec{k}\cdot\vec{r}} \tag{3.3}$$

for $\pm$ corresponding to either the bonding or anti-bonding band, or, via a proper unitary transformation, electron and hole wavefunctions in the language of semiconductors. $\theta_{\vec{k}}$ is the polar angle of the wavenumber components relative to the Dirac point (K symmetry point) of the elementary reciprocal lattice cell. The spinors come about as there are two electrons per unit cell, so forgetting the $\pm 1/2$ spin of the electrons, the valleys A and B each

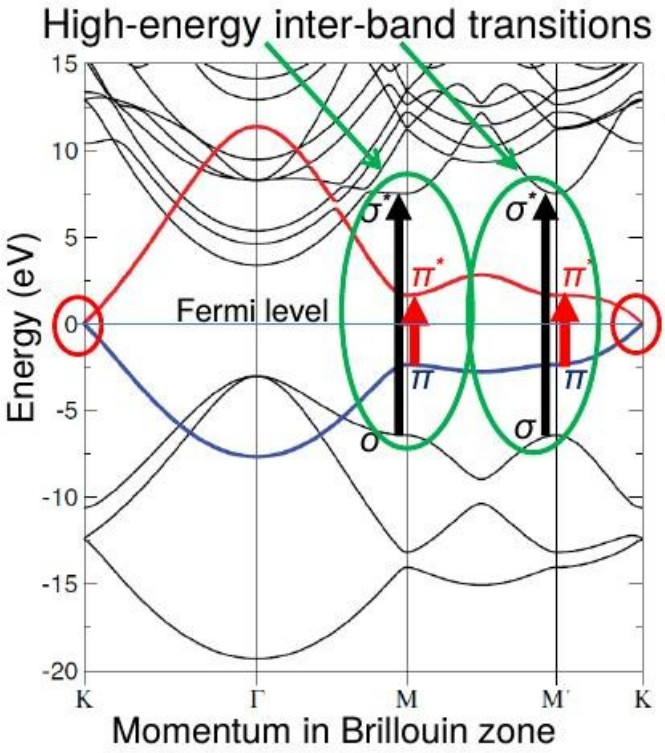

Figure 3.2: Band structure in undoped ($E_F = 0$) graphene, showing self-crossings between the electron-hole spectrum (circled red) and saddle points corresponding to symmetry points M and Γ in Figure 3.1(a) (circled green). The self-crossing has a linear dispersion in the low wavenumber limit, shown in Figure 3.3 for doped ($E_F > 0$) graphene. Adapted from [42]

make up a portion of the spinor. The $\vec{\sigma}$ in the Dirac equation above corresponds to Pauli matrices (in 2D), where the valleys are again analogous to electron spin.

Before we move on to graphene's optical properties, we make note of the fact that the density of states for energies near the Dirac points (K and K' and all edge points in the 1st Brillouin zone are all equivalent) is linear in energy just as the energy is linear in wavenumber:

$$D(E) = \frac{2|E|}{\pi(\hbar v_F)^2} \tag{3.4}$$

The property of the density of states increasing linearly with the energy levels is unique to two dimensional systems with linear energy dispersion, whereas it is constant for a 2D electron gas with quadratic energy dispersion. This quantity represents how many energy states are available for occupation at a particular energy, and hence it yields probabilities about the electron absorption of graphene that will aid us in determining optical properties of the material.

3.2 Optical and Electronic Properties

Our need for a full treatment of graphene's electronic and optical properties will be evident in each of the main projects featured in this paper. EELS will measure EM absorption by a

graphene sheet, ellipsometry will implement graphene's conductivity, and, when analyzing surface roughness, we will see the effect on graphene's plasmons themselves. Because of the two different energy regimes we are investigating, we focus on the two separately. Optical physics is primarily a feature of the low-energy spectrum, where the π bands dominate; our forays into graphene's optical properties cover the universal absorbance of frequencies, a description of low energy plasmons via a semi-classical fluid model, a discussion of the RPA approximation valid especially for linear responses to the change in polarization of the material, and of graphene's conductivity due to interband and intraband terms. Section 3.2.5 then features a semi-classical treatment of the π and σ electrons resonating according to the size of their band gaps (as in the green circled regions of Fig. 3.2); these transitions constitute the *high-energy* spectrum of graphene's electronic structure, and despite not currently being of interest in optical applications, are of interest in the analysis of transitions of the Γ and M symmetry points [46].

3.2.1 Universal Absorbance

We proceed to introduce one of graphene's most outstanding properties, which is its universal absorbance of all wavelengths of light. This is a feature that will be observed in both the ellipsometric and EELS measurements we will see later on.

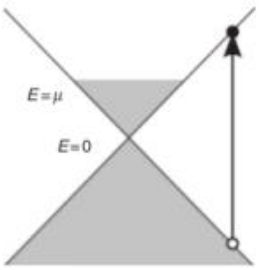

Figure 3.3: Due to the symmetry of the linear dispersion of graphene's π electron bands, a photon of energy $\hbar\omega$ will excite an electron to a state $\hbar\omega/2$ as long as $\hbar\omega > 2|\mu|$, where μ is the chemical potential. Undoped graphene has $\mu = 0$ in the tight-binding approximation, but higher approximations introduce asymmetry into the conical energy dispersion. Adapted from [26]

Let $\vec{A}(t) = \vec{A}\exp(-i\omega t)$ be the EM vector potential, so that $\vec{E}(t) = (i\omega/c)\vec{A}(t)$ by an appropriate choice of gauge. Then, in Fourier space, the Hamiltonian for particles near the Dirac point linear dispersion looks like

$$\mathcal{H} = v_F\vec{\sigma}\cdot(\vec{k} - e\frac{\vec{A}}{c}) \qquad \mathcal{H}_{int} = -\frac{1}{2}\frac{v_F e}{c}\vec{\sigma}\cdot\vec{A} = \frac{1}{2}\frac{iev_F}{\omega}\vec{\sigma}\cdot\vec{E} \tag{3.5}$$

with the 1/2 factor coming from only taking the $-i\omega$ term of the electric field (not the symmetric $+i\omega$ term). $\mathcal{H}_{int}$ represents the Hamiltonian contribution for the interband transition. To determine the absorption rate, we start with Fermi's Golden Rule, which tells us the transition probability per unit time for given energy states (in this case, at $\pm\hbar\omega/2$). It reads as

$$\text{Prob}_{i\to f} = \frac{2\pi}{\hbar}\sum_{k_c,k_v}|\langle f|H_{int}|i\rangle|^2\delta(E_c(k) - E_v(k) - \hbar\omega) \tag{3.6}$$

where c, v are indices for the conduction and valence bands, $E_c(k)$ is the energy of the final state in the conduction band, and $E_v(k)$ is the energy of the initial state in the valence band. The spinor wavefunctions for electrons and holes (conduction and valence electrons, respectively) are unitary transformations of the spinors for valleys A and B in the graphene, so we use them interchangeably. The expectation value of the interband conduction Hamiltonian is

$$|\langle e|\mathcal{H}_{int}|h\rangle|^2 = \int \psi_e^* \mathcal{H}_{int} \psi_i d^2r \tag{3.7}$$

$$= \int \frac{1}{\sqrt{2}}[1 \quad e^{-i\theta_{\vec{k}}}] e^{-i\vec{k}\cdot\vec{r}} v_F e\vec{\sigma}\cdot\frac{\vec{E}}{2i\omega}\frac{1}{\sqrt{2}}\begin{bmatrix} 1 \\ -e^{i\theta_{\vec{k}}} \end{bmatrix} e^{i\vec{k}\cdot\vec{r}} d^2\vec{r} \tag{3.8}$$

$$= v_F e\frac{|E_x|}{2i\omega}\int \frac{1}{2}[1 \quad e^{-i\theta_{\vec{k}}}]\begin{bmatrix} 0 & 1 \\ 1 & 0 \end{bmatrix}\begin{bmatrix} 1 \\ -e^{i\theta_{\vec{k}}} \end{bmatrix} d^2\vec{r} \tag{3.9}$$

$$= -v_F e\frac{|E_x|}{2\omega}\sin\theta_{\vec{k}}\int d^2\vec{r} \tag{3.10}$$

choosing the electric field to be polarized in the x-direction, and assuming an integration over a sample area $\mathcal{A} = \int d^2r$. We already see that the only wavevector dependence occurs in the polar angle in Fermi's Golden Rule, so the sum in Eq. 3.6 is equivalent to a sum over all angles. The Dirac delta function in the transition probability integral is the linear density of states from Eq. 3.4, at the energy $\hbar\omega/2$. The absorbed flux equals the total energy divided by total area, given by

$$\Phi_{abs} = \frac{1}{\mathcal{A}}\hbar\omega \text{Prob}_{h\to e} = \hbar\omega\frac{2\pi}{\hbar}v_F^2 e^2\frac{|E|^2}{4\omega^2}\sum_{\theta_{\vec{k}}}\sin^2\theta_{\vec{k}}\frac{\hbar\omega}{\pi\hbar^2 v_F^2} = \frac{e^2|E|^2}{4\hbar}. \tag{3.11}$$

Given that the incident flux for an electric field $|E|$ is $\Phi_{inc} = (c/4\pi)|E|^2$, we obtain

$$A = \Phi_{abs}/\Phi_{inc} = \frac{\pi e^2}{\hbar c} \longrightarrow 2.3\%. \tag{3.12}$$

This ratio of the absorbed to incident flux is exactly the definition of absorbance for a material. We have arrived at the result that, no matter what the frequency, graphene will absorb all energies of photon with the same probability, assuming the linear dispersion model for the graphene interband transitions is still valid. On top of this fascinating result is how high of an absorbance this is for a two-dimensional layer of carbon atoms. This quantum mechanical treatment helps show the strong interaction between electric fields and graphene we will see in the remainder of the thesis.

3.2.2 A Classical Hydrodynamic Approach to Graphene

Before delving into some advanced models, we present an elementary version of an Euler-flow hydrodynamic equation, treating the particles affected by an external source as small perturbations in the electron density $n(\vec{r}, t)$ and the current density $\vec{j}(\vec{r}, t)$ in graphene. Let $\delta n(\vec{r}, t)$ and $\delta\vec{j}(r, t)$ be these small deviations from the corresponding equilibrium, or the average values. The assumptions should be valid in the limit of small wavenumbers $q \ll k_F$, so that the response of the electrons is macroscopic [20]. Here k_F is the Fermi wavenumber, which using Eq. 3.1 is the wavenumber corresponding to the Fermi energy E_F. There is a useful relation between the electron density and the Fermi wavenumber in graphene,

$$k_F = \sqrt{\pi n_0} \tag{3.13}$$

where n_0 represents the average areal electron density of graphene, which increases with doping.

For ordinary neutral liquids, the restoring force that causes oscillations in particle density is a pressure gradient, so the classical Euler equation reads as

$$m\frac{\partial\vec{j}(\vec{r},t)}{\partial t} = -\vec{\nabla}P(\vec{r},t) \tag{3.14}$$

for $P(\vec{r},t)$ the pressure, and m the mass of the particle in the fluid. This equation is valid when the oscillations are slow enough (i.e. small ω) relative to the system's response, so that the system is always in equilibrium. The linear approximation is then that

$$\vec{\nabla}P(\vec{r},t) \approx \frac{\partial P}{\partial n}\vec{\nabla}\delta n(\vec{r},t), \tag{3.15}$$

assuming the pressure is related to the equilibrium density through an equation of state. Taking the divergence of the equation and using the continuity equation $\vec{\nabla}\cdot\vec{j} = -\frac{\partial n}{\partial t}$ yields the equation

$$\frac{\partial^2\delta n(\vec{r},t)}{\partial t^2} - \frac{1}{m}\frac{\partial P}{\partial n}\nabla^2\delta n(\vec{r},t) = 0 \tag{3.16}$$

and changing to Fourier components gives us the resonance frequency $\omega = \sqrt{\frac{1}{m}\frac{\partial P}{\partial n}}q$. Here we get our first look at what a resonance in fluids corresponds to. Putting this frequency in our equation implies that even for a low ω and q value, oscillations can exist, and we here observe a linear dependence of the frequency on the wavenumber.

However, charged liquids, which contain electrons and holes, are unique in this respect, as the main driving force is not a weakly varying pressure gradient, but instead a long-range electrostatic field that exists even at long wavelengths [21]. In this case, the Euler equation for motion will be an integration of all the charges influenced by the Coulomb potential. We obtain

$$m_e\frac{\partial\delta\vec{j}(\vec{r},t)}{\partial t} = -n_0\nabla_{\vec{r}}\int d^2r'\frac{e^2}{\epsilon|\vec{r}-\vec{r}'|}\delta n(\vec{r}',t) \tag{3.17}$$

where $\epsilon = (\epsilon_1+\epsilon_2)/2$ if the graphene is between two dielectric media [43], and m_e is the mass of the electron. This equation can be thought of as relating all the movement of charges as due to the combined electric force given by charges $\delta n(\vec{r},t)$, screened by a factor ϵ. Fourier transforming the above equation and using the same continuity equation results in

$$\left(\omega^2 - \frac{n_0q^2}{m_e}\frac{2\pi e^2}{\epsilon q}\right)\delta n(\vec{q},\omega) = 0, \tag{3.18}$$

noticing that the Fourier transform of the screened Coulomb potential in 2D is $\frac{2\pi e^2}{\epsilon q}$. This equation yields a resonant frequency of $\omega = \sqrt{2\pi n_0 e^2 q/(\epsilon m_e)}$, and we now observe square root dependence in the plasmon frequency, which is the correct behaviour for all collective eigenmodes of charged fluids in 2D.

We recall that the formula for the linear energy dispersion near the Dirac point, known as the Dirac cone, means that single-particle excitations between electrons and holes occur below the energy $\hbar\omega = \hbar v_F q$. For low enough wavenumbers, this value is smaller than the value for the plasmon frequency, meaning the plasmon will not decay into an electron-hole pair in either the conduction or valence band. We will explore later the region where the

plasmon frequency $\omega > v_F q$ decays into these pairs due to inter-band transitions, a process known as Landau damping [51]. We have pointed out before that the plasmon frequency of our graphene samples will largely be less than the frequency where the nearby conductors have their plasmon resonance - this restriction to the region below Landau damping is another reason we will be able to focus on a restricted subset of frequencies.

The factor ϵ that changes the overall potential is partially derived in later chapters (see Eq. 5.54) from a Green's function approach, and is a factor expected for all two-dimensional systems resting between two layers. Materials like substrates can interact strongly with a graphene sheet, and the effect that roughness plays into this interaction is the subject of Chapter 5.

Since the particles with their momenta near the Dirac cone exhibit a linear dispersion of their energy, and follow a Dirac spinor equation, we hinted that the traveling particles could be treated as 'massless'. These massless particles are not, however, the electrons, but rather photon-like quasi-particles which occupy the eigenstates of the energy band valleys where the conical self-crossing occurs, which we derived from the band structure. Strong pairwise electron correlations characterize graphene's electronic structure, but the quasi-particle picture presents us with a non-interacting picture, making calculations much easier.

If we consider the carrier density to be made up of these quasi-particles instead, the value m_e is no longer valid in the calculations, and instead the plasmon frequency (see Eqs. 3.29-3.33 for derivation) becomes [21]

$$\omega_p(q) = \sqrt{\frac{8E_F\sigma_0 q}{\hbar\epsilon}} \tag{3.19}$$

where $E_F = \hbar v_F k_F$ is the Fermi energy, and $\sigma_0 = e^2/(4\hbar)$ is the universal conductivity we obtained for low frequencies (causing absorbance of 2.3%). This frequency can be shown within an f-sum rule calculation [52], a derivation that outlines how the total particle number (be they electrons or quasi-particles) is conserved by forces like the Coulomb interaction that do not add or subtract to the system. This rule will be crucial once we attempt to find a hydrodynamic model that explains absorption modes for high-energy transitions in graphene, as we are necessarily making approximations about the Hamiltonian and we must ensure that the total particle 'bulk' is not changed by these assumptions.

3.2.3 Electromagnetics in Doped Graphene

Approaches to understanding graphene vary from the quantum to the macroscopic: ab initio calculations start from a density functional theory approach, building up ground states of many Schrodinger equations to determine properties on the small scale. Macroscopic theories however need a consistent and simplifying way to deal with the strongly-correlated electron systems that occur in high-density materials like graphene. For our purposes, we implement the Fermi liquid theory, which maps systems with a high electron density (which thence has strongly correlated interactions) to ones with barely interacting quasi-particles with renormalized mass (as we saw in the plasmon derivation above) [49].

The basis of Fermi liquid theory, developed by Lev Landau, shows that near the Fermi surface, which is the region of all interesting optical properties, the system has a correspondence with a free Fermi gas that obeys Fermi-Dirac statistics. Therefore electrons in the system are mapped one-to-one (as particle number must always be conserved) to weakly interacting fermionic quasi-particles. As these new quasi-particles are not definite eigenstates of the Hamiltonian, they have a finite lifetime and a renormalized mass caused by the

collective effect of all the other interactions in the system that 'dress' the particle [41]. Each electron can then be seen as having a bare part to it and a dressed portion that screens its effect on other particles in the material.

From a microscopic point of view, the theory can be developed using renormalization techniques in Quantum Field Theory (QFT). This theory predicts the central themes of the Fermi liquid theory: finite weakly interacting quasi-particles with a renormalized mass. Renormalization is a result of a divergence when summing over all possible interactions of particles (i.e. all interactions of a particle with itself, with two other particles, etc.), and choosing certain ways to renormalize in certain regimes guides our interpretation of the macroscopic properties of high density liquids.

A high density of electrons, leading to a high quasi-particle density, means that the kinetic energy for the system is much larger than the potential, and interactions that involve the kinetic part (reflected in collisions, or momentum transfer, between particles), will be heavily weighed in the renormalization.

A crude approximation for this system, known as the Hartree approximation, sums up interactions a particle has with itself, known as 'bubble' diagrams. This approximation predicts for our system infinite particle lifetimes with zero mass, since we have neglected correlations between the movement of the particles. This is expected, as treating all the new quasi-particles as not interacting will give them photon-like properties. Wanting to include the dominant effect of these correlations, we add onto this approximation what are known as 'ring' diagrams, one of the interactions representing momentum transfer. These rings are so called because an interaction at one end of the ring effectively produces a negative electron on top of the ring and a positive hole on its bottom, which together create a finite lifetime dipole, causing polarization of the medium and movement of the charges. This gives the Random Phase Approximation (RPA), also known as the time-dependent Hartree-Fock approximation for its inclusion of non-static behaviour like momentum transfer.

One way in which this RPA approximation can be seen qualitatively is in the screened Coulomb interaction in two dimensions

$$v_{sc}(q) = \frac{1}{4\pi\epsilon\epsilon_0}\frac{2\pi}{q + k_{TF}} \text{ or } v_{sc}(r) = \frac{1}{4\pi\epsilon\epsilon_0}\left\{\frac{1}{r} + \frac{\pi k_{TF}}{2}[Y_0(k_{TF}r) - H_0(k_{TF}r)]\right\}, \quad (3.20)$$

where we have Bessel Y and Struve H functions in our screened Coulomb potential equation. This expression drops off as $1/(r^3 k_{TF}^2)$, with k_{TF}^{-1} known as the Thomas-Fermi screening length. Physically, this represents an electron in the system repelling other electrons from it, and this interaction is isomorphic in properties to each electron being followed by a cloud of positive charges of width k_{TF}^{-1}, so its effect on particles outside this distance is drastically reduced. This example also shows why the interaction of quasi-particles can be considered so weak - the effective cloud that surrounds them accounts for a reduced interaction (in this case exhibited by the screened Coulomb potential).

RPA is also able to determine the linear responses we obtained from constitutive relations in EM, namely the conductivity $\sigma(q, \omega)$, polarizability $\chi(q, \omega)$ and the dielectric function $\epsilon(q, \omega)$. The inclusion of ω in these functions relating to the polarizability of the medium is evidence that the RPA is able to include correlations - ω implies that a polarization of the material moves the electrons collectively, so that a sort of inertia, or momentum transfer, is occurring on the quantum scale.

Before we proceed with explaining our RPA-derived polarizability function in terms of inter- and intra- band transitions, we briefly mention why we do not consider the case of undoped graphene. Recall that in the regime of Fermi energy $E_F = 0$, we see in Figure

3.3 that there is no longer a Fermi surface, but rather a 'Dirac point' in one dimension. Landau's Fermi liquid theory relies on electrons occupying a set of states near the Fermi level in order for the screening effect to occur. With so few electrons occupying the Fermi level (due to thermal and quantum effects), other interactions than the 'ring' diagrams will take over, and the RPA requires corrections [52]. Undoped graphene also does not include intraband transitions, which dominate at low frequencies where our plasmons are going to lie. In Section 4, where we consider interband transitions for graphene, we will make the simplifying assumption that the graphene is undoped, but for Section 5, when we study graphene plasmons existing due to intraband transitions, it is necessary that a Fermi surface exist, and we used doped graphene for that section.

Phase Space of Excitations

In our discussion about different excitations that the particle is able to take on, we will focus on the imaginary part of the polarizability $\Im\chi(q,\omega)$, as it will give us a way to analyze reasons for energy loss (and hence absorbance) in our system. To see this, we first make note of the relationship (see Appendix 2)

$$\sigma(q,\omega) = \frac{i\omega}{q^2}\chi(q,\omega), \tag{3.21}$$

meaning that $\Im\chi(q,\omega) \sim \Re\sigma(q,\omega)$. We saw in Eq. 2.40 that the absorbance of our material A under certain conditions was linearly dependent on the real part of the conductivity. This hints at the property that $\Re\sigma(q,\omega)$ gives us an idea about the nature of dissipation in our system due to current flow $\mathbf{J}$. Another way to see this is that $\Im\chi(q,\omega)$ determines how excitations couple to external charge fluctuations. For example, a fermionic excitation creates a quasi-particle/quasi-hole pair that then is moved along by a current $\mathbf{J}$, described by $\Im\chi(q,\omega)$. Plasmons are bosonic excitations in that they quantize collective behaviour, but they still exhibit the finite lifetimes of standard quasi-particles.

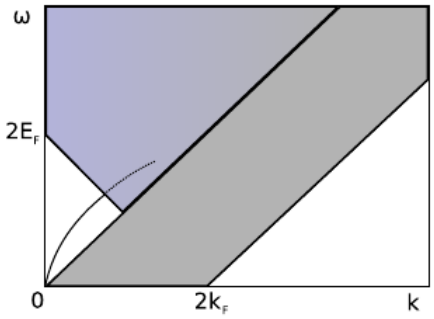

Figure 3.4: $k-\omega$ plot of the different modes of excitation. Intraband (grey) dominates the spectrum at low energies, while the interband excitations (blue) are suppressed in the $k \to 0$ limit due to the Fermi level at $\omega_F = v_F k_F$. Adapted from [51]

The intraband transitions are a result of electron excitations within conduction or valence bands, but not from one to the other. These transitions, which now dominate at low energies [33], are effective at suppressing the Coulomb interaction, and therefore for doped graphene we expect the RPA to hold.

Evaluation of $\Im\chi(q,\omega)$ within the RPA approximation yields the plasmon frequency derived from the Fermi Liquid Theory in Eq. 3.19 [22], which is a proper treatment given

the photon-like properties of the quasi-particles near the linear dispersion Dirac cone. This plasmon mode has the square root wavenumber dependence we expect from the 2D electron gas, and exists in the region $v_F q < \omega < 2E_F - q v_F$, as the other regions will cause the plasmon oscillation to decay into other modes.

3.2.4 Graphene Conductivity in the Optical Regime

We have mentioned in Chapter 2 that the difference in scale between the wavelengths of probes and plasmons in the graphene, compared to the characteristic wavenumber scales of graphene's Brillouin zone and the mean free electron path, suggests a local frequency response. This is especially valid in the Dirac cone approximation, a region where the following property holds approximately

$$0 \approx \frac{\omega}{c} \ll q \ll \frac{\omega}{v_F} \ll k_F. \tag{3.22}$$

This is known as the optical, or $q \to 0$ limit. We explore the conductivity of the material, which will yield a finite answer in this limit. This is due to the nature of the electric current $J(\omega)$ in materials, as current is an intrinsic dynamic response, whereas factors like the internal charge density, by the continuity equation, require a level of dispersion to take effect.

The optical conductivity is broken into two parts, the first being the inter-band contribution $\sigma_I = \sigma_r + i\sigma_i$, with [4]

$$\sigma_r = \sigma_0 \left(1 + \frac{1}{\pi} \tan^{-1} \frac{\hbar\omega - 2E_F}{\hbar\gamma_I} - \frac{1}{\pi} \tan^{-1} \frac{\hbar\omega + 2E_F}{\hbar\gamma_I} \right) \tag{3.23}$$

and

$$\sigma_i = -\sigma_0 \frac{1}{2\pi} \ln \frac{(\hbar\omega + 2E_F)^2 + \hbar^2\gamma_I^2}{(\hbar\omega - 2E_F)^2 + \hbar^2\gamma_I^2} \tag{3.24}$$

such that

$$\sigma_0 = \frac{e^2}{4\hbar} \tag{3.25}$$

is called the universal conductivity, and γ_I is the relaxation rate for interband transitions related to the damping of the mobile electrons in the graphene, derived under the RPA approximation. This is known as the universal conductivity as it is the same expression we showed in Eq. 3.12 for absorbance (see Eq. 2.40 to relate $\Re\sigma(\omega)$ to A) due to the inter-band transitions that absorb all frequencies below a certain threshold, where the transitions dominate for undoped graphene.

The second contribution is known as the Drude conductivity term, and has the form

$$\sigma_D = \sigma_0 \frac{4E_F}{\pi} \frac{1}{\hbar\gamma_D - i\hbar\omega} \tag{3.26}$$

derived from the intraband contribution, which becomes dominant at all frequencies for highly doped graphene (see Fig. 3.4). The relaxation rate for the Drude term is γ_D, which is derived from a measured dc mobility limited by impurities [29], allowing us to separate it from the γ_I due to interband transitions.

Based on the doping of the graphene in question, we will be exploring different regimes. There is also the non-optical regime for polarizability which we investigate in Section 5.2.2 when a description of plasmonic behaviour for a large spectrum of wavenumbers is desired [22]. Another limit that is of use to us is the limit where the interband transitions have $\gamma_I \to 0$, resulting in a total conductivity of

$$\sigma_{low}(\omega) = \frac{e^2 E_F}{\pi\hbar^2}\frac{i}{\omega + i\gamma_D} + \sigma_0\left[\Theta(\hbar\omega - 2E_F) + \frac{i}{\pi}\ln\left|\frac{\hbar\omega - 2E_F}{\hbar\omega + 2E_F}\right|\right] \tag{3.27}$$

with $\Theta(\hbar\omega - 2E_F)$ the Heaviside step function, showing the screening of low wavenumber excitations due to the Fermi surface, as in Fig. 3.4.

We see from Fig. 3.4 that the plasmon mode, which will exist for $\omega \gg qv_F$, and derived from the RPA approximation, will be dominated by this Drude conductivity term with a negligible real part (as there is negligible absorption in the plasmon region $v_F q < \omega < 2E_F - qv_F$),

$$\sigma_{plasmonics} \approx \sigma_D \approx i\frac{e^2 E_F}{\pi\hbar^2\omega}. \tag{3.28}$$

We showed in Eq. 2.59 why this conductivity suitably described the region where the plasmon is valid, and yet we could still consider our excitation to be a surface plasmon.

Based on this expression, we can derive the plasmon's resonant frequency. We combine the two dimensional continuity equation, the definition of conductivity, the definition of the electric potential and the definition of the internal charge density for the screened Coulomb interaction near a substrate, which is

$$\hat{\phi} = v(q)_{2D,s}\hat{\rho} = \frac{2\pi}{q\epsilon}\hat{\rho} \tag{3.29}$$

based on Eq. A.41 from Appendix 2.

Under the assumption of optical conductivity for graphene plasmons, this gives

$$\begin{aligned}
\omega\hat{\rho} &= \vec{q}\cdot\vec{j}(\omega) && (3.30)\\
&= \sigma(\omega)\vec{q}\cdot\vec{E}(\omega) && (3.31)\\
&= -iq^2\sigma(\omega)\hat{\phi}(q,\omega) && (3.32)\\
&= -iq^2\left(i\frac{e^2 E_F}{\pi\hbar^2\omega}\right)\left(\frac{2\pi}{q\epsilon}\hat{\rho}\right). && (3.33)
\end{aligned}$$

The plasmon frequency yields an eigenmode for the equation for non-zero $\hat{\rho}$, allowing us to cancel $\hat{\rho}$ and determine the equation for $\omega_p(q)$ from Eq. 3.19. This frequency was also derived from the dispersion relation determined in Eq. 2.58, this time in Gaussian units. [4].

It is interesting to observe that, despite the fact that our conductivity equation is derived under the quasiparticle picture within the RPA approximation, we are able to treat the particles like any other electron system that satisfies the continuity equation, the equation for current and the internal charge density. In fact, the f-sum rule for conservation of particle number mentioned earlier is a result of the application of the continuity equation on a quantum level with the quantum Hamiltonian of the system [49]. We investigate this conservation law in future chapters.

3.2.5 Two-Fluid Hydrodynamic Approach

A previously mentioned property of the graphene structure is that it contains two types of electrons depending on their location in the orbital of each carbon atom: three σ electrons and one π electron. We seek in this section to develop a model for high-energy transitions between the π and σ bands as shown in Fig. 3.2. In our development of a planar description of graphene's properties for higher energies than those where the linear dispersion model for the π-orbitals in graphene is valid, we seek to use a Hamiltonian that encodes all the features experienced by these electron types in two-dimensions via a hydrodynamic model. We use the ideas from density functional theory, which lumps collective classical and quantum mechanical properties into functionals solely dependent on the local electron density. On one hand, the Hamiltonian will contain terms seen in a classical harmonic approach to fluids with a restoring force, but on the other hand, we see the exchange interaction due to quantum indistinguishability of identical particles, now in terms of the electron density instead of wavefunctions. Effects like the periodicity of the graphene structure are ignored in favour of an electron gas against a uniform positive ion background, with various corrections included to capture the fluid effects. The two fluid Hamiltonian is [44]

$$\begin{aligned}\mathcal{H} = \sum_{\nu=\sigma,\pi} \Bigg\{ & \int d^2\mathbf{r} n_\nu(\mathbf{r}) \left[\frac{1}{2m_\nu^*} |\mathbf{p}_\nu(\mathbf{r})|^2 + \frac{\kappa_\nu}{2} |\mathbf{x}_\nu(\mathbf{r})|^2 + V(\mathbf{r}) \right] \\ & + \int d^2\mathbf{r} n_\nu(\mathbf{r}) \left[\frac{\pi\hbar^2}{2m_\nu^*} n_\nu(\mathbf{r}) - e^2 \left[\frac{32}{9\pi} n_\nu(\mathbf{r}) \right]^{1/2} \right] \\ & + \frac{e^2}{2} \sum_{\nu'=\sigma,\pi} \int\int d^2\mathbf{r} d^2\mathbf{r}' \frac{n_\nu(\mathbf{r}) n_{\nu'}(\mathbf{r})}{|\mathbf{r}-\mathbf{r}'|} \Bigg\} \end{aligned} \tag{3.34}$$

where n_ν, $\mathbf{p}_\nu$, $\mathbf{x}_\nu$, m_ν^*, and κ_ν are, respectively, the number density per unit area, the fluid momentum field, the displacement field, the effective mass, and the restoring-force constant for the ν-th electron fluid, with $\nu = \sigma, \pi$ representing the type of carrier in the fluid. We have the relation $\mathbf{p}_\nu = m_\nu^* \dot{\mathbf{x}}_\nu$, the time derivative, and we have an implicit time dependence along with the $\mathbf{r}$-dependence.

The first term represents the kinetic energy of a fluid ν, the second term the restoring force of electrons that occurs within a harmonic approximation of fluids, giving a restoring frequency $\omega_{\nu r} = \sqrt{\kappa_\nu / m_\nu^*}$, and the potential $V(\mathbf{r}) = V_g(\mathbf{r}) + V_{ext}(\mathbf{r})$ as a result of both the positive ion background and any external perturbations. The next set of terms are derived from the local density approximation (i.e. only depend on the electron density at a single point in space) to determine the exchange effects from a density functional approach, known as the Thomas-Fermi and Dirac exchange interactions. Lastly included are the electronic Coulomb interactions.

We now wish to consider the perturbations of the electrons to be small, allowing us to expand the Hamiltonian to the second-order in the perturbation by letting $n_\nu(\mathbf{r}) = n_\nu^0 + \lambda \delta n_\nu(\mathbf{r}) + \mathcal{O}(\lambda^2)$, $V_{ext} = \lambda V_{ext}$ and the velocity $\mathbf{u}_\nu(\mathbf{r}) = \lambda \delta \dot{\mathbf{x}}_\nu(\mathbf{r}) + \mathcal{O}(\lambda^2)$, where n_ν^0 is the ground state electron density of either the σ or π fluid. In order to satisfy the continuity equation, we let $\delta n_\nu(\mathbf{r}) = -n_\nu^0 \nabla \cdot \delta \mathbf{x}_\nu(\mathbf{r}) = n_\nu^0 \Delta \xi_\nu(\mathbf{r})$ where the gradient and divergence operators act in the plane of a graphene sheet, and by working in an electrostatic regime we are able to define the displacement field as being irrotational, letting $\xi_\nu(\mathbf{r})$ be the scalar

potential that generates it. Writing out the second order Hamiltonian yields

$$\begin{aligned}\mathcal{H}_2 = &\sum_\nu \int d^2\mathbf{r}\left\{\frac{m_\nu^*}{2}(|\nabla\dot{\xi}_\nu|^2 + \omega_{\nu r}^2|\nabla\xi_\nu|^2) + V_{ext}(\mathbf{r})\Delta\xi_\nu\right\} \\ &+ \sum_\nu \int d^2\mathbf{r}\left(\frac{\pi\hbar^2}{2m_\nu^*} - e^2\frac{1}{\sqrt{2\pi n_\nu^0}}\right) \times (n_\nu^0\Delta\xi_\nu)^2 \\ &+ \frac{e^2}{2}\sum_{\nu,\nu'}\int\int d^2\mathbf{r}d^2\mathbf{r}'\frac{n_\nu^0 n_{\nu'}^0}{|\mathbf{r}-\mathbf{r}'|}\Delta\xi_\nu\Delta\xi_{\nu'}\end{aligned} \tag{3.35}$$

Since this is a second order Hamiltonian, it gives us a semi-classical equation of motion for the electron fluids, containing terms analogous to the speed of propagation density and classical pressure derived from a quantum perspective. From the Hamiltonian, the Euler-Lagrange equation of motion can be derived by combining the two first-order PDEs given by Hamilton's equations to give one second order PDE for the variable ξ_ν:

$$\ddot{\xi}_\nu + \omega_{\nu r}\xi_\nu + s_\nu^2\Delta\xi_\nu = \frac{1}{m_\nu^*}(V_{ext}(\mathbf{r}) - e\Phi_{ind}(\mathbf{r})) \tag{3.36}$$

where the potential Φ_{ind} is the induced potential due to the electron fluid polarization from the small perturbative external potential satisfying the Poisson equation

$$\Delta\Phi_{ind} = 4\pi e\delta(z)\sum_{\nu=\sigma,\pi} n_\nu^0\Delta\xi_\nu(\mathbf{r}) \tag{3.37}$$

and the speed of propagation density s_ν is defined by

$$s_\nu^2 = \frac{2}{m_\nu^*}\left(\frac{\pi\hbar^2}{2m_\nu^*}n_\nu^0 - e^2\sqrt{\frac{n_\nu^0}{2\pi}}\right). \tag{3.38}$$

The term $\ddot{\xi}_\nu$ stems from the time derivative of the partial derivative of the system's Lagrangian with respect to the canonical coordinate $\dot{\xi}_\nu$, while all other terms are a result of $\partial L(t,\xi_\nu,\dot{\xi}_\nu)/\partial\xi_\nu$ in the Euler-Lagrange equation.

Transforming to Fourier components, and noticing that $V_{tot}(\mathbf{r}) = V_{ext}(\mathbf{r}) - e\Phi_{ind}(\mathbf{r})$ is the total potential of the system, we obtain

$$(-\omega^2 + \omega_{\nu r}^2 + s_\nu^2 q^2)\xi_\nu = -\frac{1}{m_\nu^*}V_{tot} \tag{3.39}$$

$$\delta n_\nu = -\frac{n_\nu^0 q^2/m_\nu^*}{\omega_{\nu r}^2 + s_\nu^2 q^2 - \omega(\omega + i\gamma_\nu)}V_{tot} = \chi_\nu(q,\omega)V_{tot} \tag{3.40}$$

which is the definition of the polarizability $\chi(q,\omega)$, relating the induced charge density with the total potential of the system. We note the addition of an imaginary damping γ_ν, which cannot be derived in the context of the Hamiltonian from DFT, but instead is a phenomenological justification of the damping that occurs in real systems. We see a similar factor occur in the QFT approach to many-body systems, considered the lifetime of quasi-particles or of oscillations. Also similar to QFT is the effective electron mass m_ν^* used in the calculations, which will be heavier than a normal electron mass due to the cloud of particles surrounding it.

Determining $\chi_\nu(q,\omega)$, which hence also gives us $\epsilon_\nu(q,\omega)$ and $\sigma_\nu(q,\omega)$, will be of much use later when we attempt a fitting of this two-fluid hydrodynamic model to explain high-energy spectroscopy data, a method that yields high-energy plasmon peaks resonating at the $\sigma \to \sigma*$ and $\pi \to \pi*$ inter-band transitions that match well with what we expect from this semi-classical electron fluid.

We note that we now have two different polarizabilities for two different regimes, allowing us to determine the response of planar graphene to external perturbations. For the linear dispersion approximation for the low-energy excitations involving only π electron bands near the two symmetry points K, K' we have (for the case of undoped graphene) already noticed the universal absorbance of graphene, which is the major contributor to this regime's polarizability. Once we look at higher energies where the plasmonic behaviour of the σ and π bonds begin to take the major roles, we can use the two-fluid two-dimensional hydrodynamic model, for which we have determined the polarizability. Reconciling these two models to determine the full spectrum of graphene's behaviour will be the subject of later chapters.

Chapter 4

Modelling Ellipsometry and EELS in Graphene

We have covered in previous chapters some of the basics of graphene and its optical properties. In our studies of rough surfaces in Chapter 5, we will focus on plasmonic behaviour, and we showed in Section 3.2.3 that these plasmons are strongest in the low wavelength/frequency regime. However, we also developed a semi-classical model for the electrons that are involved in the bonding process through σ and π orbitals, which at higher energies resonate in a fluid-like manner at different symmetry points in the graphene lattice.

Precise modeling of the low energy (and hence low frequency) regime is accomplished via the detection of changes in the polarization of light, known as ellipsometry due to the elliptical nature of electric fields that oscillate out-of-phase with each other. Less precise but having a large energy scope is the technique of EELS, which measures inelastically-scattered electrons that undergo energy loss with the material. We attempt to reconcile the data we obtain from these measurements experimentally via a combination of a hydrodynamic model with a low frequency contribution called the 'Dirac term', the universal absorbance due to interband transitions of graphene for low wavenumbers and frequencies that we explored in Sections 3.2.1 and 3.2.4. As there is an overlap between the data sets, we are able to phenomenologically determine parameters for our models that fit the data well.

4.1 Ellipsometry

We have seen in Section 2.1.3 that given the polarization of incident light, the angle at which it hits an interface, and the properties of the materials and surfaces in the system, we can determine the coefficients for the polarization of both the reflected light and transmitted light. As an experimentalist, two of these factors can be controlled, but one desires to know to great precision the optical properties of the material. Measuring reflected or transmitted light will therefore give information on the material below, which is experimentally chosen to be an interface in most cases for ease of use.

The ability for this technique to probe materials as thin as graphene, which is thinner than the light used to probe it, and its non-invasiveness, make ellipsometry ideal for measuring changes in the low energy spectrum of graphene. In our case we will consider experimental data of graphene on top of a glass substrate, as this allows the light that transmits through the graphene to pass through unhindered, while also being a neutral material that should not change heavily the electronic properties of this very tunable material. We

will speculate later in this chapter the possibility of elements and charge impurities between the graphene and glass, deposited as a result of the difficult experimental techniques used to build graphene on top of a substrate effectively. It is clear that reflection coefficients should be measured as this experimental setup allows for the measurement of light without passing through any other materials than air.

The fundamental equation of ellipsometry is [16]

$$\frac{r_p}{r_s} = \tan\psi e^{i\Delta} \tag{4.1}$$

where r_p, r_s are defined as in Eqs. 2.35-2.38, ψ is the magnitude of the difference between the different polarizations, and Δ is the phase shift. These parameters can be measured for different angles of incidence θ, and different incident energies determined by the component of the incident light parallel to the surface. Therefore our ellipsometric measurements will give us, for different energies and different θ, two parameters that in tandem should model the graphene conductivity we have in Eqs. 2.35-2.38.

It is of note that the graphene conductivity is the only unknown in the equations for r_p, r_s, so for each energy $\hbar\omega$, our amplitude and phase shift determine the conductivity. However, this system appears to be overdetermined, as two data sets have the ability to determine two free parameters. This is however a misnomer, as our conductivity contains both real and imaginary parts, corresponding to absorption and dissipation modes respectively (see Section 3.2.3). We will be starting with the model and fitting it to the data sets rather than try to extract data to create a model. This extraction in the case of three-dimensional graphene (assuming the graphene is a very thin layer) has been performed and analyzed [45], and their equations for r_p, r_s become three-layer Fresnel equations. In their case the system has three free parameters, so the thickness of the graphene must be assumed to be approximately 0.335nm as it is in the interlayer spacing of bulk graphite.

Experiments [45] were performed using a J.A.Woollam UV-IR ellipsometer, with an energy range of $0.7 - 5$ eV. We note that the size of the light beam used by this equipment requires a relatively large non-grained graphene patch, which can be challenging to find on a graphene surface assuming such a patch exists. This consideration will offer us insight into the precision of this method for materials with a small sample size.

In order to model the glass underneath (ϵ_2 in Eq. 2.35) we use experimental data for the frequency-dependent dielectric function $\epsilon_2(\omega)$, and model it via the Sellmeier equation, which is often used to model dielectric functions for light frequencies near the visible spectrum:

$$\epsilon_{2r}(\lambda) = 1 + \frac{B_1\lambda^2}{\lambda^2 - C_1} + \frac{B_2\lambda^2}{\lambda^2 - C_2} + \frac{B_3\lambda^2}{\lambda^2 - C_3} \tag{4.2}$$

where $\lambda = 2\pi/\omega$ is the wavenumber corresponding to the frequency ω, and the coefficients B_n, C_n are determined according to the model fit. Substrate materials in ellipsometry are chosen for their lack of absorption at low frequencies, hence the fact that our glass only has a real part to its dielectric function.

Given that the controlled variables in our experimental ellipsometric setup will be the angle of incidence and the in-plane frequency, our ellipsometric measurements will yield an optical ($q \to 0$) limit conductivity i.e. $\sigma(\omega)$. Is this sufficient to model graphene at low energies? We have answered this question in the low energy regime, where the universal absorbance of frequencies is wavenumber- and frequency- independent. The region where the linear dispersion model begins to break down is approximately 1 eV, after which the

hydrodynamic model for the $\pi \rightarrow \pi*$ plasmon, which we will find has a resonance near 4 eV, should achieve a better fit, with our spectrometer having an energy range up to 5 eV.

For the π electrons, let us combine our result from Eq. 3.40 for the polarizability of the π fluid with our relation Eq. A.35. This yields

$$\sigma_\pi(q,\omega) = -i\omega \frac{n_\pi^0/m_\pi^*}{\omega_{\pi r}^2 + s_\pi^2 q^2 - \omega(\omega + i\gamma_\pi)}. \tag{4.3}$$

Although it is tempting to rid ourselves of the term that results from pressure due to Thomas-Fermi and Dirac exchange interactions, we are no longer in the regime of applicability of the optical limit as defined in Eq. 3.22. Instead, the wavevector that is derived from the incident light response in ellipsometry has the form

$$q_{photon} = \frac{\omega}{c}\cos\theta, \tag{4.4}$$

which depends on the angle of incidence θ. Although we could include this in our approach, we avoid it for two reasons. The first is that in this high-energy plasmon regime, the coupling of the wavevector of the photon to that of the hydrodynamic plasmon may not be as straightforward as letting $q = q_{photon}$, and including this plasmon polariton requires a more in-depth treatment [33]. The second objection is the sense of scale, as $(s_\pi/c)^2$ is a small factor given the speed of propagation due to quantum effects is not as sizable as the speed of light. We must be careful with this statement however, as we saw in Section 2.2.1 that a metal/air or metal/glass system has the ability to sustain plasmonic modes that cause the wavenumber to approximate electrostatic behaviour, sending the system into the $q \rightarrow \infty$ regime. Thankfully, the coupling of photons to plasmons in graphene [3] is limited to small q behaviour thanks to the Landau damping that occurs for energies above the interband threshold of approximately 1 eV. For these reasons our equation for $\sigma_\pi(q,\omega)$ (and likewise for σ_σ, by the same logic) is effectively q-independent in the context of ellipsometric measurements.

4.2 Electron Energy Loss Spectroscopy

A low-loss electron energy loss spectroscopic analysis of graphene aims to use inelastic scattering of an electron beam to determine modes of energy loss in our medium (surface). This technique has the ability to map the modes of loss for up to 50 eV, allowing us to investigate both the π and σ plasmon regions, areas where the collective oscillation of electrons makes scattering at such energies occur with high frequency. We have before expressed our desire to map the response in this region via a hydrodynamic model, but we must use experimental data to verify that the two-fluid plasmons we have predicted do in fact exist. To start, we must know how one can relate the collective modes and their related polarization to the energy loss at various energies.

We begin with a straight-line trajectory for our electron, heading toward a two dimensional planar graphene sheet, thereby creating an external charge density

$$\rho_{ext} = Ze\delta(\vec{r} - \vec{v}_\parallel t)\delta(z - v_\perp t) \tag{4.5}$$

where $Z = -1$ for an electron and $\vec{v}_\parallel$ and $\vec{v}_\perp$ are velocity components parallel and perpendicular to the plane of graphene. For graphene at height $z = 0$, the induced potential will

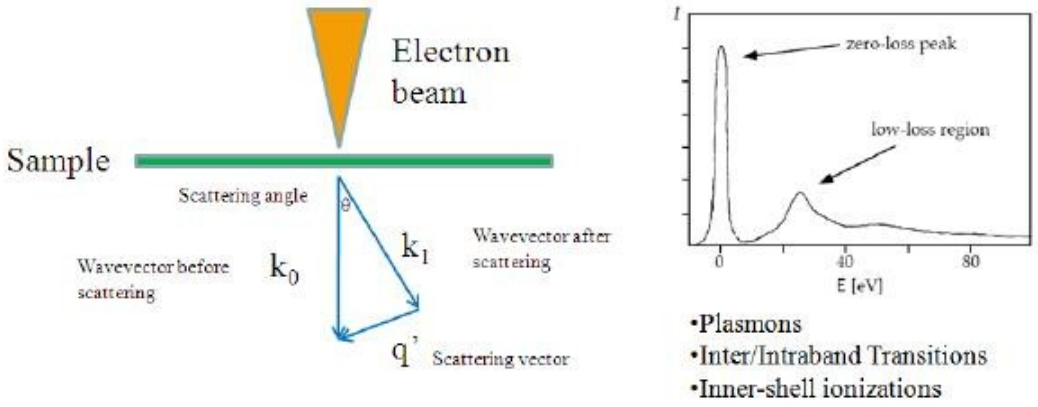

Figure 4.1: In the low-loss regime, electrons incident to the system geometry interact with interband transitions, intraband transitions and plasmon absorption in the 0-50 eV range. Beyond this, the core-loss region absorbs energies on the level of atomic bonding. The Zero Loss Peak (ZLP) comes about due to electrons that do not interact or scatter with the material, interfering with the analysis of behaviour in the 0-2 eV region. Figure adapted from [45]

decay away from z, as can be seen via the Fourier transform of the external charge density above:

$$\widetilde{\Phi}_{ind}(\vec{q}, z, \omega) = -\frac{2\pi e}{q}\widetilde{n}_1(\vec{q}, \omega)e^{-q|z|}, \tag{4.6}$$

similar to Eq. A.41 for $z = 0$, as $\widetilde{n}_1(\vec{q}, \omega)$ is the induced charge-carrier density on graphene (with $e > 0$). The polarizability now comes directly from its definition in Fourier space (recalling it is a response function),

$$\widetilde{n}_1(\vec{q}, \omega) = e\Pi_0(\vec{q}, \omega)\left[\widetilde{\Phi}_{ind}(\vec{q}, z, \omega) + \widetilde{\Phi}_{ext}(\vec{q}, z, \omega)\right]\Big|_{z=0}, \tag{4.7}$$

where $\Pi_0(\vec{q}, \omega) = -\chi(\vec{q}, \omega)$, the polarizability of the graphene sheet. Given the external charge density ρ_{ext}, we can also compute the external potential in Fourier space due to the moving electron

$$\widetilde{\Phi}_{ext}(\vec{q}, z, \omega) = \int d^2\vec{r}e^{i\vec{q}\cdot\vec{r}}\int dte^{i\omega t}\int d^2\vec{r}'dz'\frac{Ze\delta(\vec{r} - \vec{v}_\parallel t)\delta(z - v_\perp t)}{\sqrt{(\vec{r} - \vec{r}')^2 + (z - z')^2}} \tag{4.8}$$

$$= \frac{4\pi Zev_\perp}{(qv_\perp)^2 + (\omega - \vec{q}\cdot\vec{v}_\parallel)^2}e^{i(\omega - \vec{q}\cdot\vec{v}_\parallel)z/v_\perp}. \tag{4.9}$$

Combining the above three equations then yields

$$\widetilde{n}_1(\vec{q}, \omega) = -ZK(q, \omega - \vec{q}\cdot\vec{v}_\parallel)\left[\frac{1}{\epsilon(\vec{q}, \omega)} - 1\right] \tag{4.10}$$

where

$$K(q, \omega) = \frac{2qv_\perp}{(qv_\perp)^2 + \omega^2} \tag{4.11}$$

is called the kinematic factor, and as shown in Eq. A.36, there is a relation between the dielectric function and the polarizability, with $v(q) = 2\pi e^2/q$ in electrostatic units.

We still have to relate this expression to the energy loss experienced by the particle, which by definition is

$$\frac{dE_{loss}}{dt} = \int d^3\mathbf{r}\vec{j}_{ext}(\mathbf{r},t)\cdot\vec{E}_{ind}(\mathbf{r},t) \tag{4.12}$$

$$= -\int d^3\mathbf{r}\Phi_{ind}(\mathbf{r},t)\nabla\cdot\vec{j}_{ext}(\mathbf{r},t) \tag{4.13}$$

$$= \int d^3\mathbf{r}\left(\frac{\partial\rho_{ext}}{\partial t}\Phi_{ind} + \rho_{ext}\frac{\partial\Phi_{ind}}{\partial t} - \rho_{ext}\frac{\partial\Phi_{ind}}{\partial t}\right) \tag{4.14}$$

$$= \frac{d}{dt}\left(\int d^3\mathbf{r}\rho_{ext}\Phi_{ind}\right) - \int d^3\mathbf{r}\rho_{ext}\frac{\partial\Phi_{ind}}{\partial t} \tag{4.15}$$

where we implicitly used the definition of the potential Φ_{ind} under the Coulomb gauge and the continuity equation. Only the second component of this equation is the result of dissipation, as can be seen by the placement of the total time derivatives. Integrating over all time and transforming the dissipative equation to two-dimensional Fourier space gives

$$E_{loss} = i\omega\int\frac{d^2\vec{q}}{(2\pi)^2}\int\frac{d\omega}{2\pi}\int dz\widetilde{\Phi}_{ind}(\vec{q},z,\omega)\int d^2\vec{r}\int dt e^{i(\vec{q}\cdot\vec{r}-\omega t)}\rho_{ext}(r,z,t) \tag{4.16}$$

$$= i\int_0^\infty d\omega\omega\int\frac{d^2\vec{q}}{q}\left(\frac{(Ze)^2}{2\pi^2}K(q,\omega-\vec{q}\cdot\vec{v}_\parallel)\left[\frac{1}{\epsilon(\vec{q},\omega)}-1\right]\right)$$

$$\times\int dt\int d^2\vec{r}\int dz e^{i(\vec{q}\cdot\vec{r}-\omega t)}e^{-q|z|}\delta(\vec{r}-\vec{v}_\parallel t)\delta(z-v_\perp t) \tag{4.17}$$

$$= \int_0^\infty d\omega\omega P_1(\omega) \tag{4.18}$$

where the probability density of losing energy ω due to the graphene is

$$P_1(\omega) = \frac{(Ze)^2}{2\pi^2}\int\frac{d^2\vec{q}}{q}K^2(q,\omega-\vec{q}\cdot\vec{v}_\parallel)\Im\left[-\frac{1}{\epsilon(\vec{q},\omega)}\right]. \tag{4.19}$$

The factor $\Im[-1/\epsilon(\vec{q},\omega)]$ is called the loss function, and will be used in Chapter 5 to analyze energy loss due to plasmons on or near rough surfaces. Since we are working with normal electron incidence, $v_\parallel = 0$, and as graphene polarizability is close to being isotropic, we invoke $\Pi_0(\vec{q},\omega) = \Pi_0(q,\omega)$. From an experimental point of view, the integration of our wavenumber is limited by the acceptance angle of the apparatus (i.e. its ability to measure q in the below Figure), but since our kinematic factor $K(q,\omega)$ is strongly peaked at the value $q = \omega/v_\perp \ll q_c$, with q_c being the acceptance wavenumber, we can extend our integration to infinity.

Under these assumptions, we are able to write our loss probability as

$$P_1(\omega) = \frac{4e^2}{\pi v_\perp^2}\int_0^\infty dq\frac{q^2}{\left[q^2+(\omega/v_\perp)^2\right]^2}\Im\left[\frac{-1}{1+\frac{2\pi e^2}{q}\Pi_0(q,\omega)}\right]. \tag{4.20}$$

Now that we have a way to model EELS using graphene's polarizability, we wish to again ask ourselves whether the $q \to 0$ limit is sufficient for our uses. Similar to the ellipsometric

case in Section 4.1, we are able to say the speed of propagation due to quantum effects is $s_\nu \ll v_\perp$, given that our kinematic factor is peaked at $q = \omega/v_\perp$, allowing us to effectively use the wavenumber-independent conductivity.

This factor $P_1(\omega)$ is, however, only a probability, and many of the electrons passing through the graphene will not experience any sort of interaction. Although graphene has miraculously high absorbance for its dimension (approximately 2.3% as shown in Section 3.2.1), there is still a very large proportion of electrons that will be detected near 0 eV. This is known as the zero-loss peak (ZLP), and it obstructs the ability of EELS to obtain any resolution near the area between 0 and 2 eV. This is a large motivation behind using the high-resolution ellipsometric data for monolayer graphene, which is able to resolve this area clearly.

Efforts are made [45] for our data to make careful subtraction of this peak. For this task, we must note that we expect little graphene interaction for electrons below 1 eV (see Fig. 3.4) as the losses below this energy are minimal. We also expect the energy loss to be zero for zero frequency. A careful cubic interpolation removes the ZLP for these electrons, but we continue to observe a delta-like peak at approximately 2 eV (see Fig. 4.2). We posit in this thesis that this is due to interband transitions that dominate for lower energies, the same that give the universal absorbance for all frequencies. Some ab initio calculations [9] have yielded a similar low energy peak. The position of this peak near 1 eV is a result

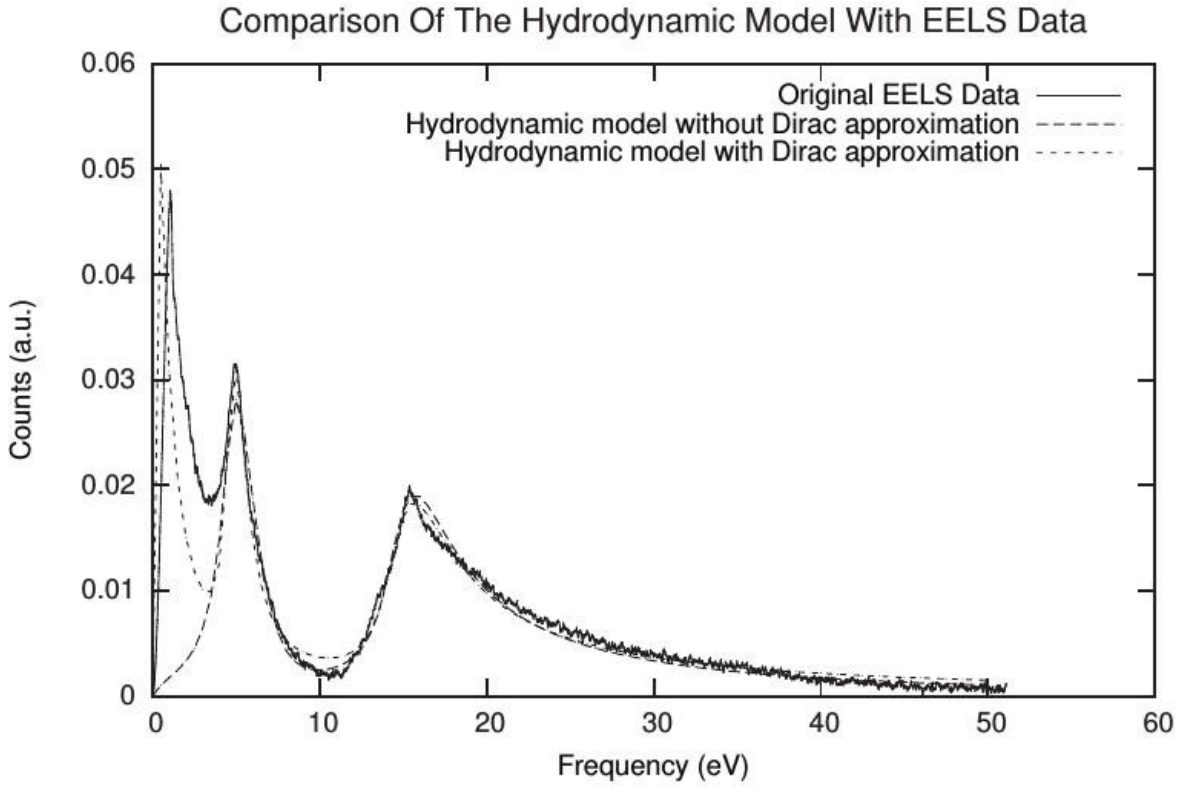

Figure 4.2: Shown are the data for EELS with the ZLP peak subtracted, along with our hydrodynamic model without the Dirac cone approximation and with it. The removal of the ZLP leaves behind a large peak, which we posit is due to the interband transitions present in low-energy graphene. Figure adapted from [36]

Hydrodynamic Parameters	Units	Pi-Plasmon	Sigma-Plasmon
n_ν^0	nm^{-2}	38.09	114.28
$\omega_{\nu r}$	eV	4.624	14.14

Table 4.1: Conductivity Parameters for Hydrodynamic Model in Section 4.2.1.

of the low-wavenumber integration over the loss function, compared to the position of the hydrodynamic peaks, which are due to being near their respective plasmon resonances. This means, for example, that if graphene had twice the universal conductivity σ_0, the peak would increase (due to more losses) but its frequency would not change. It also means the position of this peak will not depend on the electron incident velocity $v_\perp$. Corrections due to doping in the graphene however may have the ability to shift the peak for this low energy.

From an experimental point of view, we note that EELS requires a much smaller area of monolayer graphene than ellipsometry to perform accurate measurements [11]. These EEL spectra were collected in an aberration-corrected scanning transmission electron microscope, Nion UltraSTEM 100 [31]. The microscope was operated at 60 kV acceleration voltage in order to avoid knock-on damage of the lattice. A 30 mrad convergence angle, a 15 mrad collection aperture, an energy dispersion of 0.05 eV/pixel, and an electron beam with an energy resolution of 350 meV were used in the experiments.

4.2.1 Combining the Two Conductivities

The combination of two conductivity regimes requires some guesswork, as there is a lot of graphene physics occurring between in the 0-5 eV range that must be estimated using a combination of the well-understood Dirac term stemming from quantum level absorption modes and with the semi-classical two-fluid hydrodynamic flow for higher energy regimes. Our main requirement is that there is a continuous transition between the conductivities. We look at the absorbance, which is given by Eq. 2.40:

$$A = \frac{4\pi}{c}\Re\sigma(\omega), \tag{4.21}$$

noting that the universal conductivity due to the Dirac term is $\sigma_0 = 1/4$ in Gaussian units. We perform a phenomenological fit to the parameters in Fig. 4.2 for our data (see Table 4.1) and proceed to use these terms, along with the assumption that our graphene isn't doped by any impurities ($E_F = 0$), to see the absorbance data under different combinations of conductivity terms. We justified the undoped assumption phenomenologically by seeing its effect on the EELS data and by seeing the agreement with the absorption data for low energies with experiment.

Using only the hydrodynamic model, we observe zero absorbance by the graphene of low energy photons, with a peak near the π plasmon of approximately 4.62 eV, giving around 14% absorbance. By adding in the constant 2.3% absorbance we expect due to interband effects for undoped graphene in the low energy regime, this peak absorbance elevates to around 16%. A compromise between the models utilizes the Heaviside functions to separate the two regimes:

$$\sigma(\omega) = \sigma_{low}\Theta(\omega_c - \omega) + (\sigma_\pi + \sigma_\sigma)\Theta(\omega - \omega_c) \tag{4.22}$$

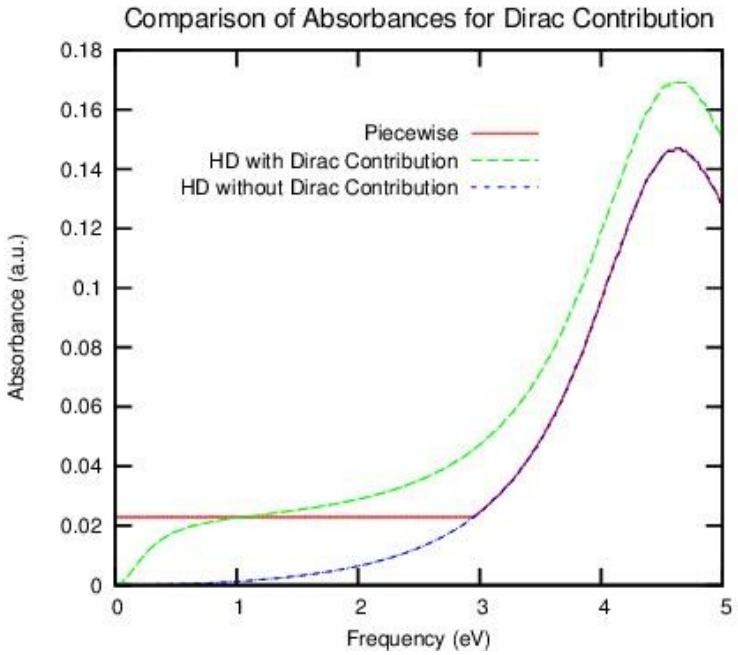

Figure 4.3: Comparison of absorbances for the HD model with and without the Dirac term, along with a piecewise combination of the two at approximately 3 eV to ensure continuity of the real part of the conductivity, which controls dissipation modes and hence absorbance.

where $\sigma_{low}(\omega)$ is defined in Eq. 3.27 for the low energy regimes, and $\sigma_\nu(\omega)$ is shown in Eq. 4.3 (with an analogous relation for the σ bonds). The intersection point of these two regimes is shown to be $\omega_c \approx 3$ eV, which is beyond the validity of the linear dispersion model near the Dirac cone, showing the simplicity of this assumption.

Experimental absorbance data [30] gives a similar peak near the value of 4.5 eV as we have in Table 4.1, and gives an asymmetry as given in the hydrodynamic model, but the experimental peak absorbance is approximately 8%, which could be due to contamination or rippling of the graphene. Unrippled pure graphene is expected to give the highest absorbance due to the collective flow of electrons in a low-dimensional system. One can then ask why the graphene continues to show around the same universal 2.3% absorbance for energies below 2 eV in experiment. This is an open question, and requires an in-depth investigation into the effect of impurities on the absorption spectra for this material. Other theoretical treatments of the absorption of graphene in this region have yielded similarly high peaks.

Due to the experimental data showing both universal absorbance and a slightly lower absorption peak, we wish to choose our Heaviside model from the above equation when checking our ellipsometric data. However, unlike for our absorption measurements, which show that the continuity of the *real* part of the conductivity for some ω_c can be achieved, this continuity does not carry over into the realm of $\Im\sigma(\omega)$. We will therefore choose the combined HD and Dirac models without the Heaviside function, keeping in mind the increased peak will predict more absorption of a certain polarization of light.

4.2.2 Checking the Ellipsometric Data

One of our main goals - that of verifying phenomenologically that the two-fluid hydrodynamic model gave an excellent fit for the plasmon peaks due to graphene's symmetry points

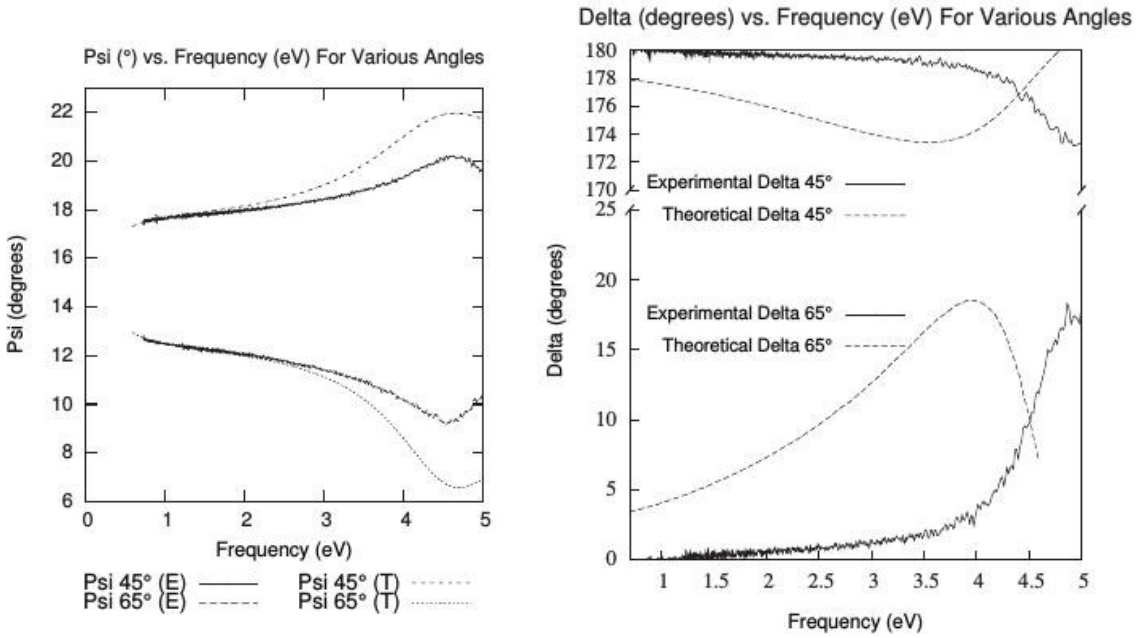

Figure 4.4: Theoretical and experimental plots of the ellipsometric parameters Δ and ψ for $\theta = 45^\circ$ and $\theta = 65^\circ$. (a) The conductivity of the graphene plays a large role in shifting ψ, more so than the energy dependent dielectric of glass. The interband contribution gives very good agreement between 0 and 3 eV, but the effect of the π-plasmon over-contributes to the polarization change. (b) This plot is broken in half to outline the ranges of angles we are investigating. Notice that due to the over-contribution, there is a flip in sign of Δ for $\theta = 45^\circ$, near 4.7 eV. For this phase shift, the Dirac contribution is eclipsed by the π-plasmon. Adapted from [36]

- has been accomplished. On top of this result, we claim that the removal of the ZLP leaves a peak that, rather than being an artifact of the removal, is evidence that the interband transitions show up in the blurred portion of the EELS spectra. To verify our parameters in this blurred region, we will compare our EELS-derived parameters for both this universal term and the 4.6 eV π-plasmon with the help of our ellipsometric data, Δ and ψ.

To recap, we input the combined conductivity $\sigma_{low} + \sigma_\pi + \sigma_\sigma$ into Eqs. 2.35 and 2.38 for the reflection coefficients of r_p and r_s, plug these factors into Eq. 4.1 and compare the values Δ and ψ to their experimentally measured values from [45]. Many angles of incidence were taken, which in Eqs. 2.35 and 2.38 changes κ_{1z} and κ_{2z}. As an example we present the angles 45° and 65°, which are indicative of the other angles between 45° and 70°, taken in 5° steps, which were measured. We note an almost mirror shift between the data of the two angles - this is due to the existence of a Brewster's angle around 60°, causing our s-polarization to disappear upon reflection i.e. $r_s = 0$.

Figure 4.4 shows side by side the values for the ellipsometric parameters Δ and ψ. Starting with ψ, the more robust of the two measurements, shows the theoretical combined HD model closely following the experimental measurement for the difference in polarized light. We anticipated that an overshoot of the π-plasmon peak would occur due to the high theoretical absorbance versus the lower experimental one due likely to contamination and rippling of the graphene sheet. In fact, by including a multiplicative factor $f = 0.5$ to the conductivity of the π-fluid σ_π in order to make the absorbance peak around 8 eV in Fig. 4.3

to match experiment, the fit to the value ψ at all angles θ is a perfect match.

The reason for this disparity can be linked to any number of factors. As the graphene in both ellipsometry and EELS is grown via Chemical Vapor Deposition (CVD), the location of water and other impurities between the graphene sheet and the glass substrate may play a large role in the changing of the reflective properties for higher energies more so than lower ones. Ripples in the graphene and its three-dimensional topology can influence the way that light comes back to the detector [54], dispersing after hitting the ripples rather than following a straight line trajectory to the ellipsometer. This effect is evidently one which would not influence the EELS measurements as much due to the incident trajectory of fast moving electrons in that setup.

Figure 4.4 also shows a theoretical plot for the parameter Δ. Here, our theoretical model, despite well approximating the magnitude of the phase shift between the r_p and r_s coefficients before and after the measurement by the ellipsometer, does not fit particularly well at any given energy. The largest phase shift experimentally occurs near 4.8 eV, whereas our theoretical treatment peaks around 4 eV. This may once again be due to factors such as contamination and rippling which do not factor in as much into the measurements for EELS.

Extraction of the refraction index $n(\omega) = \sqrt{\epsilon(\omega)}$ from [45], assuming a graphene monolayer with thickness 3.35nm and using the three-dimensional Fresnel equations, was able to obtain a dielectric function for graphene (with real parts of the function determined through Kramers-Kronig relations [10]) that was then used to determine the absorbance of the graphene in this model. The calculated absorbance matched well with previous experiments [30], with a peak around 8 eV. Although we are assuming a two-dimensional graphene layer, we know experimentally about the presence of impurities that enter below the graphene sheet. This is especially valid in Spectroscopic Ellipsometry (SE), where the experimental setup is exposed to air. Also, the presence of a third layer between the graphene and the substrate would likely have a strong effect on the phase shift of polarized light (due to the transmission/reflection at multiple surfaces rather than just one) while not having a large effect on the magnitude of the shift ψ from polarization of the graphene electrons.

In order to implement our three-layer approximation, we will make the assumption that the layer between the graphene and the substrate can be described by a local dielectric function $\epsilon_{layer}(\omega)$. We have before computed the matrices $M^{(p)}$ and $M^{(s)}$ in Section 2.1.3, describing the reflection of light for a system with graphene on top of the substrate. Using a transfer matrix formalism [60], we are able to describe in a similar way the reflection due to multiple layers. Although our $M^{(p)}$ and $M^{(s)}$ defined relations are between the first and second layer, we can generalize these relations, such that

$$\begin{bmatrix} a_2 \\ b_2 \end{bmatrix} = M_{2/3}^{(p,s)} \begin{bmatrix} a_3 \\ b_3 \end{bmatrix} \qquad\qquad \begin{bmatrix} a_1 \\ b_1 \end{bmatrix} = M_{1/2}^{(p,s)} \begin{bmatrix} a_2 \\ b_2 \end{bmatrix} \tag{4.23}$$

where a change of indices for the original $M^{(p)}$ and $M^{(s)}$ fully generalizes the result. We notice that the coefficients a, b have different meanings for s and p polarization. To account for the gap that forms between the graphene and substrate Δz, we use a 2×2 propagation matrix that gives the change in the propagation of light through the material. The overall matrix relating a_1 and b_1 (coefficients of light propagation through the first material) to a_3

and b_3 is given by

$$\begin{bmatrix} a_1 \\ b_1 \end{bmatrix} = M_{1/2}^{(p,s)} \begin{bmatrix} e^{-i\kappa_{2z}\Delta z} & 0 \\ 0 & e^{i\kappa_{2z}\Delta z} \end{bmatrix} M_{2/3}^{(p,s)} \begin{bmatrix} a_3 \\ b_3 \end{bmatrix} = \mathcal{M}^{(p,s)} \begin{bmatrix} a_3 \\ b_3 \end{bmatrix}. \tag{4.24}$$

Using this matrix $\mathcal{M}$ allows us to generalize to three-layers our reflectance and transmission coefficients

$$r_{p,s} = \frac{\mathcal{M}_{21}^{(p,s)}}{\mathcal{M}_{11}^{(p,s)}} \qquad\qquad t_{p,s} = \frac{1}{\mathcal{M}_{11}^{(p,s)}} \tag{4.25}$$

where the indices represent the elements of the 2×2 transfer matrix $\mathcal{M}$.

Unfortunately, for estimated values of ϵ between 1 and 2.5 (the dielectric function for many glass-like materials), and Δz between 1 and 3.35nm (the average 'thickness' of graphene due to its carbon atoms and perpendicular π orbitals), there is no significant change in our results from Fig. 4.4 for ellipsometry. This simplistic model ignores the possibility of polarizable media, especially water, which has an ϵ near 40. Other dielectric media are possible, but then the question arises why they do not shift the ψ if they have absorbant modes in the 0-5 eV range. Future work into the effects of contaminants on the ellipsometric response is needed for a fuller picture.

Briefly, the effects we expect from contamination are the following: for EELS, there are more opportunities for scattering events given more scatterers, and contamination is therefore believed to artificially raise the loss spectra. Analysis [45] shows that most of the spectra due to contamination comes for energies larger than 5 eV. Other effects such as rippling could serve to raise all the spectra due to $q \to 0$ being a bad approximation if many scatterers exist. We also have the fact that ellipsometric measurements require a larger area than those for EELS and are therefore more likely to use contaminated graphene, giving a plausible reason for a shift in the overall theoretical predictions. If the experimental EELS overestimates the magnitude of $\sigma_{\pi,\sigma}$, we would see a lower absorbance that matches with experiment, and a less-influential π-plasmon would, as mentioned, give better agreement with ψ.

Verifying these speculations is outside the current viable experimental realm of perfectly clean graphene and outside phenomenological models that serve to give an approximate behaviour for energy absorption and dissipation modes inside graphene.

4.3 f-sum Rule

We conclude this section by investigating the f-sum rule, mentioned in Sections 3.2.2 and 3.2.4. This is a conservation law stemming from the conservation of particle number for a given Hamiltonian. The logic is that the effect of the conductivity in graphene is to induce a planar current from an applied electric field i.e. to move electrons around. This constitutive function, and the Hamiltonian from which it was derived as an addition to the ground state energy of the system, must therefore preserve the total number of particles in the system. This applies as well to the case of quasi-particles, which have finite lifetimes, since our assumption about the Fermi liquid from which both RPA and our hydrodynamic models stem require a fixed number of particles.

The f-sum rule reads as [52]

$$\int_0^\infty \Re[\sigma(\omega)] d\omega = \frac{\pi e^2}{2m_e} n_{at} N_e \tag{4.26}$$

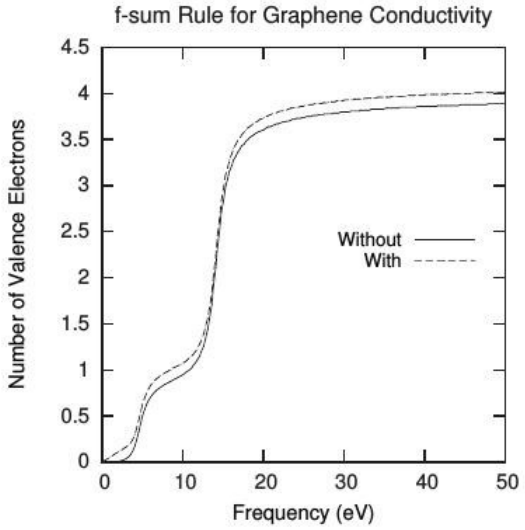

Figure 4.5: f-sum rule showing the availability of valence electrons to participate in the system. The inclusion of the Dirac term in the conductivity $\sigma(\omega) = \sigma_{low} + \sigma_\pi + \sigma_\sigma$ gives values commensurate with the expected valence electron numbers from the carbon electrons in σ and π orbitals. Figure adapted from [36]

where m_e is the mass of the electron, $n_{at} = n_\pi^0 + n_\sigma^0$ is the atomic areal density of graphene particles (noting that $3n_\pi^0 = n_\sigma^0$, as there are 3 more σ electrons than π for each carbon atom, see Table 4.1), and N_e is the number of valence electrons per carbon atom. For high energies, N_e should approach 4, as the increased frequencies allow for previously trapped electrons to flow as if behind a background of positive ions.

We can use this rule to define the number of valence electrons that participate in excitations up to a certain energy Ω [1]:

$$N_e(\Omega) = \frac{2m_e}{\pi e^2 n_{at}} \int_0^\Omega \Re[\sigma(\omega)] d\omega. \tag{4.27}$$

We see in Figure 4.5 the comparison between our hydrodynamic model with and without the additional Dirac term for undoped graphene ($E_F = 0$). The number of valence electrons suitably jumps near the plasmon peaks now that there are more valence electrons that can be involved in different types of excitations. The addition of a new mode of transition for electrons with the Dirac term increases is seen to universally increase the curve in Figure 4.5, as expected for a universal absorbance. Our number of valence electrons $N_e(\Omega)$ plateaus at 1 and 4, given the one π-electron and three σ-electrons involved in graphene bonding. This graph matches with theoretical predictions obtainable from band energy diagrams [40] about the value for $N_e(\Omega)$.

The f-sum rule lends support that the phenomenological hydrodynamic parameters we fit to the data for EELS (see Table 4.1) correctly match with the expected number of valence electrons for graphene, suggesting a clean graphene surface that yields the correct number of counts experimentally.

Chapter 5

Effects of Roughness on Graphene Plasmons

There are many elements to our investigation of how roughness on both the graphene and substrate surfaces we consider changes plasmons. How the roughnesses of the surfaces interact, the image potential effect that the substrate has on the graphene plasmons, and electronic effects present due to the crumpling and deformation of the surfaces. We investigate these properties one by one.

5.1 Characterization of Rough Surfaces

At the heart of our study are planar surfaces with stochastic height profiles. This is expected on the nano-scale, where current fabrication limits and physical properties regarding the size of atoms mean that an ideal flat surface is always just out of reach. Let us consider as an example our dielectric substrate, which, assuming it is translationally invariant, can be partially described in the following manner [13]:

$$\langle h_s(\vec{r})\rangle = 0 \tag{5.1}$$

$$\langle h_s(\vec{r})h_s(\vec{r}')\rangle = \sigma^2 C(|\vec{r}-\vec{r}'|) \text{ with } \sigma^2 = \langle h_s(\vec{r})^2\rangle \tag{5.2}$$

where $h_s(\vec{r})$ is the height in the z-direction of the graphene at the point $\vec{r}$ in the xy-plane. The averaging brackets $\langle\rangle$ are shorthand for an integration over all realizations over the surface. We note throughout the chapter the use of vector notation for two-dimensional quantities restricted to the plane.

From a probabilistic perspective, all random processes have probabilities attached to them, described by the distribution function

$$F(x,\vec{r}) = P(h_s(\vec{r}) \leq x) \tag{5.3}$$

describing the probability of the height being less than the value x. The probability density function (PDF) at the point $\vec{r}$ is then

$$f(x,\vec{r}) = \frac{\partial F(x,\vec{r})}{\partial x}. \tag{5.4}$$

We are also concerned probability-wise about how different points on a surface correlate with each other. We define the joint probability distribution to be

$$F(x_1,x_2,\vec{r},\vec{r}') = P(h_s(\vec{r}) \leq x_1, h_s(\vec{r}') \leq x_2) \tag{5.5}$$

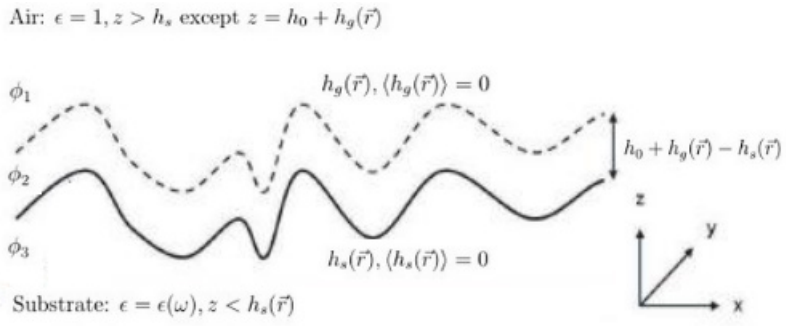

Figure 5.1: Double rough surface problem, with the mean difference between the graphene and substrate being h_0. $h_s(\vec{r})$ and $h_g(\vec{r})$ are stochastic height variations from the means 0 and h_0 for substrate and graphene, respectively. The values ϕ_1, ϕ_2 and ϕ_3 label the potentials in different regions when we seek to solve Laplace's equation for each potential. The vector $\vec{r}$ rests in the xy-plane. Adapted from [8]

and the joint PDF, describing the probability of two things happening at once, as

$$f(x_1, x_2, \vec{r}, \vec{r}') = \frac{\partial^2 F(x_1, x_2, \vec{r}, \vec{r}')}{\partial x_1 \partial x_2}. \tag{5.6}$$

These PDFs act as a sort of instantaneous probability, and they hence allow us to compute the 'moments' of our stochastic function:

$$\langle h_s(\vec{r})\rangle = \int_{-\infty}^{\infty} x f(x, \vec{r}) dx \tag{5.7}$$

$$\langle h_s(\vec{r}) h_s(\vec{r}')\rangle = \int_{-\infty}^{\infty}\int_{-\infty}^{\infty} x_1 x_2 f(x_1, x_2, \vec{r}, \vec{r}') dx_1 dx_2. \tag{5.8}$$

The first is called the mean, and the second the autocorrelation (versus regular correlation, where the two variables are not necessarily the same). This autocorrelation, as can be seen in the joint probability distribution, gives an average behaviour for how two heights on the surface are correlated. We expect of course for points $\vec{r}, \vec{r}'$ close to each other that they will be more correlated than if they were far away. This relationship will be reflected in our choice for $C(|\vec{r} - \vec{r}'|)$.

Higher-order moments can be similarly defined by determining a PDF and then integrating over all realizations of it, giving a correlation between larger collections of the stochastic process. So, for example, the function $\langle h_s(\vec{r}) h_s(\vec{r}') h_s(\vec{r}'')\rangle$ defines the correlation between three points on the surface $\vec{r}, \vec{r}', \vec{r}''$. A stochastic process is said to be fully described if all its moments are known, but of course there are infinitely many. To relate these higher moments to the first and second moments (mean and autocorrelation) we implement the Gaussian property, which says that all odd-numbered moments are zero, while all even-numbered moments are equal to the sum of the products of all permutations of h_s as paired in autocorrelation functions. For example,

$$\begin{aligned}\langle h_s(\vec{r}) h_s(\vec{r}') h_s(\vec{r}'') h_s(\vec{r}''')\rangle &= \langle h_s(\vec{r}) h_s(\vec{r}')\rangle \langle h_s(\vec{r}'') h_s(\vec{r}''')\rangle \\ &+ \langle h_s(\vec{r}) h_s(\vec{r}'')\rangle \langle h_s(\vec{r}') h_s(\vec{r}''')\rangle + \langle h_s(\vec{r}) h_s(\vec{r}''')\rangle \langle h_s(\vec{r}') h_s(\vec{r}'')\rangle. \end{aligned} \tag{5.9}$$

This theorem, a generalization of Bourret's treament of higher order moments [5], comes from the assumption that h_s follows a multivariate distribution function, where it is known

that only the mean and covariance matrix are needed to define all moments. These higher moments for certain problems will be of the order of the autocorrelation and must be treated carefully, and one of the models presented later involves our using a non-perturbative (i.e. using every moment of a stochastic process) approach to solving a problem involving the broadening of a plasmon frequency [14].

A crucial assumption we make about the macroscopic behaviour of both substrate and graphene in this thesis are their translational invariance - that on average the surface is expected to look the same everywhere. This also means there is no directional or positional dependence on any of our stochastic moments, allowing us to say, for example, that the autocorrelation only depends on $|\vec{r} - \vec{r}'|$. Although the substrate is not expected to change its structure given plasmon movement, the flexibility of the graphene likely means that its structure changes due to the interactions of strongly coupled oscillating modes, which is beyond the scope of this paper. Therefore we will make the simplifying assumption that both surfaces are translationally invariant.

We will also assume that the substrate and graphene interfaces are infinitely long. This ties in with our assumption of translational invariance, as edges are a sort of 'breeding ground' for strong plasmonic behaviour [58]. This will also simplify our transformation of our potential equations into Fourier space, a transform that highlights the effect that certain characteristic wavenumbers on the rough surface have on the graphene plasmon close to its resonance. This assumption can be justified given the locality of plasmonic effects away from the edges of a genuine graphene sample.

From an experimental point of view, it is important to point out the ergodic theorem for stationary processes. This theorem says that to determine a moment of a stationary stochastic variable (stationary in this case meaning the moment dependence is only on $|\vec{r} - \vec{r}'|$, i.e. translational invariance), it is sufficient to measure the value of $h_s(\vec{r})$ at all $\vec{r}$, and then take the arithmetic mean (i.e. use the averaging brackets $\langle\rangle$) of n-products to obtain the n-th moment. Since it is impossible experimentally to determine the value of roughness at infinitesimally small points, the moments can be defined via a limiting process

$$\langle h_s(\vec{r})\rangle = \lim_{T\to\infty} \frac{1}{4T^2} \int_{-T}^{T}\int_{-T}^{T} h_s(x,y)dxdy \tag{5.10}$$

$$\langle h_s(\vec{r})h_s(\vec{r}+\vec{r}')\rangle = \lim_{T\to\infty} \frac{1}{4T^2} \int_{-T}^{T}\int_{-T}^{T} h_s(x,y)h_s(x+x',y+y')dxdy \tag{5.11}$$

for $\vec{r} = (x,y)$ and $\vec{r}' = (x',y')$. This is one way of saying the experimenter can measure heights at various points and stochastically average them to obtain an approximate form for any of the moments. We will be using experimental data to determine roughness parameters that govern our surfaces in question.

Wavevectors are a more convenient setting to explore the effects of roughness, so the Fourier transformed surface profile function reads as

$$\widetilde{h}(\vec{k}) = \int d^2\vec{r} \exp\left(-i\vec{k}\cdot\vec{r}\right)h(\vec{r}), \tag{5.12}$$

where $\vec{k} = \hat{x}k_x + \hat{y}k_y$. The moments in k-space become

$$\langle\widetilde{h}(\vec{k})\rangle = 0, \tag{5.13}$$

$$\langle\widetilde{h}(\vec{k})\widetilde{h}(\vec{k}')\rangle = \sigma^2 g(|\vec{k}|)(2\pi)^2\delta(\vec{k}+\vec{k}'), \tag{5.14}$$

while the Gaussian property for higher moments holds just as before, verbatim in k-space. The function $g(|\vec{k}|) = \int d^2\vec{r} \exp(-i\vec{k}\cdot\vec{r})C(|\vec{r}|)$ is the Fourier transformed stationary autocorrelation. This can be seen as:

$$\langle \widetilde{h}(\vec{k})\widetilde{h}(\vec{k}')\rangle = \int d^2\vec{r} \int d^2\vec{r}' e^{-i(\vec{k}\cdot(\vec{r}-\vec{r}')+(\vec{k}+\vec{k}')\cdot\vec{r}')}\sigma^2 C(|\vec{r}-\vec{r}'|) \tag{5.15}$$

so integrating through $\vec{r}'$ forces a $(2\pi)^2\delta(\vec{k}+\vec{k}')$ term in the autocorrelation function.

It is important to note that although our real-space stochastic height profile functions have strictly real values, this is not necessarily so in Fourier space, and we must exercise caution in the difference between $\widetilde{h}(\vec{q})$ and $\widetilde{h}^*(\vec{q}) = \widetilde{h}(-\vec{q})$. The Fourier-space correlation, $g(|\vec{k}|)$, will be real valued as it represents a probabilistic likelihood of two points in k-space to be correlated.

5.1.1 EM Boundary Conditions for Rough Surfaces

Now that we have a stochastic way of describing the surface, we need to use this description to determine modified boundary conditions due to roughness. We start with the assumption of using the quasi-static approximation with the Coulomb gauge, allowing us to describe homogenous media via Laplace's equation. Considering Figure 5.1 we let $h_{s,g}(\vec{r})$ be the height profiles of the surfaces, giving the height at a planar point $\vec{r} = (x, y)$. Then our PDE with boundary conditions reads as

$$\Delta\phi_3(\vec{r}) = 0, \quad z < h_s(\vec{r}) \tag{5.16}$$

$$\Delta\phi_2(\vec{r}) = 0, \quad h_s(\vec{r}) < z < h_g(\vec{r}) \tag{5.17}$$

$$\Delta\phi_1(\vec{r}) = 0, \quad h_g(\vec{r}) < z \tag{5.18}$$

$$\phi_1|_{z=h_s(\vec{r})} = \phi_2|_{z=h_s(\vec{r})} \tag{5.19}$$

$$\phi_2|_{z=h_g(\vec{r})} = \phi_3|_{z=h_g(\vec{r})} \tag{5.20}$$

$$\frac{\partial}{\partial n}\phi_1|_{z=h_s(\vec{r})} - \frac{\partial}{\partial n}\phi_2|_{z=h_s(\vec{r})} = 4\pi\sigma \tag{5.21}$$

$$\frac{\partial}{\partial n}\phi_2|_{z=h_g(\vec{r})} - \epsilon\frac{\partial}{\partial n}\phi_3|_{z=h_g(\vec{r})} = 0 \tag{5.22}$$

$$F\phi_1|_{z\to-\infty} = \phi_3|_{z\to\infty} = 0 \tag{5.23}$$

where

$$\frac{\partial}{\partial n} = \left[1 + \left[\frac{\partial h_{s,g}(\vec{r})}{\partial x}\right]^2 + \left[\frac{\partial h_{s,g}(\vec{r})}{\partial y}\right]^2\right]^{-1/2}\left[-\frac{\partial h_{s,g}(\vec{r})}{\partial x}\frac{\partial}{\partial x} - \frac{\partial h_{s,g}(\vec{r})}{\partial y}\frac{\partial}{\partial y} + \frac{\partial}{\partial z}\right] \tag{5.24}$$

is the normal derivative to the rough surface characterized by $h_{s,g}(\vec{r})$, defined via the relation $\partial f/\partial n = \nabla f(\vec{r})\cdot\mathbf{n}$. Here we adapt the convention that σ is the surface charge density in graphene, which is in a different context than the value σ representing the root mean squared height of the surface in Eq. 5.14. Later we will develop proper perturbative Green's functions that utilize these relations.

5.1.2 Types of Rough Surfaces

The assumptions we have made so far about our rough surfaces have been standard practice: assuming that our surface is large enough that we can ignore edge effects and can say it

	H	σ (nm)	a (nm)
Fractal (G)	0.68	0.22	21.1
Fractal (S)	0.8	0.31	15
Bessel (G)	0.85	0.22	20.4
Bessel (S)	1	0.31	14.5
Gaussian (G)	1	0.22	22.3
Gaussian (S)	1	0.31	15.8

Table 5.1: Fitted values for Fig. 5.2, showing parameters for fractal, Bessel and Gaussian fits to the data. 'G' represents graphene while 'S' is the substrate

is translationally invariant (stationary), along with the subtle point that we have defined a Fourier transformed wavevector dependence that would require a flat surface to properly define. The stationary assumption allows us to determine moments of the stochastic process by an experimental sampling. The last assumption was that our height function would be similar to a multivariate Gaussian distribution, fully characterized by the mean and the autocorrelation. We will investigate three types of autocorrelation, known as Gaussian, Bessel, and Fractal surfaces, along with what is called a healing factor, derived from membrane physics to describe effects of thin films deposited on rougher surfaces [48].

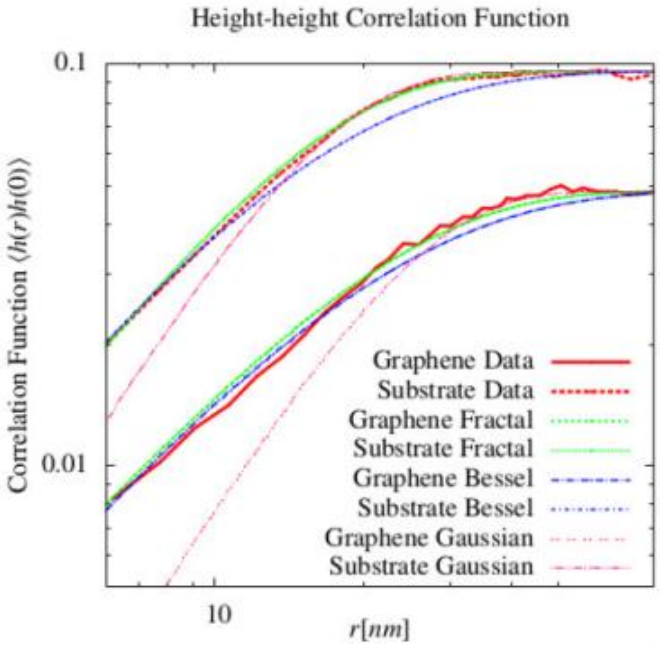

Figure 5.2: Fractal, Bessel and Gaussian correlation functions fitted to experimental data for substrate and graphene surfaces. The substrate follows the pattern $\langle h_s(\vec{r})h_s(\vec{r}')\rangle$ with parameters shown in Table 5.1. Likewise the graphene correlation function $\langle h_g(\vec{r})h_g(\vec{r}')\rangle$ has been shown in the table. The displayed data is in fact $\sigma^2_{s,g} - \langle h_{s,g}(\vec{r})h_{s,g}(\vec{r}')\rangle$. Adapted from [23] and [35]

We introduce the fractal autocorrelation function (the only piece of information we need,

given the mean is defined as 0) as

$$\langle h(\vec{r})h(\vec{r}')\rangle_F = \sigma^2 \exp\left[-\left(\frac{|\vec{r}-\vec{r}'|}{a}\right)^{2H}\right] \tag{5.25}$$

where a is known as the transverse autocorrelation length, as it describes the mean value length between two peaks or two valleys on the surface, while the factor H is known as the fractal dimension. These three parameters quantify how 'random' a surface is. Small values of a correspond to white noise, while large values imply less erratic behaviour. Likewise high σ yields a much rougher surface than $\sigma = 0$, the flat surface. The use of the fractal dimension H (also called the Hurst exponent) incorporates the idea that many surfaces exhibit a self-affine structure, such that an invariance exists where $\vec{r} \to \Lambda\vec{r}$ yields $h(\vec{r}) \to \Lambda^H h(\vec{r})$, meaning qualitatively that zooming into the surface will look very much like the original copy; this is the basis of fractals in nature [54]. We note that the values for σ are fixed by the behaviour at $|\vec{r}-\vec{r}'| \to \infty$ on the plot, when the functions in Fig. 5.2 approach $\sigma^2_{s,g}$

The typical feature of all natural correlation functions is their trailing off as the distance between points increases. Physically this means that two points infinitely far away should have no correlation, whereas two points adjacent to each other should have a lot in common. The case of white noise, $a \to 0$, implies no correlation between any points no matter their proximity, the entirely random scenario.

The Gaussian distribution is the special case of $H = 1$, so called as the autocorrelation function contains the factor $\exp(-|\vec{r}-\vec{r}'|^2)$. It is especially useful as there exists a simple analytic Fourier transform

$$g(|\vec{k}|)_G = \pi a^2 \exp\left\{-\frac{k^2a^2}{4}\right\} \tag{5.26}$$

where $g(|\vec{k}|)$ is defined in Eq. 5.14. The Bessel distribution is

$$\langle h(\vec{r})h(\vec{r}')\rangle_B = \frac{2H\sigma^2}{\Gamma(1+H)}\left[\frac{R\sqrt{2H}}{2a}\right]^H K_H\left[\frac{R\sqrt{2H}}{a}\right] \tag{5.27}$$

where Γ is the Gamma function, K_H is the second kind of Bessel function of order H, and $R = |\vec{r}-\vec{r}'|$, which has a Fourier transform

$$g(|\vec{k}|)_B = \frac{a^2}{(2\pi)^5}\left[1+\frac{a^2k^2}{2H}\right]^{-(1+H)}. \tag{5.28}$$

Since the fractal correlation function does not have an analytical expression for its Fourier transform, we can make the assumption under certain conditions that it is approximately the same as this Bessel Fourier transformed function.

Since our data is experimental, we wish to determine the autocorrelation function based on what has been measured, which requires a fit based on one of these phenomenological models. By matching our correlation functions to the data, we can determine the best fit and deduce some ideas of how the graphene bends and curls under certain conditions. Physically, the roughness of the substrate is determined by the experimental method used to construct it, but as graphene is a thin membrane that forms on top of this substrate, there is no experimental way (as of yet) to determine the behaviour of the roughness between the gap. Although we can use energy considerations to find the balance between forces like

adhesion, tension, and bending rigidity, we are concerned for our purposes on the correlation functions themselves, but we will use these forces to justify some of our models later on.

We notice two glaring properties in the table: that the graphene sheet is both smoother and has a higher value of a. This implies both that it is much smoother than the surface underneath it (like a blanket spread over a pile of knives) and that there is a mismatched correlation length, meaning the graphene does not perfectly rest on each peak and sink in each valley, but maintains much of its own structure. This is justified given that the mean spacing between the two is approximately a tenth of a nanometer. We will see that both these properties can stem from the healing assumption for thin membranes on a not strongly interacting material.

Based on the fits, it is clear that the fractal correlation function gives the overall best fit for both the substrate and the graphene, largely due to its flexibly changing parameters. However, we note that the region of most concern is the region $|\vec{r} - \vec{r}'| \to \infty$, as this corresponds to the lowest wavenumbers when a Fourier transform is performed, and the region of small q has the largest effect on the overall plasmon effect later on. This can be seen in terms of characteristic length scales, as we expect $q \sim 1/a \sim 0.1\text{nm}^{-1}$ (very small) to be near the characteristic spatial frequency of the rough surface. This makes the Gaussian profile a very attractive option, given it has an exceptional fit for $|\vec{r} - \vec{r}'| > 30\text{nm}$ and a simple analytic Fourier transform. For this reason both correlations will be considered in later chapters.

5.1.3 Healing Property for Thin Membranes

Experiments [23] and theoretical treatments both show that the graphene exhibits a roughness that partially follows the substrate surface, but how can we tell the relationship between what are now two rough surfaces? Graphene roughness is influenced by factors including thermal fluctuations, van der Waals forces, electronic orbital repulsion, and forces of lateral tension and bending rigidity that shape the graphene around the roughness of the substrate. These forces mean there is now also a correlation function between the two rough surfaces that must be taken account of. We define the gap correlation function in Fourier space as

$$\langle(\widetilde{h}_g(\vec{q}) - \widetilde{h}_s(\vec{q}'))^2\rangle = \langle\widetilde{h}_s(\vec{q})^2\rangle + \langle\widetilde{h}_g(\vec{q})^2\rangle - 2\langle\widetilde{h}_s(\vec{q})\widetilde{h}_g(\vec{q}')\rangle. \tag{5.29}$$

If we assumed that there was near perfect correlation between the two, which is given by a harmonic approximation to the adhesion potential [8], we would have $\langle\widetilde{h}_s(\vec{q})\widetilde{h}_g(\vec{q}')\rangle^2 \approx \langle\widetilde{h}_s(\vec{q})^2\rangle\langle\widetilde{h}_g(\vec{q})^2\rangle$, since each point is separated by its mean squared height, $\sqrt{\langle\widetilde{h}_{s,g}(\vec{q})^2\rangle}$, and there is hence no wavenumber dependence. However, this model ignores the elastic curvature of graphene, which partially causes the difference in the transverse correlation lengths $a_{g,s}$. We therefore consider the implementation of a healing function that describes the influence of the substrate on the adhesion of the membrane. This function relates the Fourier transformed stochastic height profiles via $\widetilde{h}_g(q) = H(q)\widetilde{h}_s(q)$, such that

$$H(q) = \left(1 + \tau^2 q^2 + \rho^4 q^4\right)^{-1} \tag{5.30}$$

is the healing function, where τ and ρ are related to the tension and bending rigidity of graphene for a rough substrate [28]. To see this, we look at the Monge representation (associating a height profile to each planar point) for the free energy of rippled graphene

[57]

$$\mathcal{F}[h_g(\vec{r})] = \int d^2\vec{r}\sqrt{1+(\nabla h_g)^2}\left\{\beta + \frac{\kappa}{2}\left(\nabla \cdot \frac{\nabla h_g}{\sqrt{1+(\nabla h_g)^2)}}\right) + V(\vec{r}, h_g)\right\}. \tag{5.31}$$

The free energy due to tension, given by the parameter β in this equation, is a constant spread out over the whole curved area of the surface, while the bending rigidity represented by κ is seen to depend on the curvature intricately. The adhesion energy $V(\vec{r}, h_g)$ can be approximated via the Lennard-Jones potential for the attraction between neutral atoms, yielding a stiffness constant k_0 that can renormalize the tension and rigidity factors by $\tau^2 = \beta/k_0$ and $\rho^4 = \kappa/k_0$. Again, we take a phenomenological approach to determining these factors by seeing how the inverse Fourier transform of the graphene height correlation function from Eq. 5.30 compares to the data we have for the real space correlation function for graphene in Fig. 5.2. We also note that we expect the healing approximation to be most valid near small k, where the approximation says the Fourier transformed graphene height correlation function approaches that of the substrate. We see that $g(|\vec{k}|)_g \approx g(|\vec{k}|)_s$ in the $\vec{k} \to 0$ limit (i.e. $\sigma_g a_g \approx \sigma_s a_s$ for each of the models), validating our point.

Our comparison, by using the Gaussian assumption for the substrate, applying the healing function to the Fourier transformed Gaussian function and then comparing the inverse transformed result to the experimental data for graphene's autocorrelation function, yields the values $\tau = 5.54$nm and $\rho = 4.46$nm. By using this healing method, we can describe the whole system, including the gap between the two surfaces, using the substrate's autocorrelation and these two coefficients for the thin graphene membrane.

5.2 Green's Functions for Single/Double Interface Problems

Figure 5.1 is a challenging problem to solve largely due to three factors: boundary conditions that are perturbative in the height profiles h_g and h_s, the roughness of our potentials and boundaries, and the correlation between the two surfaces. Throughout Chapter 5 we will attempt three methods that attempt to quantify the effect of surface roughness for the potential on a graphene surface. Below we list three different problems and the methods we consider that will be highlighted in Chapter 5 to solve them

- Rough graphene described by $h_g(\vec{r})$ above rougher substrate described by $h_s(\vec{r})$ with dielectric function $\epsilon \ldots$
  - ⋆ Section 5.2.1: First-order perturbation of boundary conditions and Laplace's equation (Section 5.1.1) in $h_g(\vec{r}), h_s(\vec{r})$, followed by smoothing method for eigenvalue problems (Appendix 1) to determine plasmon dispersion
  - ⋆ Section 5.2.2: Second-order perturbation in $h_s(\vec{r})$ of Green's function for system, Dyson series solution of full graphene-substrate interaction, must assume $h_g(\vec{r}) = 0$ to obtain plasmon dispersion
  - ⋆ Section 5.2.3: Second-order perturbation in $h_s(\vec{r})$ and $h_g(\vec{r})$ of Green's function for potential on the rough graphene surface
- Rough graphene described by $h(\vec{r})$ lying directly on top of substrate with dielectric function $\epsilon \ldots$

- ⋆ Section 5.2.1: First-order perturbation of boundary conditions and Laplace's equation (Section 5.1.1) in $h_(\vec{r})$, followed by smoothing method to determine plasmon dispersion

- Rough graphene described by $h(\vec{r})$ in free space ...

  - ⋆ Equivalent to above two methods by letting $\epsilon = 1$ for the substrate

5.2.1 Extinction of Potentials and Laplace Equation Eigenvalue Problem

As our boundary conditions and the Laplace equations in Eqs. 5.16-5.23 stand, the double interface problem contains three different potentials. We will also consider later the single interface problem, involving two different potentials, as a special case. However, using Green's second theorem, which says

$$\int_V d^3\mathbf{r}(u\Delta v - v\Delta u) = \int_\Sigma dS\left[u\frac{\partial v}{\partial n} - v\frac{\partial u}{\partial n}\right], \tag{5.32}$$

we can transform all our equations into using just a single potential. In that equation, V is defined as a volume bounded by a surface Σ. We will choose this surface to be an infinite half-sphere bounded by either the h_s or h_g surface, and since we have vanishing potentials in the infinite limit the right hand side of the Green's theorem will only include the rough surface, allowing us to use the definition of the normal vector in Eq. 5.24.

We introduce the Green's function for regions 2 and 3, G_{23}, as the solution of the equation

$$\Delta G_{23}(\vec{r},\vec{r}') = -4\pi\delta(\vec{r}-\vec{r}') \tag{5.33}$$

which, with vanishing boundary conditions at infinity, means we can write it as

$$G_{23}(\vec{r},\vec{r}') = \int \frac{d^2\vec{q}}{(2\pi)^2}\frac{2\pi}{q}e^{i\vec{q}\cdot(\vec{r}-\vec{r}')}e^{-q(z-z')} \tag{5.34}$$

with $q = |\vec{q}|$. The same definitions hold for G_{12}, which will be used for the graphene surface, except the decay factor will be $e^{-q(z'-z)}$ as this will give finite solutions as z' increases.

We multiply the definition of the Green's function by ϕ_2 on the left, and subtract it from the Green's function G_{23} multiplied by $\Delta\phi_2$ (which, in the region below the substrate surface, region 3, is 0), and then integrate the variable $\vec{r}$ over the volume V defined above. Using Green's theorem yields

$$\Theta_V(\vec{r})\phi_3(\vec{r}) = -\frac{1}{4\pi}\int_{\Sigma_{23}} dS'\left[\left[\frac{\partial}{\partial n'}G_{23}(\vec{r},\vec{r}')\right]\phi_3(\vec{r}') - G_{23}(\vec{r},\vec{r}`)\frac{\partial}{\partial n'}\phi_3(\vec{r}')\right] \tag{5.35}$$

where

$$\Theta_V(\vec{r}) = \int_V d^3\vec{r}'\delta(\vec{r}-\vec{r}') \tag{5.36}$$

which is unity if $\vec{r}$ is in the volume V and 0 otherwise. We now utilize the boundary conditions from Section 5.1.1, which for regions $2,3$ allow us to transform this into a statement about the potential in region 2:

$$0 = -\frac{1}{4\pi}\int_{\Sigma_{23}} dS'\left[\left[\frac{\partial}{\partial n'_s}G_{23}(\vec{r},\vec{r}')\right]\phi_2(\vec{r}') - \frac{1}{\epsilon}G_{23}(\vec{r},\vec{r}')\frac{\partial}{\partial n'_s}\phi_2(\vec{r}')\right]. \tag{5.37}$$

By 'flipping over' to the middle region from the top region, we eliminate any trace of the volume term, leaving a new boundary condition. We can do the same trick for the boundary condition between regions $1, 2$:

$$0 = -\frac{1}{4\pi}\int_{\Sigma_{12}} dS' \left[\left[\frac{\partial}{\partial n'_g} G_{12}(\vec{r},\vec{r}')\right]\phi_2(\vec{r}') - G_{12}(\vec{r},\vec{r})\left[\frac{\partial}{\partial n'_g}\phi_2(\vec{r}') + 4\pi\sigma(\vec{r}')\right]\right]. \quad (5.38)$$

A hybrid of these two will yield the full boundary condition for graphene directly on top of a substrate, which will be investigated later. Again, because of the outgoing boundary conditions and the Laplace's equation between the two surfaces, we choose the following form for the potential $\phi_2 = \phi$

$$\phi(\vec{r}') = \int \frac{d^2\vec{k}}{(2\pi)^2} e^{i\vec{k}\cdot\vec{r}'}(A(\vec{k})e^{-kz'} + B(\vec{k})e^{kz'}). \quad (5.39)$$

We can simplify our equations by realizing that the surface integration is defined as

$$dS = d^2\vec{r}\left[1 + \left[\frac{\partial h_{s,g}(\vec{r})}{\partial x}\right]^2 + \left[\frac{\partial h_{s,g}(\vec{r})}{\partial y}\right]^2\right]^{1/2} \quad (5.40)$$

which will eliminate the normalization term in the integration wherever the $\partial/\partial n$ term appears. It is notable that the graphene term in the second of the boundary conditions will contain this extra factor of second order form, which we will investigate in later chapters.

Beginning with Eq. 5.24 in tandem with Eq. 5.38, which now reads as

$$0 = \int d^2\vec{r}'\left[(\vec{n}'_s\cdot\nabla G_{23})\phi - \frac{1}{\epsilon}(\vec{n}'_s\cdot\nabla\phi)G_{23}\right]\Big|_{z'=h_s(\vec{r})}, \quad (5.41)$$

we plug in the derivations for the potential (Eq. 5.39), the Green's function (Eq. 5.34), and the normal vector (Eq. 5.24), to obtain

$$\begin{aligned} 0 = &\int d^2\vec{r}'\int \frac{d^2\vec{q}}{(2\pi)^2}\frac{2\pi}{q}e^{i\vec{q}\cdot(\vec{r}-\vec{r}')}e^{-qz}e^{qh_s(\vec{r}')}\int\frac{d^2\vec{k}}{(2\pi)^2}e^{i\vec{k}\cdot\vec{r}'} \\ &\Big\{[-(\nabla_{\vec{r}'}h_s(\vec{r}'))\cdot(-i\vec{q}) + q](A(\vec{k})e^{-kh_s(\vec{r}')} + B(\vec{k})e^{kh_s(\vec{r}')}) \\ &-\frac{1}{\epsilon}\left[(-(\nabla_{\vec{r}'}h_s(\vec{r}'))\cdot(i\vec{k}) - k)A(\vec{k})e^{-kh_s(\vec{r}')} + (-(\nabla_{\vec{r}'}h_s(\vec{r}'))\cdot(i\vec{k}) + k)B(\vec{k})e^{kh_s(\vec{r}')}\right]\Big\} \end{aligned} \quad (5.42)$$

We wish to expand this equation up to first-order for the exponentials, which means $e^{qh_s(\vec{r}')} \approx 1 + qh_s(\vec{r}')$, which is an approximation we will attempt to justify later, but we have set up the problem such that h_s will be very small compared to other length scales in the problem (i.e. h_0). The perturbative result is

$$\begin{aligned} 0 = \int d^2\vec{r}'\int \frac{d^2\vec{q}}{(2\pi)^2}\frac{2\pi}{q}e^{i\vec{q}\cdot(\vec{r}-\vec{r}')}e^{-qz}\int\frac{d^2\vec{k}}{(2\pi)^2}e^{i\vec{k}\cdot\vec{r}'}\Big[&A(\vec{k})(1+(q-k)h_s(\vec{r}')) \\ &\times\left((q+\frac{k}{\epsilon}) + i(\vec{q}+\frac{\vec{k}}{\epsilon})\cdot\nabla_{\vec{r}'}h_s(\vec{r}')\right) + B(\vec{k})(1+(q+k)h_s(\vec{r}')) \\ &\times\left((q-\frac{k}{\epsilon}) + i(\vec{q}+\frac{\vec{k}}{\epsilon})\cdot\nabla_{\vec{r}'}h_s(\vec{r}')\right)\Big]. \end{aligned} \quad (5.43)$$

We here invoke some Fourier transforms via the relation $\int d^2\vec{r}' e^{i(\vec{k}-\vec{q})\cdot\vec{r}'}(\cdots)$ so that

$$1 \to (2\pi)^2\delta(\vec{q}-\vec{k}), \qquad h(\vec{r}') \to \widetilde{h}(\vec{q}-\vec{k}), \qquad \nabla_{\vec{r}'}h(\vec{r}') \to -i(\vec{k}-\vec{q})\widetilde{h}(\vec{q}-\vec{k}), \tag{5.44}$$

where we have by definition the complex conjugate of the Fourier transformed height profile in our expression. Simplifying the equation, we then realize that if the total Fourier transform is 0, then each component must be given by the result

$$A(\vec{q})\frac{\epsilon+1}{\epsilon-1} + B(\vec{q}) = \int \frac{d^2\vec{k}}{(2\pi)^2}k\Big[A(\vec{k})(1-\hat{k}\cdot\hat{q}) - B(\vec{k})(1+\hat{k}\cdot\hat{q})\Big]\widetilde{h}_s(\vec{q}-\vec{k}). \tag{5.45}$$

In the case of zero roughness, this yields $A(\vec{q}) = \frac{1-\epsilon}{\epsilon+1}B(\vec{q})$.

The second equation is very similar (minus the graphene contribution), with the exception that $\epsilon = 1$ in free space, and the Green's function has now switched its sign for the outgoing perpendicular portion, so that $|z-z'| = z'-z$. After all the cancellations, it leaves us with $-2B(\vec{q})qe^{qh_0}$, which we will add to the graphene contribution, which is

$$\begin{aligned} -4\pi e^2 \int d^2\vec{r}' \int \frac{d^2\vec{q}}{(2\pi)^2}\frac{2\pi}{q}e^{i\vec{q}\cdot(\vec{r})}e^{qz}e^{-qh_0}\Bigg\{\int d^2\vec{r}'' \int \frac{d^2\vec{k}}{(2\pi)^2}\int d^2\vec{r}' e^{i(\vec{k}-\vec{q})\cdot\vec{r}'}e^{-qh_g(\vec{r}')}e^{-i\vec{k}\cdot\vec{r}''} \\ \times \chi(\vec{k},\omega)\int \frac{d^2\vec{k}'}{(2\pi)^2}e^{i\vec{k}'\cdot\vec{r}''}\Big[A(\vec{k}')e^{-k'h_g(\vec{r}'')}e^{-k'h_0} + B(\vec{k}')e^{k'h_g(\vec{r}'')}e^{k'h_0}\Big]\Bigg\}. \end{aligned} \tag{5.46}$$

This stems from the definition of the surface charge carrier density in graphene σ in terms of the potential and the polarizability, within the assumption of local screening across graphene, which is

$$\sigma(\vec{r}) = -e^2\int d^2\vec{r}''\chi(\vec{r}-\vec{r}'',\omega)\phi(\vec{r}''), \tag{5.47}$$

or fully written out,

$$\begin{aligned} \sigma(\vec{r}') = -e^2\int d^2\vec{r}''\int \frac{d^2\vec{k}}{(2\pi)^2}e^{i\vec{k}\cdot(\vec{r}-\vec{r}'')}\chi(\vec{k},\omega)\int\frac{d^2\vec{k}'}{(2\pi)^2}e^{i\vec{k}'\cdot\vec{r}''} \\ \times\Big[A(\vec{k}')e^{-k'h_g(\vec{r}'')}e^{-k'h_0} + B(\vec{k}')e^{k'h_g(\vec{r}'')}e^{k'h_0}\Big]. \end{aligned} \tag{5.48}$$

By integrating out $\int d^2\vec{r}' e^{i(\vec{k}-\vec{q})\cdot\vec{r}'}(\cdots)$ and $\int d^2\vec{r}'' e^{i(\vec{k}'-\vec{k})\cdot\vec{r}''}(\cdots)$ we have

$$e^{-qh_g(\vec{r}')} = (2\pi)^2\delta(\vec{q}-\vec{k}) - q\widetilde{h}_g(\vec{q}-\vec{k}) \tag{5.49}$$

$$e^{-k'h_g(\vec{r}'')} = (2\pi)^2\delta(\vec{k}-\vec{k}') - k'\widetilde{h}_g(\vec{k}-\vec{k}') \tag{5.50}$$

to first order in h_g.

Carrying out the calculation, we only look at the Fourier component within the larger integration, which when combined with the $-2B(\vec{q})qe^{qh_0}$ from before gives

$$\begin{aligned} 0 = -2B(\vec{q})qe^{qh_0} - 4\pi e^2\int\frac{d^2\vec{k}}{(2\pi)^2}\Big((2\pi)^2\delta(\vec{q}-\vec{k}) - q\widetilde{h}_g(\vec{q}-\vec{k})\Big)\chi(\vec{k},\omega)\int\frac{d^2\vec{k}'}{(2\pi)^2} \\ \times\Bigg[A(\vec{k}')e^{-k'h_0}\Big((2\pi)^2\delta(\vec{k}-\vec{k}') - k'\widetilde{h}_g(\vec{k}-\vec{k}')\Big) \\ + B(\vec{k}')e^{k'h_0}\Big((2\pi)^2\delta(\vec{k}-\vec{k}') + k'\widetilde{h}_g(\vec{k}-\vec{k}')\Big)\Bigg]. \end{aligned} \tag{5.51}$$

Simplification yields

$$0 = -2B(\vec{q})qe^{qh_0} - 4\pi e^2\chi(\vec{q},\omega)\Big[A(\vec{q})e^{-qh_0} + B(\vec{q})e^{qh_0}\Big] - 4\pi e^2\int\frac{d^2\vec{k}}{(2\pi)^2}\Big[k\Big(B(\vec{k})e^{kh_0} - A(\vec{k})e^{-kh_0}\Big)\chi(\vec{q},\omega) - q\chi(\vec{k},\omega)\Big(B(\vec{k})e^{kh_0} + A(\vec{k})e^{-kh_0}\Big)\Big]\widetilde{h}_g(\vec{q}-\vec{k}). \tag{5.52}$$

For a flat surface, this equation yields $0 = -2B(\vec{q})qe^{qh_0} - 4\pi e^2\chi(\vec{q},\omega)\Big[A(\vec{q})e^{-qh_0} + B(\vec{q})e^{qh_0}\Big]$, which when combined with the previous result of $A(\vec{q}) = \frac{1-\epsilon}{\epsilon+1}B(\vec{q})$ from Eq. 5.45 gives an eigenvalue equation for ω:

$$1 + \frac{2\pi e^2}{q}\chi(\vec{q},\omega)\Big[1 + \frac{1-\epsilon}{1+\epsilon}e^{-2qh_0}\Big] = 0. \tag{5.53}$$

The case of the graphene on top of the surface of a substrate is very similar, but the region worked with will only contain the term $A(\vec{q})$ as there is only an outgoing potential in the boundary conditions. There is now only one boundary condition in the problem. We obtain for this case

$$A(\vec{q})\Big[\frac{\epsilon+1}{2} + \frac{2\pi e^2}{q}\chi(\vec{q},\omega)\Big] = \int\frac{d^2\vec{k}}{(2\pi)^2}kA(\vec{k})\Big[\frac{\epsilon-1}{2}(1-\hat{k}\cdot\hat{q}) + \frac{2\pi e^2}{q}\chi(\vec{q},\omega) - \frac{2\pi e^2}{k}\chi(\vec{k},\omega)\Big]\widetilde{h}(\vec{q}-\vec{k}) \tag{5.54}$$

which again in the limit of $h \to 0$ yields the traditional flat boundary condition. This can be easily derived by setting $B(\vec{q}) = 0$ as there is no longer a middle region, and adding in the terms containing ϵ from the first boundary condition in Eq. 5.43.

The ultimate goal of these Green's functions is to determine the effect of roughness on plasmons, which are determined according to their dispersion relation i.e. the relation between the wavenumber q and ω. We have observed in previous chapters a derivation in different regimes for the polarizability of graphene (although the region where plasmons occur is best described near the linear dispersion regime, due to Landau damping), and now via these boundary conditions we can observe how the dispersion relation changes with the change in the surface properties. To link this with the RPA derivation we saw earlier, consider the case of free graphene with no roughness (see Appendix 2)

$$\epsilon(\vec{q},\omega) = 1 - v(q)\chi(\vec{q},\omega) = 1 - \frac{2\pi e^2}{q}\chi(\vec{q},\omega) = 0 \tag{5.55}$$

which is implying that in this free case $\epsilon(\vec{q},\omega) = 0$ gives the dispersion relation, a result we expect within the RPA approximation that makes the dielectric function a relation between the external and total potentials in the system. Effects like the substrate dielectric function or roughness can be seen to change the effective Coulomb potential and hence the dispersion relation. Why does this relation give us the plasmon uniquely? Notice we assumed above we could cancel $A(\vec{q})$ as if it was non-zero, but our problem is Laplace's equation with no external factors, so it will only be non-zero if there is a sustained mode not requiring

external perturbation somewhere in the system. This is uniquely satisfied by the surface plasmon [37].

We notice as a simpler example the case of graphene directly on top of the substrate, where the component of the Fourier-transformed potential component $A(\vec{q})$ appears both freely and within an integral being taken over the realization at each wavenumber of the stochastic height function. Simply trying to take the average of both sides will yield zero contribution from the stochastic variable, which has mean 0. Instead, we need a way to include effects of order higher than one (e.g. autocorrelation) while eliminating the need for the potential function $A(\vec{q})$. To do this we use the smoothing method, outlined in Appendix 1.

We begin by outlining a simpler problem presented in [14], which contains a single interface, but instead of the plasmons being induced by the graphene (i.e. $\chi(\vec{q}) = 0$), the conducting substrate has $\epsilon = \epsilon(\omega)$, which has a resonance frequency of ω_p in its bulk. We have before mentioned the existence of surface plasmons and shown they come about from an electromagnetic approach, via the photon that couples with the electron oscillations that let us describe the plasmon as a solution to the wave equation decaying away from the surface. This time, we approach the problem by seeking the dispersion equation based on the existence of a mode in the system that exists without excitation and satisfies Laplace's equation: it is because of our prior knowledge that we can then associate this dispersion equation with the solution to a surface plasmon.

Without the graphene, our boundary condition in Eq. 5.54 that allows us to solve for $A(\vec{q})$ is

$$A(\vec{q})\left(\frac{\epsilon(\omega)+1}{\epsilon(\omega)-1}\right) = \int \frac{d^2\vec{k}}{(2\pi)^2} kA(\vec{k})(1-\hat{k}\cdot\hat{q})\widetilde{h}(\vec{q}-\vec{k}) \tag{5.56}$$

We recall from Eq. 2.56 in Section 2.2.1 that for a planar interface, the equation for a surface plasmon (what we are looking for when solving Laplace's equation) satisfies $\epsilon(\omega)+1=0$, yielding a particular frequency (notice we no longer seek a dispersion equation, as a surface plasmon resonates at a unique wavenumber-independent frequency for this electrostatic regime). We expect this to change with the roughness of the surface. We notice as before that we must eliminate the factor $A(\vec{q})$ to obtain an equation for, in this case, $\gamma(\omega) = (\epsilon(\omega)+1)/(\epsilon(\omega)-1)$.

Referencing Appendix 1, our non-random matrix operator $H = \gamma(\omega)$, while the rough stochastic perturbation $V = \int \frac{d^2\vec{k}}{(2\pi)^2} k(1-\hat{k}\cdot\hat{q})\widetilde{h}(\vec{q}-\vec{k})$, so to determine an equation that operates on the function $PA(\vec{k}) = \langle A(\vec{k})\rangle$, we determine the matrix $\langle M\rangle$ up to second-order:

$$\langle M_1\rangle = \langle V\rangle = 0 \tag{5.57}$$

$$\langle M_2\rangle = \langle V\rangle + H^{-1}(\langle V^2\rangle - \langle V\rangle^2) \tag{5.58}$$

$$= \frac{1}{\gamma(\omega)} \int \frac{d^2\vec{k}}{(2\pi)^2} \int \frac{d^2\vec{k}'}{(2\pi)^2} kk'(1-\hat{k}\cdot\hat{q})(1-\hat{k}'\cdot\hat{k})\langle\widetilde{h}(\vec{q}-\vec{k})\widetilde{h}(\vec{k}-\vec{k}')\rangle \tag{5.59}$$

which will act on the potential $A(\vec{k}')$. We recall Eq. 5.14, where $g(\vec{k})$ is the Fourier-transformed autocorrelation function describing the rough properties of the substrate, while σ is the mean square deviation from flatness. This means that the total equation for $\langle A(\vec{q})\rangle$ is

$$\left(\gamma(\omega) - \frac{1}{\gamma(\omega)}\sigma^2 \int \frac{d^2\vec{k}}{(2\pi)^2} qk(1-\hat{k}\cdot\hat{q})^2 g(|\vec{q}-\vec{k}|)\right)\langle A(\vec{q})\rangle = 0 \tag{5.60}$$

and therefore the equation that determines the roughness effect in the plasmon frequency equation is

$$\gamma(\omega) = \pm\sigma\sqrt{\int \frac{d^2\vec{k}}{(2\pi)^2} qk(1-\hat{k}\cdot\hat{q})^2 g(|\vec{q}-\vec{k}|)} \text{ compared to } \gamma(\omega) = 0. \tag{5.61}$$

This equation shows a wavevector dependent splitting. To see how this comes about, one can imagine a sinusoidal or grated surface, so that the Fourier-transformed correlation function has discrete values, which would in turn yield specific wavevectors that the frequency can resonate at, due to the coupling of the length scales. The rough surface is then analogous to a continuous superposition of these gratings, causing a continuous wavenumber dependence.

Some crucial assumptions have been made in this derivation, even for this case without the graphene, namely the restriction up to first-order in the Green's function, done by assuming a linear form for the exponentials $e^{\pm kh(\vec{r})}$. We also only computed up to second order in the matrix M from Appendix 2, but larger expansions of even order (due to the Gaussian property) could be carried out. In fact, if one is able to develop an analytic form (non-perturbative) for M, the full approach for a rough eigenvalue problem (shown in Appendix 1) is a Green's function method that produces an imaginary part to the plasmon frequency. This procedure (along with keeping the full exponential) is carried out in [14], where they note that higher even order perturbations are all of the same order as the second order in their system and therefore cannot be ignored.

This discovery makes the investigation of higher-order effects in our graphene system a topic of interest throughout the remainder of the thesis. We will again be using the smoothing method when we wish to determine the effect of roughness for plasmons restrained to the graphene surface as a technique to determine the plasmon dispersion relation. We will notice some issues when trying to incorporate this idea of higher order terms into the graphene system, including the deformation and crumpling of the surface, the differential area term $\sqrt{1+(\partial h/\partial x)^2+(\partial h/\partial y)^2}$, which when expanded contains infinite even terms in the stochastic height profile h, and non-locality as a result of correlation between two surfaces.

Projection Method for Graphene System

We begin by writing out, using the method contained in Appendix 1, the values for the operators that will act on the potential $A(\vec{k})$ for the case of graphene directly on top of the substrate, shown in Eq. 5.54 which is an instructive example that provides indications for what to expect in the two surface case. The equation we wish to solve is of the form

$$\int \frac{d^2\vec{p}}{(2\pi)^2}\Big[H(\vec{q},\vec{p}) - V(\vec{q},\vec{p})\Big]A(\vec{p},\omega) = 0 \tag{5.62}$$

where

$$H(\vec{q},\vec{p}) = (2\pi)^2\delta(\vec{q}-\vec{p})\left[\frac{\epsilon+1}{2} + \frac{2\pi e^2}{q}\chi(q,\omega)\right] = (2\pi)^2\delta(\vec{q}-\vec{p})\epsilon(q,\omega) \tag{5.63}$$

$$V(\vec{q},\vec{p}) = p\left[\frac{\epsilon-1}{2}(1-\hat{p}\cdot\hat{q}) + \frac{2\pi e^2}{q}\chi(\vec{q},\omega) - \frac{2\pi e^2}{p}\chi(\vec{p},\omega)\right]\widetilde{h}(\vec{q}-\vec{p}) \tag{5.64}$$

where we point out the polarizability now only depends on the wavenumber, not on its vector components. We have shown this is a result of the assumptions about the translational

invariance of graphene. Via the Green's function method outlined in Appendix 1, this equation becomes

$$\int \frac{d^2\vec{p}}{(2\pi)^2}\Big[H(\vec{q},\vec{p}) - \langle M(\vec{q},\vec{p})\rangle\Big]\langle A(\vec{p},\omega)\rangle = 0, \tag{5.65}$$

where $\langle M\rangle = \langle V + M\langle G\rangle(V - \langle M\rangle)\rangle \approx \langle V\langle G\rangle V\rangle$, $\langle G\rangle = (G_0^{-1} - \langle M\rangle)^{-1}$ and

$$G_0 = H^{-1}(\vec{q},\vec{p}) = \frac{(2\pi)^2\delta(\vec{q}-\vec{p})}{\epsilon(q,\omega)}, \tag{5.66}$$

all by definition. Let $\langle M\rangle = (2\pi)^2\delta(\vec{q}-\vec{p})m(q,\omega)$ so that

$$\langle G\rangle = (2\pi)^2\delta(\vec{q}-\vec{p})\frac{1}{\epsilon(q,\omega) - m(q,\omega)}. \tag{5.67}$$

We note that this is reminiscent of the loss function used to determine modes of absorption

$$\text{Loss Function } = -\Im\left[\frac{1}{\epsilon(q,\omega) - m(q,\omega)}\right], \tag{5.68}$$

recalling that the imaginary component of, in this case, frequency, reflects the system's ability to absorb energy at the value of $\Re(\omega)$. The equation for the dispersion relation will hence be $\epsilon(q,\omega) - m(q,\omega) = 0$, as this reflects the region of largest energy absorption.

We are using the approximation $\langle M\rangle \approx \langle V\langle G\rangle V\rangle$, which is shorthand operator notation for saying

$$\begin{aligned}
&\langle M(\vec{q},\vec{p})\rangle = (2\pi)^2\delta(\vec{q}-\vec{p})m(q,\omega) = \int \frac{d^2\vec{p}'}{(2\pi)^2}\int \frac{d^2\vec{q}'}{(2\pi)^2}\langle V(\vec{q},\vec{p}')\langle G(\vec{p}',\vec{q}')\rangle V(\vec{q}',\vec{p})\rangle \\
&= \int \frac{d^2\vec{p}'}{(2\pi)^2}\int \frac{d^2\vec{q}'}{(2\pi)^2}(2\pi)^2\delta(\vec{p}'-\vec{q}')\frac{1}{\epsilon(\vec{p}',\omega) - m(\vec{p}',\omega)}p'p\langle\widetilde{h}(\vec{q}-\vec{p}')\widetilde{h}(\vec{q}'-\vec{p})\rangle \\
&\times\left[\frac{\epsilon-1}{2}(1-\hat{q}\cdot\hat{p}') + \frac{2\pi e^2}{q}\chi(q,\omega) - \frac{2\pi e^2}{p'}\chi(p',\omega)\right] \\
&\qquad\times\left[\frac{\epsilon-1}{2}(1-\hat{q}'\cdot\hat{p}) + \frac{2\pi e^2}{q'}\chi(q',\omega) - \frac{2\pi e^2}{p}\chi(p,\omega)\right].
\end{aligned} \tag{5.69}$$

We notice two delta functions in this expression, one from $\langle G\rangle$, and the other from the translational invariance of the system, which gives $\langle\widetilde{h}(\vec{q}-\vec{p}')\widetilde{h}(\vec{q}'-\vec{p})\rangle = \sigma^2(2\pi)^2\delta(\vec{q}-\vec{p}'+\vec{q}'-\vec{p})g(|\vec{q}-\vec{p}'|)$, yielding a dependence on a single variable. We simplify our expression as

$$\begin{aligned}
m(q,\omega) &= \sigma^2\int \frac{d^2\vec{p}'}{(2\pi)^2}\frac{g(\vec{q}-\vec{p}')p'q}{\epsilon(\vec{p}',\omega) - m(\vec{p}',\omega)} \\
&\qquad\times\left\{\left[\frac{\epsilon-1}{2}(1-\hat{p}'\cdot\hat{q})\right]^2 - \left[\frac{2\pi e^2}{q}\chi(q,\omega) - \frac{2\pi e^2}{p'}\chi(p',\omega)\right]^2\right\} \qquad (5.70)\\
&= \sigma^2\int \frac{d^2\vec{p}}{(2\pi)^2}\frac{g(\vec{q}-\vec{p})pq}{\epsilon(\vec{p},\omega) - m(\vec{p},\omega)}\left\{\left[\frac{\epsilon-1}{2}(1-\hat{p}\cdot\hat{q})\right]^2 - \Big[\epsilon(q,\omega) - \epsilon(p,\omega)\Big]^2\right\} \qquad (5.71)
\end{aligned}$$

given the definition of $\epsilon(q,\omega)$ in Eq. 5.63. This equation appears to contradict itself, as it is supposed to determine, for a certain value ω, the value of $m(q,\omega)$ that yields $\epsilon(q,\omega) - m(q,\omega) = 0$, which is a term that will be integrated over in the denominator

of its own definition. We will soon see that we can step around this issue by adding an imaginary component to the frequency, which suggests the roughness of the graphene adds some dissipation to the system, which does in fact occur physically. We notice that our expression contains $m(q,\omega)$ implicitly, and therefore must be solved iteratively. For most purposes, the value of $m(k,\omega)$ is much smaller than $\epsilon(k,\omega)$ for values of $k \neq q$, meaning a 1st or 2nd order approximation will usually suffice.

Here we employ two major assumptions in order to give an approximate form for the roughness effect on the dispersion relation. One is that the surface is describable via a Gaussian correlation function, as this allows us to write the Fourier transform of the auto-correlation in a very simple form that is easily integrable, and we have mentioned before that the Gaussian correlation function describes the surface very well from our phenomenological observations in the $q \to 0$ limit. The other is the form we use for the polarization of graphene in the optical ($q \to 0$, or $\omega \gg v_F q$) limit. For doped graphene our polarization function reads as [26]

$$\chi(q,\omega) = \frac{4e^2}{2\pi e^2}\frac{E_F}{(\hbar v_F)^2}\Big[1 - \chi_r(q,\omega) - i\chi_i(q,\omega)\Big] \tag{5.72}$$

$$= \frac{2}{\pi}\frac{E_F}{(\hbar v_F)^2}\left[1 - \frac{1+(\cdots)}{\sqrt{1-\left(\frac{qv_F}{\omega}\right)^2}} + i\frac{1+(\cdots)}{\sqrt{\left(\frac{qv_F}{\omega}\right)^2-1}}\right] \tag{5.73}$$

and doing the Taylor expansion to first order in the argument, $(qv_F/\omega)^2$, and noticing the imaginary argument will disappear for our optical limit, gives a polarizability of

$$\chi(q,\omega) \approx -\frac{E_F}{\pi}\frac{q^2}{(\hbar\omega)^2}. \tag{5.74}$$

Using the relation Eq. A.35 between conductivity and polarizability, this is exactly the Dirac conductivity term we obtained in Section 3.2.4 (Eq. 3.28), however we use this approach in order to properly treat the wavenumber response in the polarization. To recall, our region of focus (defined by the allowed phase space for the plasmon to act without decay into other modes) is $v_F q < \omega < 2E_F - qv_F$, so we are justified in both using the optical limit and in using the polarization function effects near the Dirac cone. Current research attempts to uncover higher order effects of the polarization function and energy regions beyond the Dirac cone, which we investigated using a hydrodynamic model in Chapter 4.

Given this function, we can now write $\epsilon(q,\omega)$ from Eq. 5.63 as

$$\epsilon(q,\omega) = \frac{\epsilon+1}{2} - \frac{2\pi e^2}{q}\frac{E_F}{\pi\hbar^2}\frac{q^2}{\omega(\omega+i\gamma)} = \frac{\epsilon+1}{2} - \frac{fq}{\omega^2}, \tag{5.75}$$

letting $f = 2\pi e^2 E_F/\pi\hbar^2$ and $\gamma = 0^+$. This inclusion of an imaginary damping component to the frequency will be shown to give a non-zero result for the plasmon dispersion relation. By construction, the roughness function $m(q,\omega) = m_r + im_i$. To first approximation, $m_r(p,\omega) = m_i(p,\omega) = 0$ within the integration, allowing us to use the Sokhotski-Plemelj theorem

$$\frac{1}{\epsilon(p,\omega)} \approx P.V.\frac{\omega^2}{\frac{\epsilon+1}{2}\omega^2 - fp} - i\pi\frac{\omega^2}{f}\delta\left(\frac{\epsilon+1}{2}\frac{\omega^2}{f} - p\right) \tag{5.76}$$

where *P.V.* stands for the Cauchy principal value of the integral, whereas an imaginary component occurs at the resonance frequency, where the denominator is zero, at $p = q$.

$\omega_p/v_F k_F$	$q/k_F = 0.2$	$q/k_F = 0.5$	$q/k_F = 1$
Gap, Flat Case	$0.37287 + 0I$	$0.98753 + 0I$	$2.14883 + 0I$
Full Correlation	$0.37267 + 2.7 \times 10^{-6} I$	$0.98686 + 7.8 \times 10^{-5} I$	$2.14971 + 3.4 \times 10^{-3} I$
No Correlation	$0.37171 + 2.1 \times 10^{-4} I$	$0.97636 + 8.8 \times 10^{-3} I$	$2.09026 + 0.1I$
No Gap, Flat	$0.59795 + 0I$	$0.94545 + 0I$	$1.33076 + 0I$
No Gap, Rough	$0.59837 - 6.8 \times 10^{-6} I$	$0.94604 - 1.3 \times 10^{-4} I$	$1.33790 - 1.3 \times 10^{-4} I$

Table 5.2: Table showing the shift in the normalized plasmon frequency $\omega_p/v_F k_F$ for different wavenumbers for the case of (a) flat graphene a height $h_0 = 0.42$nm above a flat substrate with $\epsilon = 3.9$ (b) a fully correlated system assuming Eq. 5.81 holds, implying the two surfaces have similar topographies (c) an uncorrelated system, where the surfaces are rough independent of each other (d) flat graphene lying directly on a flat substrate (e) rough graphene with no gap from the rough substrate it is above. $k_F = 0.2\text{nm}^{-1}$ with Gaussian correlation functions assumed for the two surfaces with parameters in Table 5.1, and the optical polarizability from Eq. 5.74.

Given the Gaussian correlation function depends on $|\vec{q} - \vec{p}|$ due to translational invariance, an angular component is involved in our integration. Expanded out, we have

$$g(|\vec{q} - \vec{p}|) = \pi a^2 \exp\left[-\frac{a^2}{4}(p^2 + q^2 - 2pq\cos\theta)\right]. \tag{5.77}$$

To eliminate this, we utilize modified Bessel functions of the first kind

$$\frac{1}{\pi}\int_0^\pi \cos^n\theta \exp\left(\frac{a^2}{2}pq\cos\theta\right) = \frac{\partial^n}{\partial\alpha^n} I_0(\alpha(p)) \tag{5.78}$$

where $\alpha(p) = \frac{a^2}{2}pq$. After some simplification, we obtain for the real part of m

$$\begin{aligned} m_r(\vec{q}) = {} & \frac{d^2a^2}{2} q\omega^2 e^{-\frac{a^2}{4}q^2} \int_{p=0}^\infty dp \frac{p^2}{\frac{\epsilon+1}{2}\omega^2 - fp} e^{-\frac{a^2}{4}p^2} \\ & \times \left\{ \left[\left(\frac{\epsilon-1}{2}\right)^2 \left(2I_0(\alpha(p)) - \left(2 + \frac{1}{\alpha(p)}\right) I_1(\alpha(p))\right)\right] - \left(\frac{f}{\omega^2}\right)^2 (p-q)^2 I_0(\alpha(p)) \right\}. \end{aligned} \tag{5.79}$$

We note that since $\frac{\epsilon+1}{2}\omega^2 = fq$ the second factor does not require the Sokhotski-Plemelj theorem to the zeroth order. However for the first term it does. This results in an imaginary term of

$$m_i(\vec{q}) = -\pi \frac{d^2a^2}{2} q^3 \frac{\omega^2}{f} e^{-\frac{q^2a^2}{2}} \left(\frac{\epsilon-1}{2}\right)^2 \left(2I_0(\alpha(q)) - \left(2 + \frac{1}{\alpha(q)}\right) I_1(\alpha(q))\right). \tag{5.80}$$

In addition to the zero-gap case, which is simplified due to having to work with only one potential component $A(\vec{q})$, we would like to compare changes in the plasmon frequency due to the gap case (Appendix 4). Many of the same derivations carry over, with the flat case plasmon frequency for two surfaces given by Eq. 5.53. As shown in Appendix 4, we are now focused on two potential components given by matrix equations, and these cause, upon averaging, cross-correlation terms to crop up. This should not be surprising, as the gap between the two surfaces is an important parameter in the effect of roughness on the plasmon frequency.

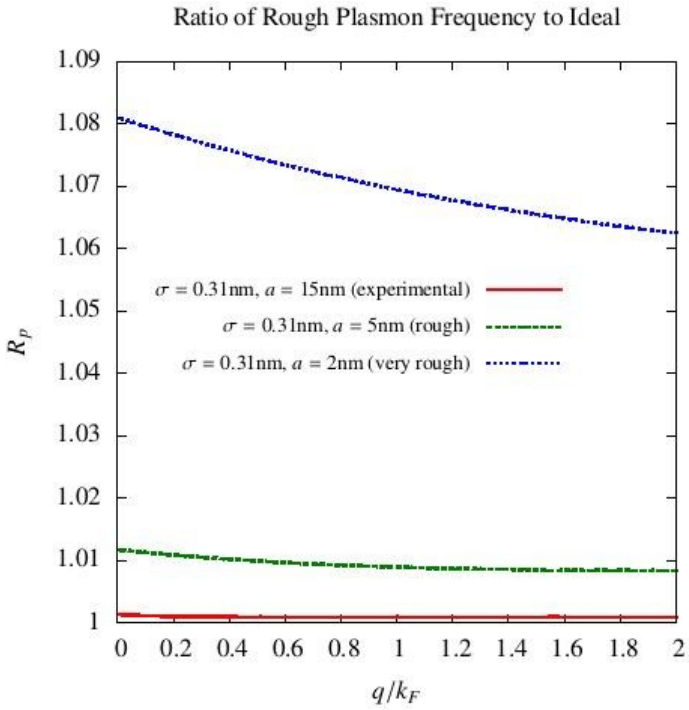

Figure 5.3: Percent difference of plasmon frequency for three different regimes of substrate/graphene roughness, assuming zero-gap. We assume $k_F = 0.2\text{nm}^{-1}$ and $\epsilon = 3.9$, using the Gaussian correlation function when computing the corrections to the frequency.

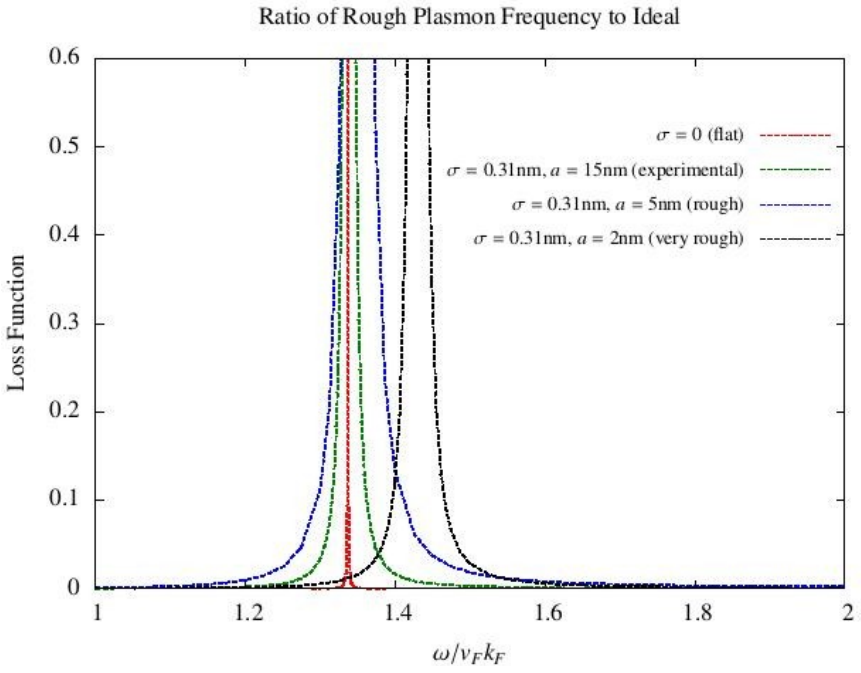

Figure 5.4: Energy loss function (Eq. 5.68) for three different regimes of substrate/grapehene roughness, with $q/k_F = 1$ chosen for display purposes, assuming zero-gap. The flat case is the ideal delta-peak, with our eigenvalue problem yielding imaginary components that make the plasmon lossy. A large enough roughness physically shifts the frequency.

For the case of a two surfaces with a finite gap, cross-correlation terms of the form $\langle \widetilde{h}_s \widetilde{h}_g \rangle$ can be approximated using the gap equation in Eq. 5.29. Assuming close adhesion,

$$\begin{aligned}\langle \widetilde{h}_s(\vec{q})\widetilde{h}_g(\vec{p})\rangle &= \sqrt{\langle \widetilde{h}_s(\vec{q})^2\rangle \langle \widetilde{h}_g(\vec{q})^2\rangle} \\ &= (2\pi)^2 \delta(\vec{q}+\vec{p})\sigma_s\sigma_g a_s a_g \exp\left[-\left(\frac{a_s^2+a_g^2}{8}\right)(p^2+q^2-2pq\cos\theta)\right] \end{aligned} \tag{5.81}$$

The inclusion of this correlation, which we call *full correlation*, is an attempt to describe the relationship between our graphene and substrate surfaces based on the model of a surface perfectly following the one below it. On the opposite side of the spectrum is the case of *no correlation*, assuming that $\langle \widetilde{h}_s \widetilde{h}_g \rangle = 0$, which will necessarily give a stronger effect on the plasmon frequency shift than the more physically justified full correlation case. We considered in Section 5.1.3 a healing method, but it is too numerically intensive to implement at this time.

Table 5.2 gives us, for three wavenumbers within or near the validity of the optical limit in Eq. 3.22, values for the plasmon frequency for five different regimes. The imaginary components come from the integration around the singularity at the plasmon frequency itself, as in Eq. 5.80. There are many things to glean from this table. One obvious observation is how different the flat case plasmon frequencies, given by Eqs. 5.53 and 5.54 respectively, are. The distinction of choosing graphene to lie directly on the substrate or even just a little above it has a profound impact on the plasmon frequency and the resulting screening. It implies that once a better understanding of the gap between graphene and its substrate evolves, that measured plasmonic behaviour can give information about the topology of the gap.

Our table also gives us an approximate value for the bifurcations due to roughness, with all our values in Table 5.2 giving a plasmon shift below 1%. Some of the corrections increase the plasmon frequency, which can be justified given that plasmon frequencies are known to bifurcate, as in Eq. 5.61. The derivation of an imaginary part to ω_p from roughness, which implies physically the damping of our plasmon, is of special note. Lastly, we mention the low q behaviour in both the gap and no gap cases, which continues to give a finite value for the plasmon frequency shift. This seems counter-intuitive given that the effects of roughness for such a spatially localized plasmon are expected to vanish, although this result could reveal new behaviour at low wavenumbers.

5.2.2 Green's Function for Non-Perturbative Case

We have so far made impressive forays into determining a change in plasmon frequencies via a first-order Green's function approach that has also yielded imaginary terms physically expected from rough surfaces. However, we have mentioned before that higher-order effects will play a role of comparable order to the second order terms in $\langle \widetilde{h}(\vec{q})\widetilde{h}(\vec{q}')\rangle$. Taking a look at the operator method in Appendix 1, it can be seen that even the fourth-order expansion for M will be very long and complicated. Therefore we will attempt in this section to take a more standard approach to determining potentials via Green's functions, namely to start by solving for the substrate with a point charge above it, proceeding to generalize it to an entire graphene sheet. This will afford us the opportunity to see the effects of higher-order correlations in the material, however, it lacks the proper treatment of electromagnetic boundary conditions in the graphene sheet as we shall see shortly.

For a substrate at $h_s(\vec{r})$, we locate a point charge above it, yielding a variation of Poisson's equation for EM potentials in homogenous media:

$$\Delta G(\vec{r},\vec{r}') = \begin{cases} -4\pi\delta(\vec{r}-\vec{r}') & z > h(\vec{r}) \\ 0 & z < h(\vec{r}) \end{cases} \tag{5.82}$$

and the z in these equations is the perpendicular height that corresponds to the $\vec{r}$ in the plane. We will have the same boundary conditions as in Section 5.1.1, except for a single surface without graphene, namely

$$\epsilon\hat{n}\cdot\nabla G(\vec{r},\vec{r}')|_{z=h_s(\vec{r})^-} = \hat{n}\cdot\nabla G(\vec{r},\vec{r}')|_{z=h_s(\vec{r})^+} \tag{5.83}$$

with the gradient being in-plane. The solution to this variant of Poisson's equation has the form [50]

$$G(\vec{r},\vec{r}') = \begin{cases} \int \frac{d^2\vec{k}}{(2\pi)^2}\left\{e^{i\vec{k}\cdot(\vec{r}-\vec{r}')}\left(\frac{2\pi}{k}\right)e^{-k|z-z'|} + A(\vec{k})e^{i\vec{k}\cdot\vec{r}}e^{-kz}\right\} & z > h(\vec{r}) \\ \int \frac{d^2\vec{k}}{(2\pi)^2}B(\vec{k})e^{i\vec{k}\cdot\vec{r}}e^{kz} & z < h(\vec{r}) \end{cases} \tag{5.84}$$

where $A(\vec{k})$ and $B(\vec{k})$ are the potential components above and below the surface, as seen previously. There is now in addition to the homogenous potentials an inhomogenous solution due to the point charge, recognized as the Fourier space transform of the Coulomb potential. We note that in the following derivations, we will make the assumption that our point charge at height z' is higher than z for all $\vec{r}$, meaning the point source is higher than any point on the rough surface, allowing us to say $|z-z'| = z'-z$. This assumption will later be explored.

In this formulation, we decide to carry out our prescription for determining the components $A(\vec{k}), B(\vec{k})$ via the two boundary conditions for continuity at the interface derived from Maxwell's equations. We recall that, given a single interface, in our first approach we used Green's second theorem to eliminate one of the components, so a system of equations with $A(\vec{k}), B(\vec{k})$ becomes solely an equation for $A(\vec{k})$. For this approach we decide to keep both potentials, leading us to two equations for two unknowns i.e. a matrix.

Our second deviation from our old method will be to expand our equations to second order in $h(\vec{r})$. This will require an expanded form for our directional derivative

$$\hat{n}\cdot\nabla = \frac{\partial}{\partial z} - (\nabla h_s(\vec{r}))\cdot\nabla - \frac{1}{2}(\nabla h_s(\vec{r}))^2\frac{\partial}{\partial z} \tag{5.85}$$

and a Fourier transform for terms of the form $h_s^2(\vec{r})$, done by performing $\int d^2\vec{r}e^{-i(\vec{k}-\vec{q})\cdot\vec{r}}$ on perturbative expansions of $e^{-qh_s(\vec{r})}$

$$e^{-qh_s(\vec{r})} \longrightarrow (2\pi)^2\delta(\vec{k}-\vec{q}) - q\widetilde{h}_s(\vec{k}-\vec{q}) + \frac{q^2}{2}\int\frac{d^2\vec{q}'}{(2\pi)^2}\widetilde{h}_s(\vec{q}')\widetilde{h}_s(\vec{k}-\vec{q}-\vec{q}') \tag{5.86}$$

to second order. What is of particular interest to us is the inhomogenous term in the potential above the surface, which means there is no longer a trivial solution $A(\vec{k}) = B(\vec{k}) = 0$ to the problem. This was crucial to us in determining the dispersion relation - seeking non-trivial solutions to Laplace's equation yielded the surface plasmon, which by definition yielded an eigenmode that could give non-zero potentials. However, the power of the Green's function technique is reflected here, as we are no longer limited in the way we have set up

the problem to just consider plasmons, and we can instead investigate potentials at any point above the surface.

Referencing Appendix 1, after computations we are able to write our problem in the form

$$(H - V)R = f \tag{5.87}$$

where f is now the term derived from the point source above the surface. Our function $R = [A(\vec{k})\ B(\vec{k})]^T$ in this case is a 2×1 vector, and H, V are matrices derived from the interface continuity equations. To determine the average potential, we write our equation as

$$\langle R \rangle = (H - \langle M \rangle)^{-1} \langle F \rangle \tag{5.88}$$

with M, F defined in Appendix 1. We mentioned before that we expanded our boundary conditions to second order in $h(\vec{r})$, and so the equation for $\langle M \rangle$ must be up to second-order as well. The equation for $\langle F \rangle$ is also written to second-order in $h(\vec{r})$. The reason it is called a non-perturbative solution is due to the non-linear way that the stochastic height function is included in the final equation for the vector R.

Our equations for the averaged potential have the form

$$\langle A(\vec{k}) \rangle = \frac{2\pi}{q} \exp(-i\vec{k} \cdot \vec{r}') \exp(-kz') a(k) \tag{5.89}$$

$$\langle B(\vec{k}) \rangle = \frac{2\pi}{q} \exp(-i\vec{k} \cdot \vec{r}') \exp(kz') b(k) \tag{5.90}$$

where $a(k), b(k)$ are known as the surface profile functions. This form comes about as $\langle R \rangle \sim \langle F \rangle$, which is the term containing the free solution to Laplace's equation due to the point source, causing the terms $\frac{2\pi}{q} \exp(-i\vec{k} \cdot \vec{r}') \exp(\pm kz')$ to appear. Lastly, for ease of calculation, we invoke the Gaussian correlation function found in Eq. 5.26 for the autocorrelation of the Fourier transformed height profile $\widetilde{h}(\vec{k})$ in the expressions for $\langle M \rangle$ and $\langle F \rangle$.

The equations for these surface profile functions are given in Appendix 3. By writing $\langle A(\vec{k}) \rangle$ in this form, we can write for the average potential above the surface

$$\langle G(\vec{r}, \vec{r}') \rangle = \int \frac{d^2\vec{k}}{(2\pi)^2} \exp(i\vec{k} \cdot (\vec{r} - \vec{r}')) g(k, z, z'). \tag{5.91}$$

Our Fourier coefficient is

$$g(k, z, z') = \frac{2\pi}{k} \left[\exp(-k|z - z'|) + a(k) \exp(-k(z + z')) \right], \tag{5.92}$$

where $a(k)$ is the surface profile function as defined in Appendix 3.

Now that we have determined the Green's function for a point source, we would like to apply this to a graphene sheet. If we wish to determine the effect of the substrate roughness on graphene, we must look at the image charge effect. This is the physical effect of electrons in the graphene inducing charge in the substrate which in turn affects the graphene electrons, ad infinitum. We have seen this before in Section 3.2.2 for a graphene sheet directly on top of the substrate, causing the Coulomb potential to be screened by a factor $(\epsilon + 1)/2$. To examine this self-interaction, we must determine the full Green's function for the graphene system, which is [43]

$$G(k, z, z') = g(k, z, z') + e^2 \int dz'' g(k, z, z'') \chi(k, \omega) G(k, z'', z') \delta(z'' - (h_0 + h_g(\vec{r}))). \tag{5.93}$$

The full Green's function $G(k,z,z')$ should not be confused with $\langle G(\vec{r},\vec{r}')\rangle$, the average Green's function due to a charge near a rough surface. Eq. 5.93 can be seen to come about based on the equation for the Fourier transformed potential

$$\widetilde{\phi}(z) = \int dz' g(k,z,z')[\widetilde{\rho}(k,z') + e^2\chi(k,\omega)\delta(z' - (h_0 + h_g(\vec{r})))\widetilde{\phi}(z')], \tag{5.94}$$

which says that the total potential at point z is due to the Fourier transformed external charge density $\widetilde{\rho}(z')$ at all other points z' and the charge density due to the graphene, which due to its two-dimensional form is uniquely located at $h_0 + h_g(\vec{r})$. Our $G(k,z,z')$ above is then a solution to

$$\widetilde{\phi}(z) = \int dz' G(k,z,z')\widetilde{\rho}(z'), \tag{5.95}$$

the definition of the Green's function. In order to obtain an analytic form for this Green's function, we will assume that $h_g(\vec{r}) = 0$, so the graphene is flat. This allows us to write

$$G(k,z,z') = g(k,z,z') + e^2 g(k,z,h_0)\chi(k,\omega)G(k,h_0,z') \tag{5.96}$$

with the same equation giving us

$$G(k,h_0,z') = g(k,h_0,z') + e^2 g(k,h_0,h_0)\chi(k,\omega)G(k,h_0,z'). \tag{5.97}$$

Rearranging the above equation and plugging back into our full Green's function yields

$$G(k,z,z') = g(k,z,z') - \frac{e^2\chi(k,\omega)g(k,z,h_0)g(k,h_0,z')}{1 + e^2\chi(k,\omega)g(k,h_0,h_0)}. \tag{5.98}$$

For Coulomb interactions within graphene we can also set $z = z'$, so that

$$G(k,h_0,h_0) = \frac{2\pi/k}{[1 + a(k)\exp(-2kh_0)]^{-1} + (2\pi e^2/k)\chi(k,\omega)}. \tag{5.99}$$

Our Green's function relates the potential to the charge density, so when the Green's function is very large, this reflects a sizable charge oscillation occurring. We can see that our Green's function will be largest when the denominator is 0. We therefore suggest that this denominator yields the plasmon dispersion relation between q and ω. We can observe this from the flat case, which gives

$$1 + \left(1 + \frac{1-\epsilon}{1+\epsilon}e^{-2kh_0}\right)\frac{2\pi e^2}{k}\chi(k,\omega) = 0. \tag{5.100}$$

This is exactly the flat case plasmon dispersion relation we obtained in Section 5.2.1 in Eq. 5.53. Assuming we use the form for the graphene polarizability in the optical limit in Eq. 5.74, this yields an exact formula for ω in terms of the wavenumber k:

$$\omega^2 = \left(1 + \frac{1-\epsilon}{1+\epsilon}e^{-2kh_0}\right)fk. \tag{5.101}$$

Here we observe the square-root wavenumber dependence that is a property of two-dimensional electronic systems.

Figure 5.5 investigates the percentage change in the plasmon frequency and the change in the energy loss function due to roughness by analyzing three different regimes that have

been mentioned briefly in Section 5.1.3. The properties of being fully correlated (FC) or not correlated (NC) relate to the assumption made about the substrate-graphene correlation function:

$$\langle \widetilde{h}_s(\vec{q})\widetilde{h}_g(\vec{q}')\rangle_{FC} = \sqrt{\langle \widetilde{h}_s(\vec{q})^2\rangle\langle \widetilde{h}_g(\vec{q})^2\rangle}, \qquad \langle \widetilde{h}_s(\vec{q})\widetilde{h}_g(\vec{q}')\rangle_{NC} = 0. \tag{5.102}$$

The third regime, "very rough", assumes $a_s = 1$nm and $\sigma_s = 0.38$nm, giving a surface resembling more white noise than a genuine physical substrate used in experiments.

One may question why the factors for the graphene roughness and the gap correlation function are coming about when we assumed that graphene was flat, in order to compute the Dyson series. Theoretically, the assumption of flatness can be relaxed to a degree by instead changing the relative roughness of the substrate underneath. For example, although we know physically that the graphene has $\sigma_g = 0.22$nm and the substrate has $\sigma_s = 0.31$nm, if they are fully correlated we suggest this system should behave similarly to flat graphene with $\sigma_s = 0.09$nm. Likewise, with no correlation, the effective $\sigma_s = \sqrt{\sigma_s^2 + \sigma_g^2} = 0.38$nm. Under these assumptions, we use the gap correlation function from Eq. 5.29 instead of the traditional $\langle \widetilde{h}_s(\vec{q})\widetilde{h}_s(\vec{q}')\rangle$ in the surface profile function $a(q)$.

We use the Gaussian correlation regime for both the substrate and graphene autocorrelation, although we could just as well use the fractal or Bessel correlation forms. We have however confirmed in Section 5.1.2 that in the low wavenumber limit, the three forms are convergent, and there is therefore minimal difference in the percent difference of the plasmon frequency. One main advantage of the image potential method is that, despite its simplicity, it allows us to see the effects that different choices of the correlation function make.

In Fig. 5.5, where we analyze the change in frequency assuming the polarizability from Eq. 5.74, we seek plasmons in the range where Landau damping does not occur, for $0 \leq q/k_F < 1$. This is known as the ideal plasmon, as it neglects the effects of finite lifetime and scattering from charged impurities which would yield a perfect delta-peak in the energy loss function. We notice that even for a substrate which is similar in character to white noise, the roughness of the substrate affecting flat graphene is approximately 2%. Our image potential method also suggests that in the low wavenumber limit roughness becomes entirely negligible, an effect contrary to what we observed in Fig. 5.3. This suggests that the assumption of flat graphene is the main contributor in the plasmon frequency shift at low wavenumbers.

A reason for this small effect been suggested in [50], where the collective roughness of the substrate is said to be equivalent to a thin dielectric layer on top of a flat substrate. Thus, the relatively large average distance between graphene and substrate helps explain the small effect that changing a or σ has on the plasmon dispersion relation. The effect of the roughness in our plots is to make the plasmon frequency lower, but there is an equivalent branch the plasmon divides into making the frequency increase. We recall the dispersion relation for a surface plasmon on a substrate generally splits into two branches in the presence of surface roughness, as seen in Eq. 5.61.

We notice that although we now have a result which includes a non-perturbative rough surface profile function, a few assumptions needed to be made to obtain this result. Clearly letting $h_g(\vec{r}) = 0$, given the experimental data we have available, is a very rough approximation. In addition to the fact that this assumption implies flat graphene, it also implies that the local gap height between the substrate and graphene is negligible i.e. that the substrate is far enough away that the substrate surface appears as a flat surface with some correlations. This is another very rough approximation, given how close the two surfaces can

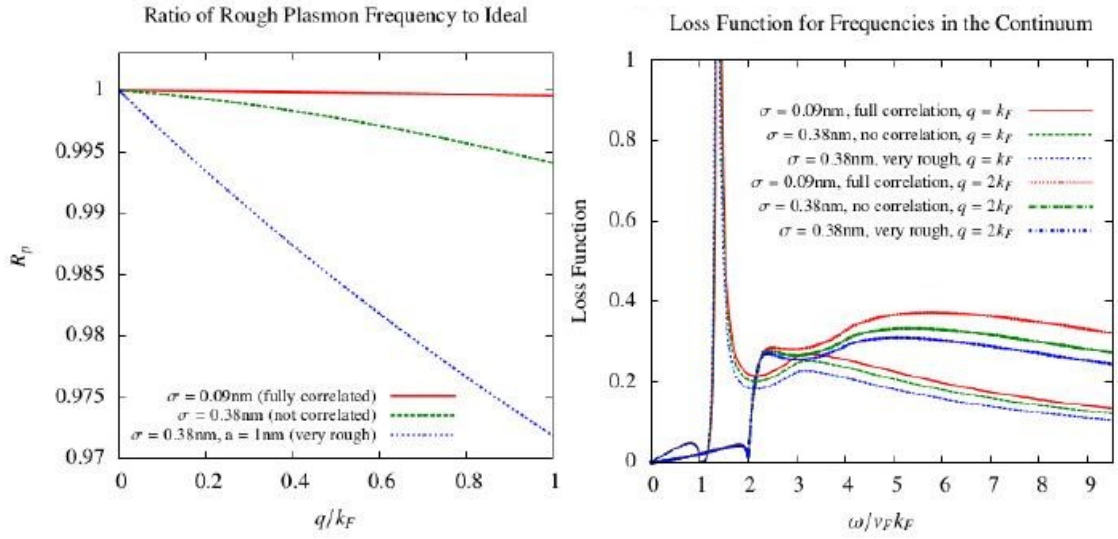

Figure 5.5: Percent difference of plasmon frequency and energy loss function for three different regimes of grapehene roughness. We assume $h_0 = 0.42$nm, $E_F = 0.1$eV and $\epsilon = 3.9$, with a_g, σ_g, σ_s and a_s in Table 1 using the Gaussian correlation function. $a_s = 1$ is used in the "very rough" regime. Adapted from [35]

be (as seen in Section 5.1.3 on thin membranes). One result of this assumption of a large distance between the graphene and substrate surfaces is that any point on the graphene will be higher than every point on the substrate, so that the approximation $|z - z'| = z' - z$ is valid for graphene at z'. An attempt to rectify these properties is given in the next section.

Determining the plasmon dispersion is one way to look at how roughness changes the frequencies that our system resonates at. Under the assumption of optical limit polarizability, we see that the relation between k and ω is very simple. However, one of the powerful tools at our disposal via this Green's function approach is that we have determined something similar to an effective dielectric function in the denominator. We will be able to look at what is called the loss function, just as in Eq. 5.68. Although under the traditional optical limit we will be observing a delta peak for such a function, an expanded model [22] that includes imaginary parts to the polarizability and wavenumbers beyond just linear dispersion near the Dirac cone are thereby considered in order to see the effects of roughness in regions where $\Im\chi(k, \omega)$ is non-zero (such as the region of Landau damping beyond the Fermi wavenumber $k > k_F$). Implementing such models is numerically intensive for the plasmon dispersion in Section 5.2.1, and for that section we therefore stick to the optical limit polarizability. This restrains us to discussing the roughness in the low k limit, but this is the region where the plasmon is strongest and is therefore of the most interest.

Figure 5.5 also shows the energy loss dispersion for two different wavevectors, $q = k = k_F$, where the plasmon just enters the electron-hole continuum (see Fig. 3.4), and $q = k = 2k_F$, where it is deep into the continuum, both chosen for a specific wavenumber q to highlight the change in absorption for different energies. One can see that moving deep into the region of heavy losses obliterates the delta-peak reminiscent of the lossless plasmon. The figure shows that roughness has its largest effect in the region of Landau damping, where the asymmetric broadening of the plasmon decreases by approximately 5% from the fully correlated case, which we mentioned was nearly equivalent to the case of flat graphene hovering over a flat

substrate.

5.2.3 Green's Function in Perturbative Case

The assumption of flat graphene, for which the non-perturbative case made the assumption, requires rectification. To do this, recall for the flat case we let $z = z' = h_0$ in the expression for Eq. 5.92, which is the Fourier-transformed equation for the Green's function in Eq. 5.84, using our derivation that the potential $A(\vec{q})$ could be written via a surface profile function $a(q)$ as in Eq. 5.89. Instead of this approach, we deign to construct a function similar to $g(k, z, z')$ in Eq. 5.92, but with our heights, given by $z = h_0 + h_g(\vec{r})$ and $z' = h_0 + h_g(\vec{r}')$ plugged into Eq. 5.84 to properly treat the potential on the surface of rippled graphene. Once these heights are inputted, our new Green's function, which will be a second-order perturbation of the Green's function for the potential on flat graphene above a flat substrate, can be computed.

Now, to second order in both $h_s(\vec{r})$ and $h_g(\vec{r})$, we must retain the factors up to second order only in our perturbation of Eq. 5.84, including perturbations of the potential component $A(\vec{q})$ shown in Eq. A.60. Looking at this equation, the inhomogenous term and A_0 will contain up to 2nd order in h_g, A_1 will contain up to first order in h_g and first order in h_s (and will therefore involve the correlation between the two surfaces), and A_2, the second-order perturbation in h_s to the homogenous component of the potential $A(\vec{q})$ above the surface, is expanded to zeroth-order in h_g as assumed in the flat case.

We begin by rewriting our desired problem in Fourier space, letting $\psi(\vec{r}) = \phi(\vec{r}, h_g(\vec{r}))$ be the local potential on graphene. Using our equation for the charge density due to the polarizability,

$$\begin{aligned}
\psi(\vec{p}) &= \int d^2\vec{r} e^{-i\vec{p}\cdot\vec{r}} \psi(\vec{r}) \\
&= -e^2 \int d^2\vec{r} e^{-i\vec{p}\cdot\vec{r}} \int d^2\vec{r}' G(\vec{r}, \vec{r}', h_g(\vec{r}), h_g(\vec{r}')) \int d^2\vec{r}'' \int \frac{d^2\vec{p}'}{(2\pi)^2} e^{i\vec{p}'\cdot(\vec{r}'-\vec{r}'')} \chi(\vec{p}') \psi(\vec{r}'') \\
&= -e^2 \int \frac{d^2\vec{p}'}{(2\pi)^2} \chi(\vec{p}') \psi(\vec{p}') \int d^2\vec{r} \int d^2\vec{r}' e^{i(\vec{p}'\cdot\vec{r}' - \vec{p}\cdot\vec{r})} g(\vec{r}, \vec{r}', h_g(\vec{r}), h_g(\vec{r}')) \\
&= -e^2 \int \frac{d^2\vec{p}'}{(2\pi)^2} \chi(\vec{p}') \psi(\vec{p}') \widetilde{g}(\vec{p}, \vec{p}'), \qquad (5.103)
\end{aligned}$$

which implicitly defines $\widetilde{g}(\vec{p}, \vec{p}')$. Before, our Green's function for the point source was $g(k, z, z')$, but now we know exactly the location of the graphene, but we also acknowledge that there may be some non-locality in the coupled substrate-graphene system, and we must therefore include a dependence of both $\vec{p}, \vec{p}'$. Our desire is to determine this function $\widetilde{g}(\vec{p}, \vec{p}')$ to second order in our height profiles $h_s(\vec{r})$ and $h_g(\vec{r})$ as additions to our previous framework. Later we will consider the effects of graphene crumpling and surface terms and their effect on this Green's function. We note that this Green's function does not require a Dyson expansion as does $\widetilde{g}(\vec{k}, z, z')$, as Eq. 5.103 includes graphene's response already.

We note that it is desirable for our Green's function $\widetilde{g}(\vec{p}, \vec{p}')$ to be only $\vec{p}$-dependent, as our Green's relation would then become an eigenvalue problem - we will touch on this later.

In the equation's current form, however, it is not terribly useful to us; this is because $\psi(\vec{p})$ is itself rough, yet we need some way to determine a dispersion relation from it. We have two options set before us: in Section 5.2.1 we used the equation for the potential along with a potential extinction method and a smoothing operator technique to directly

determine the dispersion relation from a matrix equation for $\langle A(\vec{k})\rangle$. In Section 5.2.2 we worked directly with the Green's function under the assumption of flat graphene being affected by the average effect of the rough substrate beneath it. To continue in the spirit of the Green's function method then, we implement Bourret's approximation [5]

$$\langle\psi(\vec{p})\rangle = -e^2 \int \frac{d^2\vec{p}'}{(2\pi)^2}\chi(\vec{p}')\langle\psi(\vec{p}')\rangle\langle\widetilde{g}(\vec{p},\vec{p}')\rangle. \tag{5.104}$$

This common approximation used in stochastic processes is in fact equivalent to our first-order approximation from Eq. A.12 for $\langle M_1\rangle$. We make the definition in text from now on that $\widetilde{g} = \langle\widetilde{g}(\vec{p},\vec{p}')\rangle$.

We begin with the potential due to the free Coulomb interaction at the point $z = h_0 + h_g(\vec{r})$ due to a point source at a height $z' = h_0 + h_g(\vec{r}')$.

$$\widetilde{g}_{free} = \int d^2\vec{r}\int d^2\vec{r}' e^{i(\vec{p}'\cdot\vec{r}'-\vec{p}\cdot\vec{r})}\int \frac{d^2\vec{k}}{(2\pi)^2}\frac{2\pi}{k}e^{i\vec{k}\cdot(\vec{r}-\vec{r}')}e^{-k|h_g(\vec{r})-h_g(\vec{r}')|} \tag{5.105}$$

We can switch temporarily to real coordinates, where our Coulomb potential reads as

$$\begin{aligned}\widetilde{g}_{free} &= \int d^2\vec{r}\int d^2\vec{r}' e^{i(\vec{p}'\cdot\vec{r}'-\vec{p}\cdot\vec{r})}\frac{1}{\sqrt{(\vec{r}-\vec{r}')^2+(h_g(\vec{r})-h_g(\vec{r}'))^2}} \\ &\approx \int d^2\vec{r}\int d^2\vec{r}' e^{i(\vec{p}'\cdot\vec{r}'-\vec{p}\cdot\vec{r})}\frac{1}{|\vec{r}-\vec{r}'|}\left\{1-\frac{1}{2}\frac{(h_g(\vec{r})-h_g(\vec{r}'))^2}{(\vec{r}-\vec{r}')^2}\right\}\end{aligned} \tag{5.106}$$

The average of the height profiles yields the autocorrelation. This correlation will be dependent on $|\vec{r}-\vec{r}'|$, and since this is the only variable, we shift our integration to depend on $\vec{r}_- = \vec{r}-\vec{r}'$. Using Eq. 5.14 we obtain

$$\widetilde{g}_{free} = \widetilde{g}_{0,free} + \widetilde{g}_{2,free} = (2\pi)^2\delta(\vec{p}-\vec{p}')\int\frac{d^2\vec{r}_-}{|\vec{r}_-|}\left[1-\sigma_g^2\frac{1-C_g(|\vec{r}_-|)}{|\vec{r}_-|^2}\right]e^{-i\vec{p}\cdot\vec{r}_-}. \tag{5.107}$$

This perturbative expansion, like its counterpart for flat graphene, contains a local wavevector response. Using a Gaussian correlation function as in Eq. 5.26 yields an analytic form for this Green's function

$$\widetilde{g}_{free} = (2\pi)^2\delta(\vec{p}-\vec{p}')\frac{2\pi}{p}\left\{1-(\sigma_g p)^2\left[-1+\frac{\sqrt{\pi}}{2}e^{-2\beta^2}\left[(\beta+\frac{1}{\beta})I_0(2\beta^2)+\beta I_1(2\beta^2)\right]\right]\right\} \tag{5.108}$$

$$\to \frac{2\pi}{p}\left[1-\left(\frac{\sigma_g}{a_g}\right)^2 pa_g\right] \text{ for } pa_g \ll 1 \text{ and } \to \frac{2\pi}{p}\left[1-\left(\frac{\sigma_g}{a_g}\right)^2\right] \text{ for } pa_g \gg 1 \tag{5.109}$$

with $\beta = pa_g/2$, and a_g the transverse correlation length of graphene as shown in Table 5.1. Comparing these results with Table 5.1 shows that roughness does not have a large effect to 2nd order in either limiting case on the overall Green's function for the free part. This however shows that much rougher surfaces require careful consideration.

The expansion of the image potential (the second term in Eq. 5.92) due to a flat substrate (A_0) follows similar lines of reasoning, yielding the Green's function $\widetilde{g}_{00}+\widetilde{g}_{02}$ (zeroth order in h_s, zeroth and 2nd order in h_g).

$$\begin{aligned}\widetilde{g}_{00}+\widetilde{g}_{02} &= (2\pi)^2\delta(\vec{p}-\vec{p}')\frac{2\pi}{p}\frac{1-\epsilon}{1+\epsilon}e^{-2ph_0}+\frac{1-\epsilon}{1+\epsilon}\int\frac{d^2\vec{k}}{(2\pi)^2} \\ &\times\frac{2\pi}{k}e^{-2kh_0}\int d^2\vec{r}\int d^2\vec{r}' e^{-i((\vec{k}-\vec{p}')\cdot\vec{r}'-(\vec{k}-\vec{p})\cdot\vec{r})}\frac{1}{2}k^2(h_g(\vec{r})+h_g(\vec{r}'))^2,\end{aligned} \tag{5.110}$$

forgetting the first-order contribution as it averages to 0. Again the correlation function yields a translational invariance, so upon averaging the integration can be shifted.

$$\widetilde{g}_{02} = (2\pi)^2\delta(\vec{p}-\vec{p}')\frac{2\pi}{p}\frac{1-\epsilon}{1+\epsilon}\Bigg[e^{-2ph_0}+ \int\frac{d^2\vec{k}}{(2\pi)^2}\frac{2\pi}{k}e^{-2kh_0}k^2\int d^2\vec{r}_- e^{i(\vec{k}-\vec{p})\cdot\vec{r}_-}\sigma_g^2[1+C_g(|\vec{r}_-|)]\Bigg]. \tag{5.111}$$

This portion of the Green's function again gives a local wavenumber response.

Now, our perturbation must consider the correlation between the first-order perturbation in the substrate with that in the graphene. We therefore use A_1 as shown in Appendix 3 to obtain

$$\widetilde{g}_{11} = \int d^2\vec{r}e^{-i\vec{p}\cdot\vec{r}}\int d^2\vec{r}'e^{i\vec{p}'\cdot\vec{r}'}\int\frac{d^2\vec{k}}{(2\pi)^2}e^{-kh_0}e^{i\vec{k}\cdot\vec{r}} \times 4\pi\frac{1-\epsilon}{(\epsilon+1)^2}\int\frac{d^2\vec{q}}{(2\pi)^2}e^{-i\vec{q}\cdot\vec{r}'}e^{-qh_0}(\epsilon+\hat{k}\cdot\hat{q})\widetilde{h}_s(\vec{k}-\vec{q})[1-kh_g(\vec{r})-qh_g(\vec{r}')] \tag{5.112}$$

$$= 4\pi\frac{\epsilon-1}{(\epsilon+1)^2}\int\frac{d^2\vec{k}}{(2\pi)^2}e^{-kh_0}\int\frac{d^2\vec{q}}{(2\pi)^2}(\epsilon+\hat{k}\cdot\hat{q})\widetilde{h}_s(\vec{k}-\vec{q})e^{-qh_0}[k\widetilde{h}_g(\vec{p}-\vec{k})+q\widetilde{h}_g(\vec{q}-\vec{k}')]. \tag{5.113}$$

Upon averaging, we obtain

$$\widetilde{g}_{11} = 4\pi\frac{\epsilon-1}{(\epsilon+1)^2}\int\frac{d^2\vec{k}}{(2\pi)^2}ke^{-kh_0} \times[(\epsilon+\hat{k}\cdot\hat{p})e^{-ph_0}\langle\widetilde{h}_s(\vec{p}-\vec{k})\widetilde{h}_g(\vec{p}-\vec{k})\rangle+(\epsilon+\hat{k}\cdot\hat{p}')e^{-p'h_0}\langle\widetilde{h}_s(\vec{p}'-\vec{k})\widetilde{h}_g(\vec{p}'-\vec{k})\rangle] \tag{5.114}$$

with integration parameters changed appropriately to yield a single integration.

We have in this cross-correlation Green's function perturbation a response that is both $\vec{p}$ and $\vec{p}'$ dependent, dashing our hopes of perturbatively solving our potential as an eigenvalue problem as mentioned above, unless we assume zero correlation between the surfaces.

Lastly, we write $\widetilde{g}_{20}$, which combines A_2 from Appendix 3 with the zeroth order of $z' = h_0 + h_g(\vec{r}')$ for a trivial definition:

$$\widetilde{g}_{20} = \int d^2\vec{r}e^{-i\vec{p}\cdot\vec{r}}\int d^2\vec{r}'e^{i\vec{p}'\cdot\vec{r}'}\int\frac{d^2\vec{k}}{(2\pi)^2}e^{-kh_0}e^{i\vec{k}\cdot\vec{r}}A_2(\vec{k},z'=h_0). \tag{5.115}$$

This expression for $\widetilde{g}_{20}$, just like $\widetilde{g}_{02}$, will contain a local wavevector response $\delta(\vec{p}-\vec{p}')$. These four derivations are the four we show, as the others when averaged are zero due to being of first-order in either h_g or h_s.

One major caveat of using the Green's function formalism is our ability to include various other effects that occur in the graphene monolayer due to effects not obtainable from boundary conditions in the Laplace's equation. One is the electronic response of crumpling, and the other is the area of graphene and its effect on the conductivity that we must be careful in handling. Current investigations into the nature of graphene reveal that the rough surface of the graphene plays a role in the low mobility of charges in the sheet. This, along with the effect of charged impurities in the substrate [2], are thought to be major players in the movement of graphene's free electrons.

Considering these effects brings up new questions about how to consider the roughness effects on the potential in graphene. One is that there is, in addition to the out-of-plane roughness, which we have modeled based on the Monge representation, an in-plane roughness, caused by the shift of spacings in the lattice between carbon atoms in the graphene sheet. Another is whether our assumption about the flat effect of our polarizability, $\chi(q,\omega)$, is justified given our other assumptions and our inclusion of second-order deformation of our sheet in the Green's function.

The crumpling of graphene, mediated by long-wavelength phonons coupling with graphene's electrons [38], contribute to strain and tension in the material, and these phonons, in a way analogous to the EM fields created by traveling photons, create a scalar potential V_1 and a vector potential A due to both in-plane and out-of-plane strains. As these are potentials, they would come about in our expression for the conductivity of the graphene, a variation of our expression in Eq. 5.47 in Fourier space [18, 19]:

$$\sigma(q) = -e^2\chi(q,\omega)\left(\widetilde{\phi}(q) + \widetilde{V}_1(q) + \frac{\omega}{q}\hat{q}\cdot\widetilde{A}(q)\right) \tag{5.116}$$

with $\chi(q,\omega)$ the flat polarizability from before. These potentials, derived from similar energy considerations that led us to write the free energy functional in Eq. 5.31, are not added directly into the Green's function but they do play a role in the final potential equations, and are implicitly already averaged over second-order terms in h_g (although under a different formalism using deformation tensors from elasticity theory).

Now we are faced with the question of how to properly incorporate the area of the graphene sheet in our calculations. In our derivations in Section 5.2.1 and their respective eigenvalue problem, we were able to write an equation up to first-order in our substrate (or substrate-graphene system), and hence neglect the factor $\sqrt{1+(\nabla h_g)^2}$ which would appear in the boundary conditions for graphene. In order to be consistent with the eigenvalue problem in our calculations in this section, should we include this factor in our polarizability and hence our conductivity? As shown in Appendix 3 and in Eq. 5.85, the differential area factor is what gives a second-order term in the directional derivative. If we include it as an addition to our flat case conductivity, it results in a renewed definition for $\sigma(\vec{r})$ [57]

$$\sigma(\vec{r},\omega)_{diff} = -e^2\int d^2\vec{r}''\sqrt{1+(\nabla h_g(\vec{r}''))^2}\chi(\vec{r}-\vec{r}'',\omega)\phi(\vec{r}''), \tag{5.117}$$

with which we would be forced to make a Bourret-like approximation if an averaged form for the potential is to be extracted from this equation. This approximation however is questionable and comes about solely due to our using a flat estimation for the polarizability, and its inclusion is hence an open question.

We are faced with a final question in this chapter - are we are able to construct a full Green's function, starting from a graphene point source, that includes the self-interaction of the graphene and hence the plasmonic behaviour? We have seen an issue in Eq. 5.114, where the non-local wavevector response yields a Green's function $\widetilde{g}(\vec{p},\vec{p}')$, unlike the local dependence we see elsewhere. This implies that given correlation between the substrate and graphene surfaces, the potential $\langle\psi(\vec{p})\rangle$ cannot be separated out as an eigenvalue problem. What if we assume there is a negligible substrate-graphene correlation? There remains an issue with attempting to determine a full Green's function perturbatively: the perturbative orders of the heights do not match. To see this, let our potential $\langle\widetilde{\psi}(\vec{p})\rangle = \psi_0(\vec{p}) + \psi_2(\vec{p})$,

separating portions of the function based on their order in height profiles h_s or h_g. Then

$$\psi_0(\vec{p}) = -e^2 \int \frac{d^2\vec{p}'}{(2\pi)^2} (\widetilde{g}_{0,free}(\vec{p},\vec{p}') + \widetilde{g}_{00}(\vec{p},\vec{p}'))\chi(\vec{p}')\psi_0(\vec{p}') \tag{5.118}$$

$$\psi_2(\vec{p}) = -e^2 \int \frac{d^2\vec{p}'}{(2\pi)^2} \chi(\vec{p}')[(\widetilde{g}_{2,free} + \widetilde{g}_{02} + \widetilde{g}_{11} + \widetilde{g}_{20})\psi_0 + (\widetilde{g}_{0,free} + \widetilde{g}_{00})\psi_2], \tag{5.119}$$

by Eq. 5.103. The first equation, ψ_0, is a system with both a flat substrate and flat graphene a height h_0 above it, and can be seen to yield the flat plasmon dispersion when a non-zero ψ_0 is induced by the plasmon it describes. We can do this as the local response of the Green's function $\widetilde{g}_{0,free}(\vec{p},\vec{p}') + \widetilde{g}_{00}(\vec{p},\vec{p}')$ turns the zeroth order solution into an eigenvalue problem.

Similarly, the equation we have developed for ψ_2 is the second order correction to the potential on the surface of the graphene. This equation is in itself quite useful, as it gives the perturbative correction to the potential for a system with no external charges, so the plasmon dispersion will be the set of wavenumbers and frequencies that constitute the non-zero values of the potential for this equation.

However, are we able to combine the Green's functions into one large function that allows us to determine the plasmon relation? This is seen not to be the case, as there will be 'mixing' between terms of second order in the Green's function and terms of second order in the potential ψ_2 if this is attempted, yielding values of fourth order in the potential $\psi(\vec{p})$ which we did not account for. This is the ultimate issue with attempting to determine a perturbative form for the total Green's function. This should not be too surprising looking at the equations above - solving for ψ_0 will yield the flat plasmon dispersion, after which there is no way from the equation for ψ_2 to change the dispersion. The perturbed potential does however give us information about the effect of roughness on the potential, as we see in Eq. 5.109.

As it stands, there are now two consistent ways to determine the plasmon dispersion: one from the potentials themselves via an eigenvalue problem, and the other from a self-consistent Dyson equation for the point-source Green's function. These yield the same answers in the limit of no roughness despite being entirely different approaches. The question about which method yields the best interpretation for how plasmons behave on a rough surface is open, but both methods have their merits.

A summary of the three methods outlined in this Chapter, as well as the pros and cons of the methods are found in a table on the next page.

Methods for Solving Doubly Rough Surface Plasmon Dispersion for Graphene

First-Order Expansion with Smoothing Method to Second-Order

- Using Green's Second Theorem, this method turns the three-potential problem into one with just ϕ_2, expands boundary conditions to first order, then uses the smoothing method for eigenvalue problems with stochastic variables (Appendix 1) to determine a self-consistent plasmon dispersion correction
- Can be generalized easily to graphene on top of the substrate, free graphene, and for a frequency-dependent substrate that can sustain its own plasmons
- Advantages: Gives both real and imaginary corrections to plasmon dispersion equation; self-consistent treatment of roughness
- Disadvantages: Only expands boundary conditions to first-order, neglecting substrate-graphene interactions and other second-order effects; numerically challenging: requires iterative computation and works best for low roughness and low wavenumber

Image Potential in Non-Perturbative Regime

- Approaching the problem from a Green's Function perspective, this method computes $g(\vec{k}, z, z')$ for a point charge above the graphene, computes the average non-perturbative effect of the substrate underneath, and uses a Dyson series to determine the full Green's function for the self-potential induced by the graphene, giving the plasmon dispersion
- Can only be used for graphene above the substrate, under the flexible assumption that each point on the graphene is above the highest peak on the substrate surface
- Advantages: Allows for full graphene wavenumber spectrum analysis through an energy-loss function; self-consistent plasmon dispersion
- Disadvantages: Assumes flat graphene; neglects substrate-graphene interactions and other second-order effects

Image Potential in Perturbative Regime

- Using Bourret's approximation, we obtain a second-order Green's function based on the roughness of the substrate and graphene involved in the boundary conditions. Allows for computation of the potential on the graphene surface, on average
- Advantages: Can include effects such as crumpling of the graphene and the differential area of the graphene.
- Disadvantages: Perturbative Green's function cannot be used to deduce plasmon dispersion equation due to order mismatch; non-local wavenumber means eigenvalue problem only defined under special conditions

Chapter 6

Conclusion

6.1 Summary

Investigating graphene and all its intricate complexities is a task not attempted by the author. The breadth and scope of the research being done experimentally and theoretically in everything from its opto-electronic properties to its use as a membrane in biology to its tremendous breaking strength makes it a fascinating area to pursue. For this thesis, we decided to investigate graphene plasmonics in two different contexts: one where plasmons that occur due to saddle points in the graphene energy band structure create absorbance patterns that we modeled semi-classically via a hydrodynamic model, and another where we utilized electromagnetic PDEs and their boundary conditions on rough surfaces to determine the overall effect of roughness on the behaviour of plasmons restrained to the graphene surface.

Two main themes spanned both of these topics. The first is our postulate that graphene, due to its monolayer thickness, should be treated as a two-dimensional material. Given the physical size of atoms, this is still an approximation, but the limited dimensions that electrons and holes are restricted to on the graphene sheet make our conjecture plausible. We extended this theory to experimental areas like Electron Energy Loss Spectroscopy and Ellipsometry, experimental methods commonly used in the analysis of thin films, where our conjecture and the results that follow from it gave us a new way to interpret results about the reflectance of light and the absorption modes of two dimensional materials; based on our assumptions we derived that a peak in the spectra for electron energy loss is likely due to linear energy dispersion for low energy electrons in monolayer graphene. Our postulate also allowed us to implement graphene as a boundary condition in Maxwell's equations, which we then used to derive perturbative results for the effect that a rough surface (with roughness also factored into the boundary conditions) would have on the resonance of electron oscillations.

Both of these topics spanned many aspects of the theory of light and matter in the context of a graphene sheet, and to arrive at any useful result requires consistent but careful use of assumptions in our theories. The second theme of this thesis has been the exploration of different regimes within which our various approximations would hold. In the introductory chapters we introduced many of them, including the quasi-static approximation, the optical limit of graphene, the isotropy of graphene, the Random Phase Approximation, the hydrodynamic model for π and σ plasmons, and the validity of Maxwell's equations for a nano-scale structure. In the context of modeling spectroscopy data, we made assumptions

about the nature of inelastic scattering in graphene and of light reflection from a rippled interface, and for roughness we explored different methods that implemented differing ways of cataloging the effects of rippled surfaces as well as phenomenologically and theoretically determining the correlation function of graphene. Although not results in themselves, much of our research is motivated by our need to make better and better approximations as our knowledge of graphene's material and electrical properties expands.

Starting from the basics of electromagnetism, we derived conditions required for plasmons to exist and ways to determine the plasmon dispersion relation. Our exploration of the electronic properties of graphene led us into RPA results derived from a combination of a tight-binding approximation and Fermi Liquid theory, yielding a conductivity that we used in the theoretical modeling of electron loss spectra and of polarization light changes upon interaction with monolayer graphene. A need to describe the surface that these properties exhibited themselves on led us into a mathematical investigation into the nature of rippling on graphene and the stochastic ways to describe it and the effect the rippling has on plasmons.

Ultimately, our thesis presented many ideas about the nature of graphene. The main one was the constant emphasis on graphene's effectively two-dimensional structure and how this will change our approach to spectroscopic analysis and in computing the plasmon dispersion. We presented the idea that a proper subtraction of the zero-loss peak in EELS done on small graphene flakes should maintain a sharp peak due to interband transitions in the regime of very low energies. Also shown was that our two-fluid HD model combined with a Dirac term is able to predict effects such as the asymmetric energy loss spectra, placement of the absorbance peak, fluctuations in light polarization and the valency of carbon's orbital electrons at certain energies. We illustrated the solvability of stochastic systems via a proper treatment of the rough perturbations to the flat potential and the flat boundary conditions, giving numerical predictions for graphene based on measured stochastic properties of the material. These numerical plots showed in different regimes the regions where roughness affected graphene the most. For one method we extracted a damping term from an eigenvalue solution to the dispersion relation, suggesting mathematically that rippling forces the eventual decay of the plasmon, although this remains speculation.

6.2 Future Work

Many of the next steps that can be undertaken have been alluded to in previous chapters, and we elaborate on them below.

Our theoretical models for the spectroscopic data analyzed in Chapter 4, despite making useful predictions, are a long way away from being able to predict the spread of experimental data from our two-dimensional model. The reconciliation of the two regimes of conductivity from Section 4.2.1, due to its discontinuity in the imaginary space, can be further improved by incorporating approximate models for the electronic effects in the 1-3eV range, although the advantage of our model is its simplicity and explanatory power. Results may also be improved by developing a theory for the effective polarization of water molecules and other impurities wedged beneath the graphene sheet. For this investigation, we can in fact incorporate some of our framework from Chapter 5 and consider a stochastic treatment of impurities that influence the electronic structure of the graphene, thereby changing the response of the graphene to incident photons or electrons. From a theoretical standpoint, checking the Kramers-Kronig relations to ensure our conductivity is a proper response function,

and verifying the f-sum rule holds for the Hamiltonian used to generate our semi-classical conductivity will in future work help validate our theory and our hypothesis that treating graphene as two-dimensional is valid in our systems of consideration.

Since our modeling in Chapter 4 is mostly as a tool to analyze the general trend of data, corrections to it can be checked against experiment. Our perturbative analysis in Chapter 5 has yet to be compared to experimental analysis of plasmon loss and dispersion on a graphene surface, although similar analysis for plasmons on rough dielectrics with surface modes reveal a good match between theory and experiment [50]. Future work will attempt to determine of the three methods considered which is the best in predicting the change in the frequency over time for different regimes, and more powerful numerical techniques can reveal the effects that using the Gaussian correlation function versus the healing assumption or the fractal correlation function have on the plasmon dispersion and the energy loss of our plasmons. Another technique of interest would be the comparison of the roughness effects between graphene laying directly on the surface of the substrate compared to the system of smooth graphene on a rougher substrate with gaps between. A large divergence in the results may reveal that assuming zero gap between graphene and its substrate is not valid in some regimes of graphene plasmonics. An analysis of the coupling of phonon modes to the Dirac plasmon for low energies [34], done by a suitable choice of dielectric, may reveal roughness to have a stronger effect here than on the plasmon alone.

Perhaps of most interest in future work is investigating via our smoothing method the effects of charged impurities on the low energy Dirac plasmon for doped graphene - if the impurities or contaminants in the substrate are stochastically spread, they will individually raise or lower the local Fermi energy in graphene, causing the fluctuation in the Fermi energy to now be a stochastic parameter. We have good models to predict the autocorrelation of the Fermi energy fluctuation due to substrate impurities [2] and can therefore determine the potential on the surface as in Section 5.2.1 and thence find the shift in the plasmon dispersion relation via an eigenvalue problem. It is likely that this Fermi energy shift can have a large effect on the overall plasmonic behaviour of the substrate, as has been suggested in some studies [19].

Bibliography

[1] I. Abril, R. Garcia-Molina, C. D. Denton, F. J. Pérez-Pérez, and N. R. Arista. "Dielectric description of wakes and stopping powers in solids". *Physical Review A* **58** (1998).

[2] R. Anicic. "Effects of the Dielectric Environment on the Electrical Properties of Graphene". MA thesis. University of Waterloo, (2013). URL: `http://hdl.handle.net/10012/7804`.

[3] P. Avouris and M. Freitag. "Graphene Photonics, Plasmonics, and Optoelectronics". *IEEE Journal of Selected Topics In Quantum Electronics* **20** (2014).

[4] Y. V. Bludov, A. Ferreira, N. M. R. Peres, and M. I. Vasilevskiy. "A Primer On Surface Plasmon-Polaritons In Graphene". *International Journal Of Modern Physics B* **27** (2013).

[5] R. Bourret. "Ficton theory of dynamical systems with noisy parameters". *Canadian Journal of Physics* **43** (1965), 619–639.

[6] H. Buljan, M. Jablan, and M. Soljacic. "Graphene plasmonics: Damping of plasmons in graphene". *Nat Photon* **7** (2013). News and Views, 346–348.

[7] A. H. Castro Neto, F. Guinea, N. M. R. Peres, K. S. Novoselov, and A. K. Geim. "The electronic properties of graphene". *Rev. Mod. Phys.* **81** (2009), 109–162.

[8] W. G. Cullen, M. Yamamoto, K. M. Burson, J. H. Chen, C. Jang, L. Li, M. S. Fuhrer, and E. D. Williams. "High-Fidelity Conformation of Graphene to SiO2 Topographic Features". *Physical Review Letters* **105** (2010).

[9] V. Despoja, D. Novko, K. Dekanić, M. Šunjić, and L. Marušić. "Two-dimensional and π plasmon spectra in pristine and doped graphene". *Physical Review B* **87** (2013), 075447.

[10] M. Dressel. *Electrodynamics of solids: optical properties of electrons in matter*. Cambridge University Press, (2002).

[11] R. F. Egerton. *Electron energy-loss spectroscopy in the electron microscope*. Vol. 233. Springer, (1996).

[12] L. Falkovsky. "Optical properties of graphene". *arXiv preprint arXiv:0806.3663* (2008).

[13] G. A. Farias and A. Maradudin. "Effect of surface roughness on the attenuation of surface polaritons on metal films". *Physical Review B* **27** (1983), 7093.

[14] G. A. Farias and A. A. Maradudin. "Surface plasmons on a randomly rough surface". *Physical Review B* **28** (1983), 5675.

[15] M. Freitag, T. Low, W. Zhu, H. Yan, F. Xia, and P. Avouris. "Photocurrent in graphene harnessed by tunable intrinsic plasmons". *Nat Commun* **4** (2013).

[16] H. Fujiwara. *Spectroscopic ellipsometry: principles and applications*. John Wiley & Sons, (2007).

[17] F. J. García de Abajo. "Nonlocal effects in the plasmons of strongly interacting nanoparticles, dimers, and waveguides". *The Journal of Physical Chemistry C* **112** (2008), 17983–17987.

[18] M. Gibertini, A. Tomadin, F. Guinea, M. I. Katsnelson, and M. Polini. "Electron-hole puddles in the absence of charged impurities". *Physical Review B* **85** (2012), 201405.

[19] M. Gibertini, A. Tomadin, M. Polini, A. Fasolino, and M. Katsnelson. "Electron density distribution and screening in rippled graphene sheets". *Physical Review B* **81** (2010), 125437.

[20] G. Giuliani and G. Vignale. *Quantum theory of the electron liquid*. Cambridge university press, (2005).

[21] A. N. Grigorenko, M. Polini, and K. S. Novoselov. "Graphene plasmonics". *Nature Photonics* **6** (2012), 749–758.

[22] E. H. Hwang and S. Das Sarma. "Dielectric function, screening, and plasmons in two-dimensional graphene". *Phys. Rev. B* **75** (2007), 205418.

[23] M. Ishigami, J. Chen, W. Cullen, M. Fuhrer, and E. Williams. "Atomic structure of graphene on SiO2". *Nano letters* **7** (2007), 1643–1648.

[24] M. Jablan, M. Soljacic, and H. Buljan. "Plasmons in Graphene: Fundamental Properties and Potential Applications". *Proceedings of the IEEE* **101** (2013), 1689–1704.

[25] J. D. Jackson and J. D. Jackson. *Classical electrodynamics*. Vol. 3. Wiley New York etc., (1962).

[26] M. I. Katsnelson. *Graphene: Carbon in two dimensions*. Cambridge University Press, (2012).

[27] M. I. Katsnelson. "Graphene: carbon in two dimensions". *Materials Today* **10** (2007), 20–27.

[28] E.-A. Kim and A. C. Neto. "Graphene as an electronic membrane". *EPL (Europhysics Letters)* **84** (2008), 57007.

[29] F. H. Koppens, D. E. Chang, and F. J. Garcia de Abajo. "Graphene plasmonics: a platform for strong light–matter interactions". *Nano letters* **11** (2011), 3370–3377.

[30] V. G. Kravets, A. N. Grigorenko, R. R. Nair, P. Blake, S. Anissimova, K. S. Novoselov, and A. K. Geim. "Spectroscopic ellipsometry of graphene and an exciton-shifted van Hove peak in absorption". *Physical Review B* **81** (2010).

[31] O. Krivanek, G. Corbin, N. Dellby, B. Elston, R. Keyse, M. Murfitt, C. Own, Z. Szilagyi, and J. Woodruff. "An electron microscope for the aberration-corrected era". *Ultramicroscopy* **108** (2008), 179–195.

[32] H. W. Kroto, J. R. Heath, S. C. O'Brien, R. F. Curl, and R. E. Smalley. "C60: Buckminsterfullerene". *Nature* **318** (1985), 162–163.

[33] T. Low and P. Avouris. "Graphene Plasmonics for Terahertz to Mid-Infrared Applications". *ACS Nano* **8** (2014), 1086–1101.

[34] X. Luo, T. Qiu, W. Lu, and Z. Ni. "Plasmons in graphene: Recent progress and applications". *Materials Science & Engineering R-Reports* **74** (2013), 351–376.

[35] K. A. Lyon and Z. Mišković. "The effects of the substrate surface roughness on graphene plasmons". *Electronic, Photonic, Plasmonic, Phononic And Magnetic Properties Of Nanomaterials*. Vol. 1590. AIP Publishing. 2014, pp. 163–167.

[36] K. A. Lyon, Z. Mišković, A. C. Diebold, and J.-C. Idrobo. "Modeling ellipsometry and electron energy loss spectroscopy of graphene". *Electronic, Photonic, Plasmonic, Phononic And Magnetic Properties Of Nanomaterials*. Vol. 1590. AIP Publishing. 2014, pp. 158–162.

[37] S. A. Maier. *Plasmonics: Fundamentals and Applications: Fundamentals and Applications*. Springer, (2007).

[38] J. L. Manes. "Symmetry-based approach to electron-phonon interactions in graphene". *Physical Review B* **76** (2007).

[39] A. Maradudin. *Electromagnetic surface excitations on rough surfaces*. Springer, (1986), pp. 57–131.

[40] A. Marinopoulos, L. Reining, A. Rubio, and V. Olevano. "Ab initio study of the optical absorption and wave-vector-dependent dielectric response of graphite". *Physical Review B* **69** (2004), 245419.

[41] R. D. Mattuck. *A guide to Feynman diagrams in the many-body problem*. Courier Dover Publications, (2012).

[42] Z. Mišković. *Interaction of Graphene with Charged Particles*. Presentation.

[43] Z. Mišković, P. Sharma, and F. Goodman. "Ionic screening of charged impurities in electrolytically gated graphene". *Physical Review B* **86** (2012), 115437.

[44] D. J. Mowbray, S. Segui, J. Gervasoni, Z. Mišković, and N. R. Arista. "Plasmon excitations on a single-wall carbon nanotube by external charges: Two-dimensional two-fluid hydrodynamic model". *Physical Review B* **82** (2010).

[45] F. Nelson. "Study of the Dielectric Function of Graphene from Spectroscopic Ellipsometry and Electron Energy Loss Spectroscopy". PhD thesis. University of Albany, State University of New York, (2012).

[46] F. J. Nelson, J. C. Idrobo, J. D. Fite, Z. L. Mišković, S. J. Pennycook, S. T. Pantelides, J. U. Lee, and A. Diebold. "Electronic excitations in graphene in the 1-50 eV range-The Π and $\Pi + \sigma$ peaks are not plasmons". *Nano Letters* (2014).

[47] L. Novotny and B. Hecht. *Principles of nano-optics*. Cambridge university press, (2012).

[48] G. Palasantzas and G. Backx. "Fluctuation properties of interfaces and membranes bounded by self-affine surfaces". *Physical Review B* **55** (1997), 9371.

[49] D. Pines and P. Nozières. *The theory of quantum liquids*. Addison-Wesley, (1990).

[50] T. S. Rahman and A. A. Maradudin. "Effect of surface roughness on the image potential". *Physical Review B* **21** (1980), 504.

[51] J. Sabio González. "Interactions in novel low-dimensional quantum systems: arrays of cold atoms and graphene monolayers". PhD thesis. Universidad Complutense de Madrid, Servicio de Publicaciones, (2010).

[52] J. Sabio, J. Nilsson, and A. H. C. Neto. "f-sum rule and unconventional spectral weight transfer in graphene". *Physical Review B* **78** (2008).

[53] F. Schwierz. “Graphene transistors”. *Nature Nanotechnology* (2010), 487–496.

[54] I. Simonsen. “Optics of surface disordered systems”. *The European Physical Journal Special Topics* **181** (2010), 1–103.

[55] N. Stander, B. Huard, and D. Goldhaber-Gordon. “Evidence for Klein Tunneling in Graphene *p-n* Junctions”. *Phys. Rev. Lett.* **102** (2009), 026807.

[56] T. Stauber and G. Gómez-Santos. “Plasmons in layered structures including graphene”. *New Journal of Physics* **14** (2012), 105018.

[57] P. S. Swain and D. Andelman. “Supported membranes on chemically structured and rough surfaces”. *Physical Review E* **63** (2001), 051911.

[58] V. Volkov and S. Mikhailov. “Edge magnetoplasmons: low-frequency weakly damped excitations in inhomogeneous two-dimensional electron systems”. *Sov. Phys. JETP* **67** (1988), 1639–1653.

[59] A. V. Zayats, I. I. Smolyaninov, and A. A. Maradudin. “Nano-optics of surface plasmon polaritons”. *Physics reports* **408** (2005), 131–314.

[60] T. Zhan, X. Shi, Y. Dai, X. Liu, and J. Zi. “Transfer matrix method for optics in graphene layers”. *Journal of Physics-Condensed Matter* **25** (2013).

Appendix A

Appendix

A.1 Smoothing Method

The smoothing method follows a procedure in [39] to turn equations of the form

$$(H - V)R = f \tag{A.1}$$

into the form

$$(H - \langle M\rangle)\langle R\rangle = \langle F\rangle \tag{A.2}$$

where H, V are $n \times n$ matrices, R, f are $n \times 1$ column vectors, and V, R and f have the property of being stochastic. We include the additional caveat that H, V are similar to response functions and are not related in functional form to either R or f. By definition, they cannot be determined exactly, but their behaviour can be estimated based on averaging techniques. For example, if a function $\zeta(\vec{r}_\parallel)$ is a stochastic function over all planar radii $\vec{r}_\parallel$, then $\langle\zeta(\vec{r}_\parallel)\rangle$ tells you the average over all realizations, while $\langle\zeta(\vec{r}_\parallel)\zeta(\vec{r}'_\parallel)\rangle$ is an autocorrelation that gives you the average relationship between points on a plane.

Being able to put the first equation into a form that only measures the average of the variables considered is a great leap forward in determining properties about R. Usually the matrix V is a small stochastic perturbation of the larger, deterministic matrix H, and knowing the function $H - \langle M\rangle$ yields analytic properties about the average of our function R.

We introduce the operator P, which acts on a function f by $Pf = \langle f\rangle$. Its counterpart, Q, acts via $Qf = f - \langle f\rangle$, and represents fluctuations from the average of f. These operators act on everything after them. Starting from the first equation, noting that $f = P(f) + Q(f)$, we have

$$P(HR) - P(VR) = P(f) \longrightarrow HP(R) - P(VP(R)) - P(VQ(R)) = P(f) \tag{A.3}$$

$$Q(HR) - Q(VR) = Q(f) \longrightarrow HQ(R) - Q(VP(R)) - Q(VQ(R)) = Q(f) \tag{A.4}$$

$$(H - QV)QR = QVPR + Qf \tag{A.5}$$

$$QR = (H - QV)^{-1}QVPR + (H - QV)^{-1}Qf \tag{A.6}$$

Plugging this last equation into the first yields

$$HPR - PVPR - PV(H - QV)^{-1}QVPR = PV(H - QV)^{-1}Qf + Pf \tag{A.7}$$

$$(H - P(V + V(H - QV)^{-1}QV))PR = P(V(H - QV)^{-1}Qf + f). \tag{A.8}$$

This is our essential equation, as it shows there is an analytic way to represent the average of the functions in a consistent way. We proceed in this way as it is almost never the case that $P(VR) = PVPR$, which would give us a simple expression for $\langle R \rangle$. This is most obvious by considering a matrix V such that $PV = 0$, so the incorrect method would conclude that there is no average effect.

We have deduced the stochastic functions

$$M = V + V(H - QV)^{-1}QV \qquad F = f + V(H - QV)^{-1}Qf. \tag{A.9}$$

We now show that M is also equal to $V + MH^{-1}QV$, via a perturbative expansion in powers of QV.

$$\begin{aligned} M &= M_1 + M_2 + M_3 + \cdots \\ &= V + M_1 H^{-1} QV + M_2 H^{-1} QV + \cdots \\ &= V + VH^{-1}QV + VH^{-1}QVH^{-1}QV + \cdots \\ &= V + V(I + H^{-1}QV + H^{-1}QVH^{-1}QV + \cdots)H^{-1}QV \\ &= V + V(H - QV)^{-1}QV = M \end{aligned} \tag{A.10}$$

which shows the equivalency, using the geometric series expansion and hence the assumption that V is small compared to H. Multiplying the left side of $M = V + MH^{-1}QV$ by VM^{-1} and the right side by $V^{-1}M$ gives us another equivalency, $M = V + VH^{-1}QM$.

As we mentioned, the value V is generally small compared to H, so we will now be able to solve $\langle M \rangle$ via a perturbative expansion in V:

$$M = M_1 + M_2 + M_3 + \cdots \tag{A.11}$$

$$M_1 = V \longrightarrow \langle M_1 \rangle = \langle V \rangle \tag{A.12}$$

$$M_2 = V + VH^{-1}QV \longrightarrow \langle M_2 \rangle = \langle V \rangle + H^{-1}(\langle V^2 \rangle - \langle V \rangle^2) \tag{A.13}$$

$$M_3 = V + M_2 H^{-1} QV \tag{A.14}$$

where we note that this last averaging will have terms of the form $QVQV$ which when expanded become quite large.

It is interesting to observe that the averaged form of $\langle M \rangle$ does not depend on either f or R. Therefore any $n \times 1$ matrix R will yield the same factor $H - \langle M \rangle$ in its averaged form equation.

Although we now have an analytic form for M, a perturbative approach must be taken to each order we would like, and therefore the full function $\langle M \rangle$ can never be fully determined. We therefore proceed with a Green's function like method that eliminates the factors R, f, and shows that this approach, and the non-linearities it invokes, produces values for $\langle M \rangle$ reminiscent of self-energies that appear in many-body problems, giving an imaginary part to what, for H, M real valued matrices, is a surprising result. Although the two values of $\langle M \rangle$ will be perturbationally equivalent, this Green's function approach shows the non-perturbative result for $\langle M \rangle$ yields a complex-valued self energy [14].

Let $H^{-1} = G_0$, $(H - V)^{-1} = G$ and I be the identity (now using matrices in place of

vectors), so that

$$(H - V)G = I \longrightarrow (H - PM)PG = I \text{ or } (H - \langle M\rangle)\langle G\rangle = I \tag{A.15}$$
$$PG = G_0 + G_0PMPG \tag{A.16}$$
$$G = G_0 + G_0VG \tag{A.17}$$
$$G = G_0 + G_0VPG + G_0VQG \tag{A.18}$$
$$(I - G_0VQ)G = G_0 + G_0VPG \tag{A.19}$$
$$G = (I - G_0VQ)^{-1}G_0 + (I - G_0VQ)^{-1}G_0VPG \tag{A.20}$$
$$G = G_0 + G_0(I - G_0VQ)^{-1}VPG \tag{A.21}$$
$$\text{but } M = V + G_0VQM \longrightarrow M = (I - G_0VQ)^{-1}V, \tag{A.22}$$

where (A.16) follows from multiplying both sides of (A.15) by G_0, and (A.17) follows from our definitions of G and G_0.Therefore

$$G = G_0 + G_0MPG = G_0 + G_0VG \longrightarrow VG = MPG \tag{A.23}$$

This tidbit will allow us to derive an expression for M that can be computed perturbatively. In the expression $G = G_0 + G_0VG$, let $V = \langle M\rangle + (V - \langle M\rangle)$, so $G = G_0 + G_0\langle M\rangle G + G_0(V - \langle M\rangle)G$, which can be written as

$$(I - G_0\langle M\rangle)G = G_0(I + (V - \langle M\rangle)G). \tag{A.24}$$

Let G_1 be the solution for the first component of V:

$$G_1 = G_0 + G_0\langle M\rangle G_1 \tag{A.25}$$
$$G_1 = (I - G_0\langle M\rangle)^{-1}G_0 \tag{A.26}$$
$$G = G_1(I + (V - \langle M\rangle)G) \tag{A.27}$$

where (A.27) follows from (A.24). Now we have

$$G_1 = G_0 + G_0\langle M\rangle G_1 \text{ and } PG = G_0 + G_0\langle M\rangle PG \longrightarrow G_1 = PG \tag{A.28}$$

This yields, based on our derivation $G = G_1(I + (V - \langle M\rangle)G)$,

$$G = \langle G\rangle + \langle G\rangle(V - \langle M\rangle)G \tag{A.29}$$

Transforming via $VG\langle G\rangle^{-1}(\cdots)G^{-1}\langle G\rangle$ gives

$$VG = V\langle G\rangle + VG(V - \langle M\rangle)\langle G\rangle \tag{A.30}$$
$$M\langle G\rangle = V\langle G\rangle + M\langle G\rangle(V - \langle M\rangle)\langle G\rangle \tag{A.31}$$
$$M = V + M\langle G\rangle(V - \langle M\rangle), \tag{A.32}$$

yielding a final analytic value for M. If H, M are simple enough matrices, this result combined with the Gaussian property for higher order moments will give a non-perturbative solution to $\langle M\rangle$.

A.2 Linear Response Theory in Two Dimensions

Frequently we have encountered linear response theory in our treatment of electromagnetic problems and in graphene. The conductivity σ relates the current density to the electric field, the dielectric function ϵ relates the electric field due to external charges to the total field, and the polarizability χ relates the internal charge density to the total electric field. These are all intertwined but as the dimensionality of the problem changes, so does the dimensionality of the parameters σ, χ. ϵ relates two portions of an electric field, and therefore maintains its form.

We wish to derive the general relation between $\sigma(q,\omega)$ and $\chi(q,\omega)$. We start with the continuity equation in Fourier space:

$$\omega\rho_{int} = \vec{q}\cdot\mathbf{J}_{int} = \sigma\vec{q}\cdot\mathbf{E}_{tot}. \tag{A.33}$$

By definition we also have

$$\mathbf{E}_{tot} = -i\vec{q}\phi_{tot} + i\omega\mathbf{A} \text{ and } \rho_{int} = \chi(q,\omega)\phi_{tot} \tag{A.34}$$

with $(\vec{q},\omega)$ in all other variables implicitly. We note however that the vector potential $\mathbf{A}$ is gauge invariant, so within the Coulomb gauge we are able to choose $\nabla\cdot\mathbf{A} = 0$, and in this gauge the vector potential disappears from the final equation. It is important to note that our relation is only valid within this gauge, unless we work within an electrostatic approximation where $\partial\mathbf{A}/\partial t = 0$ always. Combining these all yields

$$\sigma(q,\omega) = \frac{i\omega}{q^2}\chi(q,\omega) \tag{A.35}$$

We recall another general form for the relation between the polarizability χ and the dielectric function ϵ,

$$\epsilon(q,\omega) = 1 - v(q)\chi(q,\omega) \tag{A.36}$$

where $v(q)$ is the unscreened Coulomb potential, a value that is equal to different values depending on the dimension of the problem:

$$v(q)_{3D} = \frac{1}{4\pi\epsilon_0}\frac{4\pi}{q^2} \qquad v(q)_{2D} = \frac{1}{4\pi\epsilon_0}\frac{2\pi}{q} \tag{A.37}$$

This definition stems from separating out the potential due to external and internal contributions

$$\phi_{tot} = \phi_{ext} + v(q)\chi(q,\omega)\phi_{tot} \longrightarrow \phi_{tot} = \frac{\phi_{ext}}{1 - v(q)\chi(q,\omega)} = \frac{\phi_{ext}}{\epsilon(q,\omega)} \tag{A.38}$$

We can see that we re-obtain our EM relation in three dimensions between ϵ and σ from Eq. 2.9

$$\epsilon(q,\omega) = 1 - \frac{1}{4\pi\epsilon_0}\frac{4\pi}{q^2}\chi(q,\omega) = 1 - \frac{1}{4\pi\epsilon_0}\frac{4\pi}{q^2}\left(\frac{q^2}{i\omega}\right)\sigma(q,\omega) = 1 + \frac{i\sigma(q,\omega)}{\epsilon_0\omega} \tag{A.39}$$

This same process using the two dimensional k-space Coulomb potential gives

$$\epsilon(q,\omega)_{2D} = 1 + \frac{iq}{2\epsilon_0\omega}\sigma(q,\omega)_{2D} \tag{A.40}$$

We also mention the relation between the internal potential and the internal charge density using (A.36) and (A.38), along with the definition of the internal charge density:

$$\phi_{int} = (1 - \epsilon(q,\omega))\phi_{tot} = v(q)\chi(q,\omega)\phi_{tot} = v(q)\rho_{int}, \tag{A.41}$$

which is applicable in any dimension.

A.3 Perturbative Potentials and Non-Perturbative Surface Profile Functions

Surface profile functions for a point charge above a randomly rough surface describe the average potential induced by the point charge. They have the form [50]

$$a(k) = \frac{1}{\epsilon+1}\frac{M_{22}(k)h_1(k) - M_{12}h_2(k)}{|M(k)|} \tag{A.42}$$

$$b(k) = \frac{1}{\epsilon+1}\frac{M_{11}(k)h_2(k) - M_{21}h_1(k)}{|M(k)|} \tag{A.43}$$

where $|M(k)|$ is the determinant of the matrix M. We define the variable $\xi = ak$, and the function

$$J_n(\xi) = e^{-\xi^2/4}\int_0^\infty du e^{-u^2/\xi^2}u^2 I_n(u) \tag{A.44}$$

$$= \frac{1}{16}\pi^{1/2}e^{-\xi^2/8}\xi^5\left\{I_{n/2-1}(\frac{1}{8}\xi^2) + \left[1 + \frac{4}{\xi^2} - \frac{4n}{\xi^2}\right]I_{n/2}(\frac{1}{8}\xi^2)\right\}. \tag{A.45}$$

Our matrix elements are

$$M_{11}(k) = 1 + \frac{1}{2}\frac{\sigma^2}{a^2}\xi^2 - 4\frac{\sigma^2}{a^2}\frac{1}{\xi^2}\frac{\epsilon-1}{(\epsilon+1)^2}\left((\epsilon - \frac{1}{2})J_0 + \frac{4\epsilon}{\epsilon-1}J_1 - \frac{1}{2}J_2\right) \tag{A.46}$$

$$M_{12}(k) = -4\frac{\sigma^2}{a^2}\frac{1}{\xi^2}\frac{\epsilon(\epsilon-1)}{(\epsilon+1)^2}\left(\frac{3}{2}J_0 - 2J_1 + \frac{1}{2}J_2\right) \tag{A.47}$$

$$M_{21}(k) = 4\frac{\sigma^2}{a^2}\frac{1}{\xi^2}\frac{\epsilon-1}{(\epsilon+1)^2}\left(\frac{3}{2}J_0 - 2J_1 + \frac{1}{2}J_2\right) \tag{A.48}$$

$$M_{22}(k) = 1 + \frac{1}{2}\frac{\sigma^2}{a^2}\xi^2 - 4\frac{\sigma^2}{a^2}\frac{1}{\xi^2}\frac{\epsilon-1}{(\epsilon+1)^2}\left(\frac{1}{2}(\epsilon-2)J_0 + \frac{4\epsilon}{\epsilon-1}J_1 + \frac{1}{2}\epsilon J_2\right) \tag{A.49}$$

and functions

$$h_1(k) = (1-\epsilon)\left(1 + \frac{1}{2}\frac{\sigma^2}{a^2}\xi^2 + 2\frac{\sigma^2}{a^2}\frac{1}{\xi^2}\frac{1}{\epsilon+1}\left[J_2 + (2\epsilon+1)J_0\right]\right) \tag{A.50}$$

$$h_2(k) = 2\left(1 + \frac{1}{2}\frac{\sigma^2}{a^2}\xi^2 + \frac{\sigma^2}{a^2}\frac{1}{\xi^2}\frac{1-\epsilon}{\epsilon+1}\left[J_2 + \frac{4(\epsilon+1)}{\epsilon-1}J_1 - J_0\right]\right). \tag{A.51}$$

The surface profile functions in the flat case are

$$a(k)_{\sigma=0} = \frac{1-\epsilon}{1+\epsilon} \tag{A.52}$$

$$b(k)_{\sigma=0} = \frac{2}{1+\epsilon}. \tag{A.53}$$

We note that there is no directional-dependence in the surface profile functions, as the autocorrelation of the height profile function is also not directionally-dependent as a result of the translational invariance we assume about the substrate surface.

The two boundary conditions can be written up to second order perturbations as follows. The first, a result of continuity of the tangential electric field at the interface, is written as

$$0 = \int \frac{d^2\vec{q}}{(2\pi)^2}\Bigg\{\frac{2\pi}{q}e^{-i\vec{q}\cdot\vec{r}'-qz'}\left[(2\pi)^2\delta(\vec{k}-\vec{q}) + q\widetilde{h}(\vec{k}-\vec{q}) + \frac{q^2}{2}\alpha\right] + A(\vec{q})\left[(2\pi)^2\delta(\vec{k}-\vec{q}) - q\widetilde{h}(\vec{k}-\vec{q}) + \frac{q^2}{2}\alpha\right] - B(\vec{q})\left[(2\pi)^2\delta(\vec{k}-\vec{q}) + q\widetilde{h}(\vec{k}-\vec{q}) + \frac{q^2}{2}\alpha\right]\Bigg\} \tag{A.54}$$

letting $\alpha = \int \frac{d^2\vec{q}'}{(2\pi)^2}\widetilde{h}(\vec{q}')\widetilde{h}(\vec{k}-\vec{q}-\vec{q}')$.

The second boundary condition, which expresses the continuity of the normal components of the electric displacement vector D, reads as

$$0 = \left\{\frac{\partial}{\partial z} - [\nabla h_s(\vec{r})]\cdot\nabla - \frac{1}{2}[\nabla h_s(\vec{r})]^2\frac{\partial}{\partial z}\right\}\int \frac{d^2\vec{q}}{(2\pi)^2}e^{i\vec{q}\cdot\vec{r}} \left\{\frac{2\pi}{q}e^{-i\vec{q}\cdot\vec{r}'}e^{-q|z-z'|} + A(\vec{q})e^{-qz} - \epsilon B(\vec{q})e^{qz}\right\}\Bigg|_{z=h_s(\vec{r})}. \tag{A.55}$$

Expanding to second order in the known coefficients yields

$$0 = \int \frac{d^2\vec{q}}{(2\pi)^2}e^{i\vec{q}\cdot\vec{r}}\Bigg\{2\pi e^{-i\vec{q}\cdot\vec{r}'}e^{-qz'}\left[1 - i\hat{q}\cdot\nabla h + qh - iqh\hat{q}\cdot\nabla h - \frac{1}{2}(\nabla h)^2 + \frac{q^2}{2}h^2\right] - A(\vec{q})q\left[1 + i\hat{q}\cdot\nabla h - qh - iqh\hat{q}\cdot\nabla h - \frac{1}{2}(\nabla h)^2 + \frac{q^2}{2}h^2\right] - \epsilon B(\vec{q})q\left[1 - i\hat{q}\cdot\nabla h + qh - iqh\hat{q}\cdot\nabla h - \frac{1}{2}(\nabla h)^2 + \frac{q^2}{2}h^2\right]\Bigg\} \tag{A.56}$$

where h is short for $h_s(\vec{r})$ in these equations.

Via the Fourier transform shown in Section 3.2.2, along with the relations

$$\int d^2\vec{r}e^{-i(\vec{k}-\vec{q})\cdot\vec{r}}(\nabla h)^2 = -\int \frac{d^2\vec{Q}}{(2\pi)^2}\vec{Q}\cdot(\vec{k}-\vec{q}-\vec{Q})\widetilde{h}(\vec{Q})\widetilde{h}(\vec{k}-\vec{q}-\vec{Q}) \tag{A.57}$$

$$i\vec{q}\cdot\int d^2\vec{r}e^{-i(\vec{k}-\vec{q})\cdot\vec{r}}h\nabla h = -\int \frac{d^2\vec{Q}}{(2\pi)^2}\vec{q}\cdot\vec{Q}\widetilde{h}(\vec{Q})\widetilde{h}(\vec{k}-\vec{q}-\vec{Q}) \tag{A.58}$$

$$i\vec{q}\cdot\int d^2\vec{r}e^{-i(\vec{k}-\vec{q})\cdot\vec{r}}\nabla h = -\vec{q}\cdot(\vec{k}-\vec{q})\widetilde{h}(\vec{k}-\vec{q}), \tag{A.59}$$

one can rewrite the second boundary condition in the same form as the first boundary condition. These two equations form the matrix equation used in Section 3.2.2 to determine the non-perturbative solutions to $A(\vec{k}), B(\vec{k})$. It becomes clear that expanding this equation to any more than second-order would be an exercise in tedium.

To determine the perturbative solutions for the potentials $A(\vec{k}), B(\vec{k})$ to second order in the height profile h_s

$$A(\vec{k}) = A_0(\vec{k}) + A_1(\vec{k}) + A_2(\vec{k}) + (\cdots) \tag{A.60}$$

(likewise for B), we group terms of order n in the potential expansion with terms of order $2-n$ in the stochastic height profile, similar in spirit to perturbative solutions in quantum mechanics with expansions to n-th order in the energy and wavefunctions. The solutions to 1st and 2nd order for these potentials are

$$\begin{bmatrix} A_1(\vec{k}) \\ B_1(\vec{k}) \end{bmatrix} = -4\pi \frac{\epsilon - 1}{(\epsilon+1)^2} \int \frac{d^2\vec{q}}{(2\pi)^2} e^{-i\vec{q}\cdot\vec{r}'} e^{-qz'} \widetilde{h}(\vec{k} - \vec{q}) \begin{bmatrix} \epsilon + \hat{k}\cdot\hat{q} \\ -1 + \hat{k}\cdot\hat{q} \end{bmatrix} \tag{A.61}$$

$$\begin{aligned} \begin{bmatrix} A_2(\vec{k}) \\ B_2(\vec{k}) \end{bmatrix} &= -4\pi \frac{\epsilon - 1}{(\epsilon+1)^3} \int \frac{d^2\vec{q}}{(2\pi)^2} \int \frac{d^2\vec{Q}}{(2\pi)^2} e^{-i\vec{Q}\cdot\vec{r}'} e^{-Qz'} q\widetilde{h}(\vec{k} - \vec{q})\widetilde{h}(\vec{q} - \vec{Q}) \\ &\times \begin{bmatrix} \epsilon(\epsilon-1) + 2\epsilon\hat{q}\cdot(\vec{Q}+\vec{k}) - (\hat{k}\cdot\hat{q})(\hat{q}\cdot\hat{Q})(\epsilon-1) \\ -(\epsilon-1) - 2\hat{Q}\cdot\hat{q} + 2\epsilon(\hat{k}\cdot\hat{q}) - (\hat{k}\cdot\hat{q})(\hat{q}\cdot\hat{Q})(\epsilon-1) \end{bmatrix} \end{aligned} \tag{A.62}$$

A.4 Smoothing Method for Finite-Gap Case

Combining equations from Section 5.2.1 into matrix form yields

$$\begin{aligned} &\int \frac{d^2\vec{p}}{(2\pi)^2} \Bigg((2\pi)^2 \delta(\vec{q} - \vec{p}) \begin{bmatrix} \frac{1+\epsilon}{1-\epsilon} & 1 \\ W(q)e^{-qh_0} & [1+W(q)]e^{qh_0} \end{bmatrix} - \\ &p \begin{bmatrix} \widetilde{h}_s(\vec{q}-\vec{p})(1-\hat{q}\cdot\hat{p}) & -\widetilde{h}_s(\vec{q}-\vec{p})(1+\hat{q}\cdot\hat{p}) \\ \widetilde{h}_g(\vec{q}-\vec{p})[W(p)+W(q)]e^{-ph_0} & \widetilde{h}_g(\vec{q}-\vec{p})[W(p)-W(q)]e^{ph_0} \end{bmatrix} \Bigg) \begin{bmatrix} A(\vec{p}) \\ B(\vec{p}) \end{bmatrix} = \begin{bmatrix} 0 \\ 0 \end{bmatrix} \end{aligned} \tag{A.63}$$

where $W(q) = (2\pi e^2/q)\chi(q,\omega)$, recalling that ω is not involved in our integrations, allowing us to write our edited dielectric function as $W(q)$. Here we perform the same perturbation as the smoothing method did for graphene on top of a substrate as done in Section 5.2.1. As we now have matrices, we define $\epsilon(q,\omega)$ via a matrix equation as:

$$H(\vec{q},\vec{p}) = (2\pi)^2\delta(\vec{q}-\vec{p}) \begin{bmatrix} \frac{1+\epsilon}{1-\epsilon} & 1 \\ W(q)e^{-qh_0} & [1+W(q)]e^{qh_0} \end{bmatrix} = (2\pi)^2\delta(\vec{q}-\vec{p})\epsilon(q,\omega) \tag{A.64}$$

We likewise make the approximation $\langle M\rangle = \langle V + M\langle G\rangle(V - \langle M\rangle)\rangle \approx \langle V\langle G\rangle V\rangle$. Our only change in definition is that for the loss function, which now will take on the form

$$\text{Loss Function } = -\Im\left[\frac{1}{\det[\epsilon(q,\omega) - m(q,\omega)]}\right]. \tag{A.65}$$

This extends the analogy of the plasmon dispersion being given by the relation $\epsilon(q,\omega) - m(q,\omega) = 0$ to matrices. Analyzing this loss function gives indications about where the plasmon modes lie.

Our matrix $\langle G(\vec{p},\vec{q})\rangle$ is now defined as an inverse calculation

$$\begin{aligned} \langle G\rangle = (2\pi)^2\delta(\vec{q}-\vec{p}) &= (2\pi)^2\delta(\vec{q}-\vec{p}) \begin{bmatrix} h_{11}(q) - m_{11}(q) & h_{12}(q) - m_{12}(q) \\ h_{21}(q) - m_{21}(q) & h_{22}(q) - m_{22}(q) \end{bmatrix}^{-1} \\ &= (2\pi)^2\delta(\vec{q}-\vec{p}) \begin{bmatrix} g_{11}(q) & g_{12}(q) \\ g_{21}(q) & g_{22}(q) \end{bmatrix}, \end{aligned} \tag{A.66}$$

recalling that to make a first-order iterative approximation to $M \approx \langle V\langle G\rangle V\rangle$, we take $m_{ij}(q) = 0$ in the expression for $\langle G\rangle$. The terms $g_{ij}(q)$, by nature of being defined as the components of the inverse matrix, contain the determinant of $H - \langle M\rangle$ in their denominator. This equivalent situation in Section 5.2.1 forced us to implement the Sokhotski-Plemelj theorem to justify integration over a singularity.